2014

MODEL ANALYSIS AND PREDICTIVE CONTROL OF DOUBLE ELECTRODE SUBMERGED ARC WELDING PROCESS FOR FILLET JOINTS WITH ROOT OPENING

Yi Lu
University of Kentucky, louis.lu212@gmail.com

STUDENT AGREEMENT:

I represent that my thesis or dissertation and abstract are my original work. Proper attribution has been given to all outside sources. I understand that I am solely responsible for obtaining any needed copyright permissions. I have obtained needed written permission statement(s) from the owner(s) of each third-party copyrighted matter to be included in my work, allowing electronic distribution (if such use is not permitted by the fair use doctrine) which will be submitted to UKnowledge as Additional File.

I hereby grant to The University of Kentucky and its agents the irrevocable, non-exclusive, and royalty-free license to archive and make accessible my work in whole or in part in all forms of media, now or hereafter known. I agree that the document mentioned above may be made available immediately for worldwide access unless an embargo applies.

I retain all other ownership rights to the copyright of my work. I also retain the right to use in future works (such as articles or books) all or part of my work. I understand that I am free to register the copyright to my work.

REVIEW, APPROVAL AND ACCEPTANCE

The document mentioned above has been reviewed and accepted by the student's advisor, on behalf of the advisory committee, and by the Director of Graduate Studies (DGS), on behalf of the program; we verify that this is the final, approved version of the student's thesis including all changes required by the advisory committee. The undersigned agree to abide by the statements above.

Yi Lu, Student

Dr. YuMing Zhang, Major Professor

Dr. Cai-Cheng Lu, Director of Graduate Studies

MODEL ANALYSIS AND PREDICTIVE CONTROL OF DOUBLE ELECTRODE SUBMERGED ARC WELDING PROCESS FOR FILLET JOINTS WITH ROOT OPENING

DISSERTATION

A dissertation submitted in partial fulfillment of the requirements for the degree of Doctor of Philosophy in the College of Engineering at the University of Kentucky

By

Yi Lu

Lexington, Kentucky

Co-Directors: Dr. YuMing Zhang, Professor of Electrical and Computer Engineering and Dr. Lawrence E. Holloway, Professor of Electrical and Computer Engineering

Lexington, Kentucky

ABSTRACT OF DISSERTATION

MODEL ANALYSIS AND PREDICTIVE CONTROL OF DOUBLE ELECTRODE SUBMERGED ARC WELDING PROCESS FOR FILLET JOINTS WITH ROOT OPENING

Submerged Arc Welding (SAW) for fillet joints is one of the major applications in the shipbuilding industry. Due to the requirement for the weld size, a sufficient amount of metal must be deposited. In conventional SAW process, the heat input is proportional to the amount of metal melted and is thus determined by the required weld size. To meet this requirement, an excessive amount of heat is applied causing large distortions on the welded structures whose follow-up straightening is highly costly. In order to reduce the needed heat input, Double-Electrode (DE) technology has been practiced creating the Double-Electrode SAW (DE-SAW) method for fillet joints. The reduction in the heat input, however, also reduces the penetration capability of the process, and the ability to produce required weld beads has to be compromised. To eliminate the unwanted side effect after using DE-SAW, a root opening between the panel and the tee has been proposed in this dissertation to form a modified fillet joint design. Experimental results verified that the use of root opening improves the ability of DE-SAW to produce the required weld beads at reduced heat input and penetration capability. Unfortunately, the use of root opening decreases the stability of the process significantly. To control

the heat input at a minimally necessary level that guarantees the weld size and meanwhile the process stability, a feedback is needed to control the currents at their desired levels. To this end, the fillet DE-SAW process is modeled and a multivariable predictive control algorithm is developed based on the process model. Major parameters including the root opening size, travel speed and heat input level have been selected/optimized/minimized to produce required fillet weld beads with a minimized heat input based on qualitative and quantitative analyses. At the end of this dissertation, a series of experiments validated the feasibility and repeatability of the predictive control based DE-SAW process for fillet joints with root opening.

KEYWORDS: Submerged Arc Welding (SAW), Fillet Joint, Double-Electrode (DE), Predictive Control, Root Opening

Yi Lu

Feb 18, 2014

MODEL ANALYSIS AND PREDICTIVE CONTROL OF DOUBLE ELECTRODE SUBMERGED ARC WELDING PROCESS FOR FILLET JOINTS WITH ROOT OPENING

By

Yi Lu

Dr. YuMing Zhang

_____

Director of Dissertation

Dr. Cai-Cheng Lu

_____

Director of Graduate Studies

Feb 18, 2014

_____

Date

ACKNOWLEDGEMENTS

This research is funded by the Navy under contracts N65538-08-M-0049 and N00024-09-C-4140 and Kentucky Cabinet for Economic Development (CED) Office of Commercialization and Innovation through Kentucky Science and Engineering Corp. under agreements KSTC-184-512-08-038 and KSTC-184-512-09-067. I would like to gratefully and sincerely thank my advisor, Dr. YuMing Zhang, for his guidance, patience, support, and most importantly, his encouragement during my graduate studies at University of Kentucky. Also thanks to my dissertation committee members Drs. Alan T. Male, Larry Holloway and Yuan Liao for their help both in my graduate courses and my dissertation research. Moreover, my appreciation is also given to my colleagues from Adaptive Intelligent Systems LLC and Welding Research Lab: Xiangrong Li, Jinsong Chen, Kun Qian, Zeng Shao, Chenglin Yi, Yi Huang, Xiaoji Ma, Weijie Zhang, Yan Shao, Yukang Liu and Kehai Li. Last but most important, I want to express my deep gratitude to my parents and girlfriend for their love, faith in me, and long-term solid support for my work.

Table of Contents

List of Tables

List of Figures

Chapter 1 Introduction

1.1 Background

Submerged arc welding (SAW) is a widely used arc welding process. Similarly as conventional gas metal arc welding (GMAW) and flux-cored arc welding (FCAW), it melts a continuously fed consumable solid or flux cored electrode wire to deposit metal into the work-piece. In SAW process, however, the consumable wire and arc are better shielded from atmospheric contamination because of being “submerged” under a blanket of granular, fusible flux. However, excessive heat is also applied to the work-piece causing the distortion whose follow-up straightening is highly costly. If the heat input into the work-piece can be reduced effectively, then the distortion and required straightening will be reduced.

Double-Electrode SAW (DE-SAW) is a process developed recently to reduce the heat input associated with SAW. It is considered as a new application of Double-Electrode technology. Except for the change from gas shielding to flux shielding so as to realize the advantages associated with SAW, the principle of the electrical circuit remains unchanged. That is, in DE-SAW, the total welding current still divides into the base metal current and the bypass current after it melts the main wire. Since part of the current is bypassed without flowing into the work-piece, the heat input into the work-piece is reduced. When the metal from the bypass wire melted by the bypass arc is added into the work-piece, the reduced heat input is added back but the metal deposition is increased. The DE-SAW is thus capable of depositing the same amount of metal at reduced heat

input or depositing more metal at the same heat input. Of course, the DE-SAW for fillet joints is more challenging than the butt joints. That is why a root opening between the tee and the panel has to be introduced in this research.

Undoubtedly, the feedback control of the fillet DE-SAW process with root opening is indispensable. After all, the application of the Double-Electrode technology merely provides a platform for reducing the heat input and increasing the metal deposition; the accurate control of the heat input and penetration during the welding process, especially after the introduction of a root opening between the tee and the panel, depends on the precise output of welding currents. Therefore, finding out a reasonable and effective control algorithm and then building up a reliable control system based on this algorithm to control the welding currents and thereby help the DE-SAW process reduce the heat input, the distortion as well as the required straightening of the work-piece is really meaningful to the welding industry. And that is the motivation of this paper.

1.2 Objectives

The ultimate goal of this dissertation research is to develop a control system for fillet joint DE-SAW process with root opening based on the analysis to the principles and model, so that the heat input into the work-piece can be reduced and the welding process can be maintained at a steady status. Meanwhile, the metal deposition rate and penetration ability need be controlled appropriately as well, so that the quality of the welds can be guaranteed.

Some proposed objectives for this research are listed below:

1. Apply the Double-Electrode technology to the submerged arc welding (SAW) process to build a DE-SAW process.
2. Introduce a root opening between the tee and the panel to form a modified fillet joint, so that the required penetration ability can be reduced in the fillet DE-SAW process.
3. Identify the process model of the fillet DE-SAW process with root opening.
4. Based on the dynamic incremental model of the fillet DE-SAW process, develop an advanced control algorithm to feedback control the base metal current and the bypass current, so that the heat input and penetration ability can be controlled and maintained at a stable status.
5. By through a series of practical experiments, prove the effectiveness of the control system as well as the feasibility and repeatability of the fillet DE-SAW process with root opening.
6. Compared with the conventional SAW process, illustrate the advantages of the fillet DE-SAW with root opening under advanced control on heat input reduction and welding quality.
7. After verifying the feasibility and effectiveness of the predictive control system with small work pieces, conduct the same control on large panels to simulate a more practical welding environment.
8. Based on on-site requirements, simplify/ modify the control system so that the system can be transplanted to the practical welding processes in a more convenient way.

1.3 Organization

To document this research, this dissertation is divided into 8 chapters and organized as follows:

Chapter 1 Introduction: gives a brief introduction to the issues occurred in the fillet joint welding using the conventional SAW and DE-SAW, and the control approaches used in this research.

Chapter 2 Review of Double-Electrode Technology: As the precursor and key part of DE-SAW process, the fundamental principle, developments and extension of Double-Electrode technology have been reviewed in this chapter.

Chapter 3 DE-SAW and Use of Root Opening: discusses the advent of DE-SAW and why an intentionally designed root opening between the tee and panel of the fillet joint has to be used. Also, the necessity of effective control in fillet DE-SAW with root opening is discussed.

Chapter 4 Parameters Selection: by through a series of open-loop experiments on the fillet joint work-pieces with a root opening, the root opening size, travel speed of the tractor, and the total heat input (i.e. the initial main wire feed speed) have been selected, optimized and minimized based on quantitative and qualitative approaches.

Chapter 5 Process Modeling: by analyzing the melting physical process, an incremental model of the fillet joint DE-SAW process with root opening has been established.

Chapter 6 Predictive Control Algorithm Design: in terms of the process incremental model, the predictive control algorithm has been developed.

Chapter 7 Experiments and Analysis: by through a series of experiments conducted on fillet joint welds with a root opening, the performance of the predictive DE-SAW control algorithm has been tested and analyzed. Also, after compared with the conventional SAW, the advantages of the fillet DE-SAW with root opening under advanced control on heat input reduction and welding quality has been illustrated well. At the end of this chapter, the predictive control system has been conducted on large panels to simulate a more practical welding condition in shipyards.

Chapter 8 Base on the on-site requirements of the shipyards, the predictive control system is simplified so that the portability of the control system can be increased. Also, at the end of this chapter, the simplified predictive control system has been conducted on large panels to simulate a more practical welding condition in shipyards.

Chapter 9 Conclusion and Future Work: the contents of this dissertation, especially the performance and outcome by using the root opening and predictive control algorithm in fillet DE-SAW are summarized; some prospective works are proposed.

Chapter 2 Review of Double-Electrode Technology

DE-GMAW can be considered as the precursor of DE-SAW. Before discussing the algorithm and control system design of the fillet joint DE-SAW process, it is necessary to review the invention and development of the Double-Electrode technology.

2.1 Background

Previously, two technologies have been developed to modify GMAW for faster deposition: Tandem GMAW [1, 2] and Variable-Polarity GMAW (VP-GMAW) [3-7]. In Tandem GMAW, two torches have been integrated into one bigger torch, and two close arcs are independently established between their own wire and the work-piece in parallel and are adjusted by their own GMAW power supply. In essence, Tandem GMAW is still considered two parallel conventional GMAW processes. It allows the deposition speed be doubled without increasing the arc pressure. For VP-GMAW, liquid droplets are still detached during the reverse polarity (wire positive) period, but the welding wire can be melted faster during the straight polarity (wire negative) period [3, 8]. It was found that to melt the welding wire at the same rate, the base metal heat input could be “up to 47%” less than the conventional pulsed GMAW [8]. Thus, when the allowed base metal heat input is given, VP-GMAW may also double the deposition speed. Modifications by adding a laser to form hybrid laser-arc processes [9-16] can penetrate deeper to reduce the needed deposition. However, the resultant process is no longer a pure arc welding process and many advantages associated with arc welding have to be compromised.

The double-electrode GMAW [17, 18] and its variants are introduced to increase the deposition rate without increasing the heat input, reduce the heat input without compromising the deposition speed, or freely provide the needed heat input and deposition speed as desired in different applications which typically use GMAW or its variants. For conventional GMAW and its variants, the base metal current is exactly the same as the wire current, i.e., the current flows through the wire. This is the fundamental principle not only for GMAW but also for all other conventional arc welding processes in which an arc must be established between an electrode and the work-piece. Because of this fundamental principle, while the wire current needs to be increased to raise the deposition rate, the base metal current increases exactly the same regardless of the actual requirement of the work-piece. The DE-GMAW changes this principle by introducing a bypass channel such that the deposition speed no longer needs to be proportional to the heat input applied into the work-piece.

In this chapter, the principle, developments and extension of the DE-GMAW are reviewed and discussed in a roughly chronological order.

2.2 Principle of Double-Electrode GMAW

Fig. 2.1 demonstrates the principle of the DE-GMAW process and its variants where the main electrode is a consumable wire. The main power supply, main torch/electrode and work-piece form the conventional GMAW process and the main loop. The bypass torch added next to the main torch provides an additional electrode to form an additional arc, i.e., the bypass arc, with the main electrode and closes the bypass loop. In Fig. 2.1, the

bypass arc is powered by an added second power supply but it may also be powered by the same main power supply as will be mentioned later in this chapter.

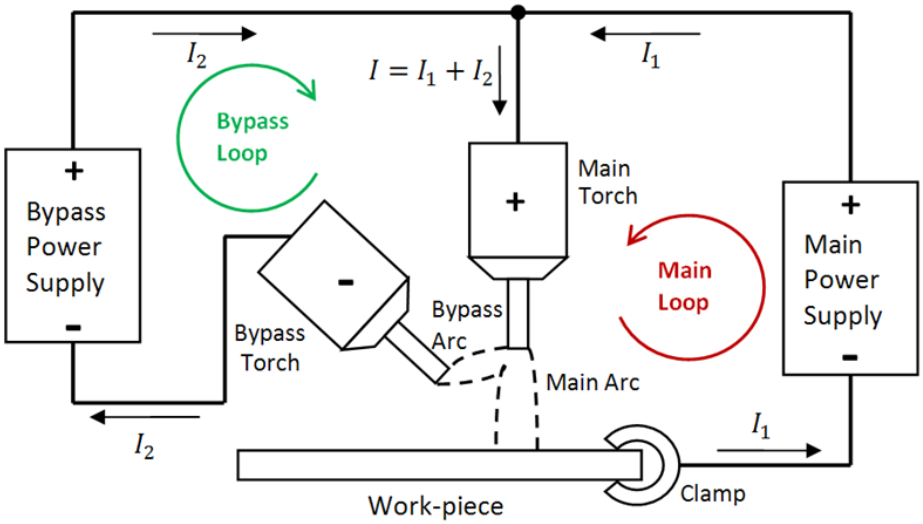

Fig. 2.1 Current relationship in DE-GMAW process

The wire current I (also known as total current or melting current), base metal current I_1 and bypass current I_2 have also been denoted as I_m, I_{bm} and I_{bp} respectively in some literature. They will be both used in order to match with the literatures cited.

The main loop represents the path through which the base metal current (I_1) flows while the bypass loop represents the path through which the bypass current (I_2) flows. In Fig. 2.1, the positive terminals of the two power supplies are connected together as a common positive terminal connecting to the main torch. The work-piece (or base metal) and bypass electrode are connected with the negative terminals of the main and bypass power supply respectively. This is a modification from the standard straight polarity GMAW system, although it is also possible from a reverse-polarity GMAW system. In the system shown in Fig. 2.1, the wire current

$$I = I_1 + I_2 \tag{2.1}$$

where I is the total welding current that melts the wire. The division of the wire current I into the base metal current I_1 and bypass current I_2 provides Double-Electrode GMAW the fundamental to reduce the heat input into the work-piece while maintaining the melting rate.

For non-consumable DE-GMAW, the heat that melts the wire is

$$H_{wire} = (V_{anode} I + k_1 I^2)\Delta t \tag{2.2}$$

where V_{anode} is the anode voltage, $k_1 > 0$ is a constant, and Δt is the time interval. In addition to H_{wire} brought into the work-piece by the melted wire, the main arc also directly applies its cathode heat

$$H_{cathode} = V_{cathode} I_1 \Delta t \tag{2.3}$$

into the work-piece. Omitting the resistive heat ($k_1 I^2$) yields

$$H_{wire} \approx V_{anode} I \Delta t \tag{2.4}$$

Further, omitting the heat input into the work-piece due to the arc column radiation, the total heat input into the work-piece is

$$H \approx (V_{anode} I + V_{cathode} I_1)\Delta t \tag{2.5}$$

The range of the proportion "p" of the wire melting heat in the total heat applied into the work-piece can be used to measure the controllability of the heat input of the process as quantified by:

$$p = H_{wire}/H \approx V_{anode} I/((V_{anode} I + V_{cathode} I_1) \tag{2.6}$$

For convenience, this dissertation refers "p" as the deposition efficiency. A greater deposition efficiency "p" implies a lower heat input procedure/process and a larger range of the deposition efficiency "p" implies a better heat input controllability. It is apparent that "p" increases as I_1 decreases (or I_2 increases) for the same I. By adjusting I_2, "p" is adjusted and reaches its minimum:

$$p_0 = V_{anode}/(V_{anode} + V_{cathode}) \tag{2.7}$$

when $I_1 = I$ or $I_2 = 0$, i.e., when the process becomes the conventional GMAW process. Hence, the non-consumable DE-GMAW can increase the melting speed without changing the heat input (or reduce the heat input without reducing the melting speed) and the increase in melting speed (or reduction in heat input) can be controlled by modifying the bypass current.

For consumable DE-GMAW, the bypass wire is melted and the heat is added back into the work-piece such that

$$H_{wire} \approx (V_{anode}I + V_{cathode}I_2)\Delta t \tag{2.8}$$

$$H \approx (V_{anode} + V_{cathode})I\Delta t \tag{2.9}$$

$$p = \frac{H_{wire}}{H} = (V_{anode}I + V_{cathode}I_2)/\,(V_{anode} + V_{cathode})I = p_0 + \Delta p \tag{2.10}$$

Where:

$$\Delta p = V_{cathode}I_2/\,(V_{anode} + V_{cathode})I \tag{2.11}$$

Again, when $I_2 = 0$, i.e., when the process becomes the conventional GMAW process, then $\Delta p = 0$. Hence, the consumable DE-GMAW can increase the melting speed without changing the heat input (or reduce the heat input without reducing the melting speed) and

the increase in melting speed (or reduction in heat input) can be controlled by adjusting the bypass current.

2.3 Non-Consumable DE-GMAW Using Constrained Bypass Arc

A non-consumable DE-GMAW uses a non-consumable bypass electrode to realize the general DE-GMAW system shown in Fig. 2.1. Its feasibility was first verified using a PAW torch to provide the non-consumable second electrode in 2004 at the University of Kentucky [17, 18] as shown in Fig. 2.2. The purpose of using PAW torch was to ease the establishment of the bypass arc because the pilot arc can easily provide a reliable channel bridging the main arc and the tungsten second electrode. In fact, the constrained pilot arc can overcome the possible effects on the ignition of the bypass arc from variations in the bypass torch installation. Hence, although the bypass arc can only be established after the main arc has been established, the existence of the bypass channel prior to the main arc is helpful for minimizing the delay from the establishment of the main arc to the establishment of the bypass arc. The DE-GMAW process can thus be successfully established almost as soon as the main arc is ignited.

Two 12 by 6 by 0.5 inch plates were used to form a 60° groove as shown in Fig. 2.2, and joined together using PAW as a root pass before being used as the work-piece for DE-GMAW experiments. In the weld shown in Fig. 2.2, the groove is sufficiently filled in a single pass at the travel speed of 6.6 in/min with a bypass current at 100 A. Under the same welding conditions (same main wire feed speed and same travel speed), the work-piece was burned through in the conventional GMAW process. The effectiveness of the

bypass method for heat input and arc pressure reductions without reducing the melting speed is demonstrated.

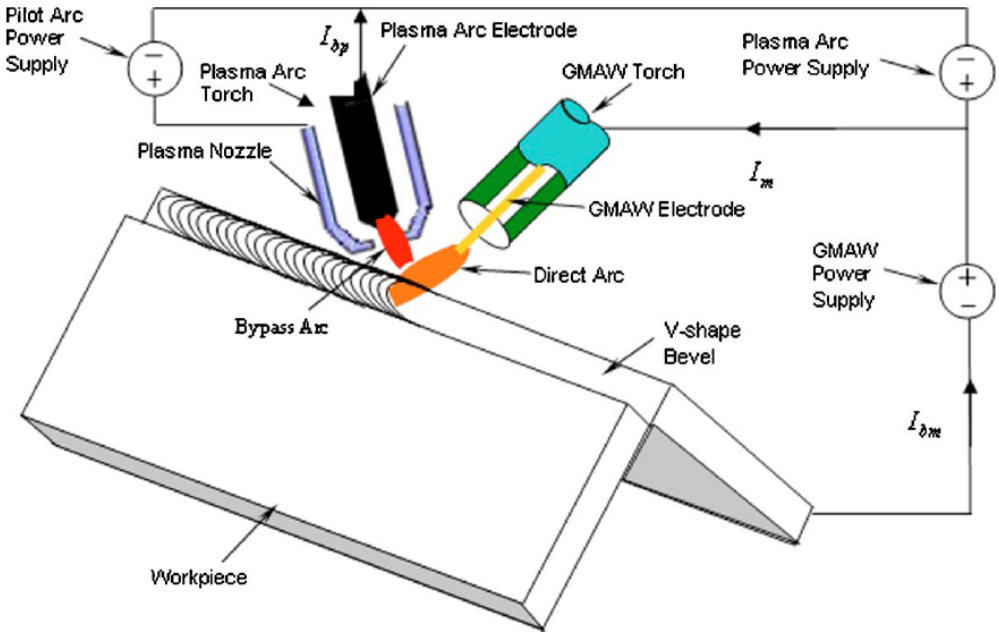

Fig. 2.2 Non-consumable DE-GMAW experimental system using a PAW torch [17]

Where, I_m, I_{bm}, and I_{bp} stand for the melting, base metal and bypass current respectively and correspond to I, I_1 and I_2 respectively in Fig. 2.1.

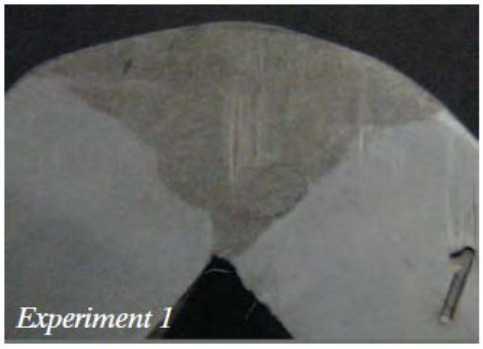

Fig. 2.3 Cross-section of weld made by non-consumable DE-GMAW using plasma bypass arc I_{bp} =100 A, I_{bm} =145 A [17]

2.4 Non-Consumable DE-GMAW Using Unconstrained Bypass Arc

While the pre-existence of a constrained pilot arc can ease the ignition of the bypass arc after the main arc has been established, its associated high cost for the equipment and the inconvenient large size of the bypass torch are all unwanted. In the non-consumable DE-GMAW system shown in Fig. 2.4, the PAW torch in Fig. 2.2 is replaced by a GTAW torch. The bypass power supply is replaced by a bypass control circuit which controls the passing bypass current at the desired level. The main GMAW power supply provides $I_m = I_{bm} + I_{bp}$, i.e., $I = I_1 + I_2$ in Fig. 2.1. Since the tungsten electrode is much easier to emit electrons then the work-piece, the majority of the current provided by the power supply would be bypassed such that the bypass current may exceed the desired level. The bypass control circuit provides an approach to reduce the bypass current to its desired level. The current principle $I = I_1 + I_2$ of DE-GMAW as shown in Fig. 2.1 is unchanged.

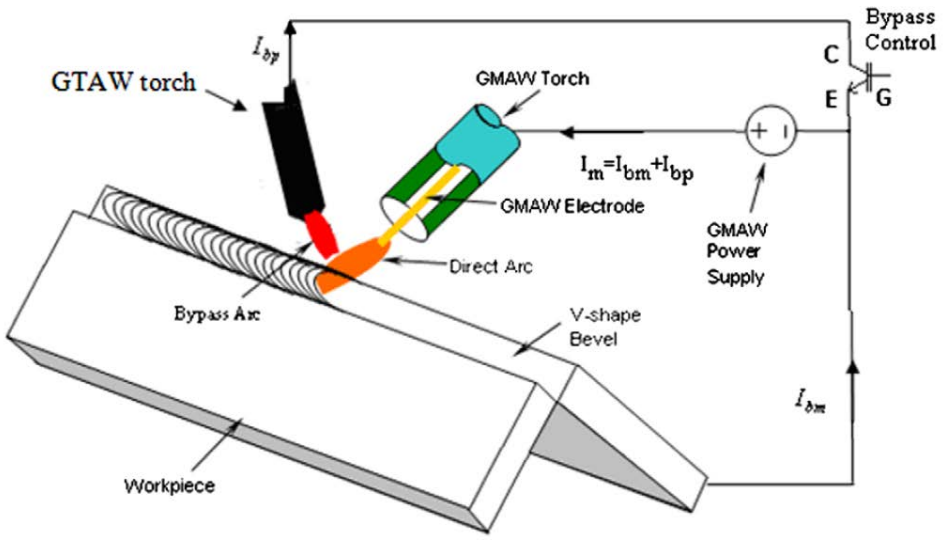

Fig. 2.4 Principle of non-consumable DE-GMAW [17]

In the system in Fig. 2.4, the bypass control circuit is an Insulated Gate Bipolar Transistor (IGBT) which controls the on and off of the bypass loop. However, if no current sensors are used to provide the feedback to control the switch of the IGBT, this non-consumable DE-GMAW system would work in the open loop mode. Proper welding parameters, especially the proportion of the on-off ratio and the wire feed speed which controls the total current, must be set carefully to obtain the currents at their desired levels.

The non-consumable DE-GMAW circuit was analyzed as shown in Fig. 2.5 [17]. The GMAW (main) arc and bypass arc were represented by their equivalent resistances. The two arcs are approximated as two resistors in parallel with the same voltage. The current distribution is thus determined by their resistances. Their corresponding current will be inversely proportional to their resistance. Since the equivalent resistance of the bypass arc is much smaller, an adjustable power resistor should be added to control the bypass current. On the other hand, the total current is determined by the wire feed speed. The currents can therefore be controlled in reasonable ranges.

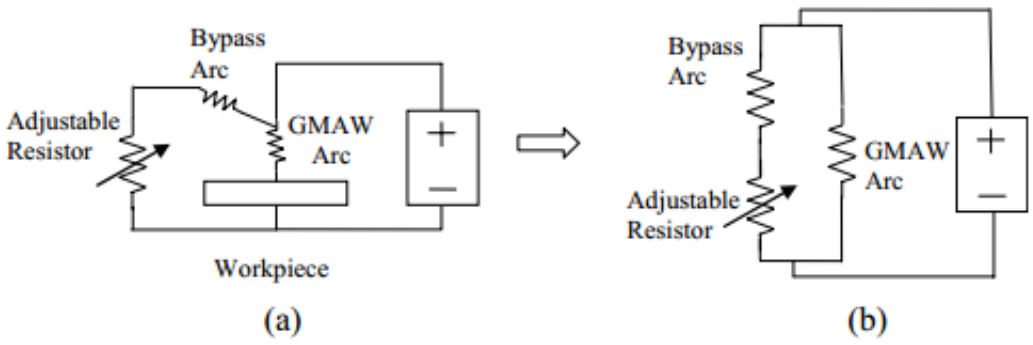

Fig. 2.5 Equivalent circuit of a single power supply based non-consumable DE-GMAW system [18]

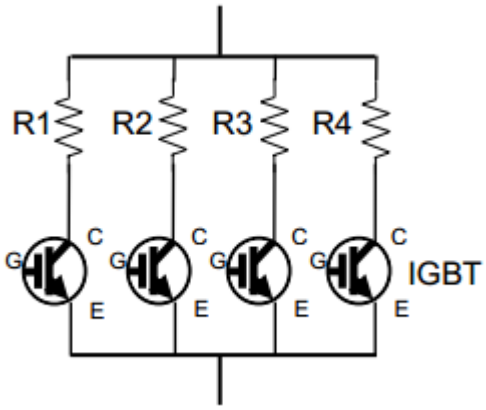

Fig. 2.6 Adjustable resistor [18]

The adjustable power resistor has been formed using four parallel power resistors with each in series with an IGBT (see Fig. 2.6) as its on-off control switch [18]. The resistance for each resistor has been designed such that the parallel circuit can provide adequate resolution for the resultant resistance incorporated with the on-off switch of the resistors. Fig. 2.7 shows the recorded currents for a control experiment using the non-consumable DE-GMAW process and control system shown in Fig. 2.4~2.6.

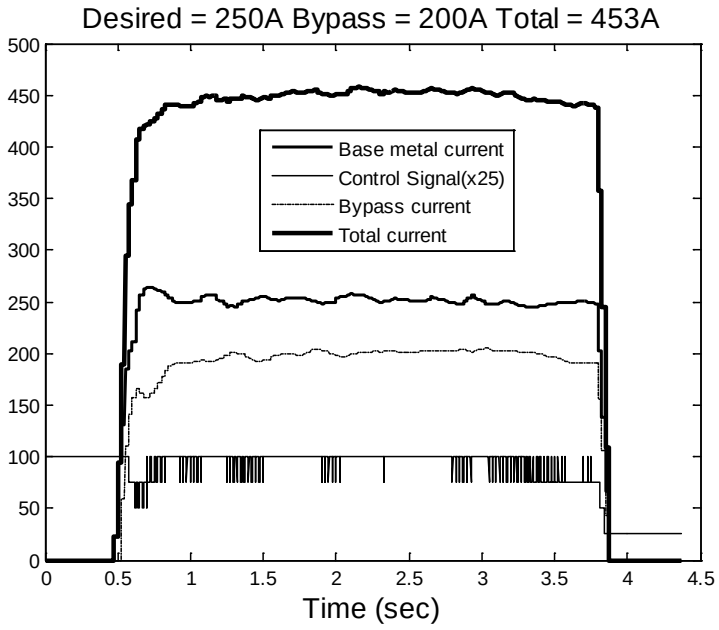

Fig. 2.7 A control example [18]. The bypass current is adjusted by changing the equivalent resistance of the power resistor to maintain the base metal current around the desired value that is 250 A

Fig. 2.8 shows an example weld made on a lap joint, formed by 2 mm on 2 mm thick low carbon steel sheet, with the non-consumable DE-GMAW process and control system shown in Fig. 2.4~2.6. The travel speed was 1.65 m/min (65 IPM) while the wire was fed in at 14.0 m/min (550 IPM). The welding voltage was 32 volts. From this example weld, it can be seen that the DE-GMAW process made acceptable weld at a high speed. However, when applying the conventional GMAW by setting the bypass current to zero, the lap-joint formed by two 2 mm low carbon steel sheets was burned through [18].

Fig. 2.8 Comparison of weld on lap joint made by controlled DE-GMAW and conventional GMAW process [18]

2.5 Metal Transfer in Non-Consumable DE-GMAW Using Unconstrained Bypass Arc

The American Welding Society (AWS) classifies the metal transfer into three primary modes: spray transfer, globular transfer, and short-circuiting transfer. In the spray transfer, the liquid metal droplets transfer into the weld pool across the arc gap with diameters similar to or smaller than that of the wire. The International Institute of Welding (IIW) further classifieds the spray transfer mode into the projected spray (or drop spray), streaming spray, and rotating spray. In the globular transfer, the liquid metal droplets are also transferred across the arc gap but with diameters much greater than that of the wire. In the short-circuiting transfer, the melted metal is transferred when the droplet is in contact with the weld pool. For conventional GMAW, metal transfer plays a critical role in determining the arc stability and weld quality. In DE-GMAW, the dependence of the arc stability and weld quality on the metal transfer still exists.

A major issue in GMAW is that it requires a current higher than the critical current [19] to produce the desired spray mode. However, such a high current may not be desired by the application. Specifically, in conventional GMAW, the current flows from the wire approximately around the wire axial direction. This direction determines the net effect of the electromagnetic force - the major detaching force, needed to produce the spray transfer. Under this condition, the current needs to be greater than the critical current in order to supply a sufficient detaching force for the spray transfer. However, in DE-GMAW, the current from the wire flows into two directions: around the wire axial direction and toward the bypass electrode. The condition in the conventional GMAW that

determines the net effect of the distributed electromagnetic force field as the detaching force is changed. The metal transfer in DE-GMAW should be related to both the base metal current and bypass current [20-22].

Studies found that, when the total current is high enough, the droplet forms a stream which bridges the electrode wire and the weld pool. Partial welding current can flow through the stream to the work-piece. However, the current path from the solid electrode wire to the work-piece still exists because of the existence of the main arc. This is a metal transfer that falls into the definition of neither the free flight transfer nor the bridge transfer. It has been referred to as the contacting stream spray transfer because of its similarity to the conventional stream spray transfer and the conventional short-circuiting transfer.

In greater detail, when the bypass arc is present, partial melting current is forced to flow to the bypass electrode. Because the bypass tungsten electrode is at a different direction from the cathode on the work-piece, the bypass current forms an angle with the base metal current which flow from the droplet to the cathode on the work-piece. As a result, the convergence of the current in conventional GMAW is undermined so that the net electromagnetic force shifts toward becoming a detaching force. Hence, although the total current may be smaller than the critical current, the metal transfer still changes to the spray mode after the bypass arc is introduced. In addition to the change of the transfer mode, the effect of the bypass arc on the droplet trajectory can also be observed.

In the series of experiments shown in Fig. 2.9 [20], the total current is approximately the same (the wire feed speed is the same) but the bypass current varies. It can be seen that the droplets associated with the higher bypass current changed from globular transfer to spray transfer and became smaller with higher droplet rate. This suggests that the electromagnetic force was further shifted toward being a detaching force although the total current remained unchanged.

(a) Bypass current = 0

(b) Bypass current = 72amps

(c) Bypass current = 108amps

Fig. 2.9 Metal transfer experiments. WFS: 6.4 m/min (250IPM), diameter 1.2 mm steel wire. (a), (b), and (c) used different bypass currents

2.6 Consumable DE-GMAW and Analysis

In non-consumable DE-GMAW, although extra heat input and arc force have been reduced, the energy absorbed by the bypass electrode is wasted. If the bypass electrode is a consumable wire, the waste can be eliminated while still providing the advantages associated with DE-GMAW. The resultant process is the consumable DE-GMAW shown in Fig. 2.10 and its heat input controllability as represented by the range of the deposition efficiency p has been discussed earlier in Section 2.2 and especially mathematically analyzed in Eq. (2-8) ~ (2-11). The consumable wire is fed through a GMAW torch as the bypass electrode. In Fig. 2.10, two power supplies running at the CV mode are used to provide the base metal and bypass current. The main wire is primarily melted by the anodes of the main arc and bypass arc whose currents are the base metal current and bypass current respectively. The bypass wire is primarily melted by the cathode of the bypass arc. The main wire feed speed thus controls the sum of the base metal and bypass current, i.e., the total current $I = I_1 + I_2$, and the bypass wire feed speed determines the bypass current I_2.

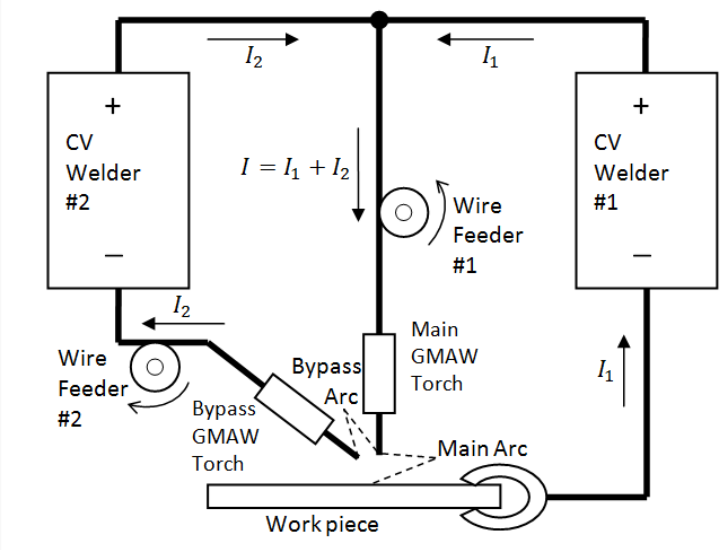

Fig. 2.10 Principle of consumable DE-GMAW

In Fig. 2.10, two CV power supplies are used. In such a CV power supply based system, the total current and bypass current depend on the corresponding wire feed speed and voltage setting. First, the CV mode controls the length of the main arc, at a desired level corresponding to the setting of CV Welder #1 in Fig. 2.10, to balance the melting with the feeding of the main wire. The actual total current is the result of the adjustment on the melting current for the main wire. In the meantime, the actual bypass current is the result of the adjustment on the melting current for the bypass wire. When the actual bypass current is determined by the need to balance the melting and feeding for the bypass wire, the balance of the main wire determines the base metal current. Hence, balancing the melting with feeding for the two wires controls the base and bypass current. Second, the equilibriums, as determined by the voltage settings of the two CV power supplies, control the degrees of the balances. This is because that the realized arc lengths as a result of the balances affect the wire extensions and the wire extensions determine the resistive heats on the wires. As the resistive heats increase, the needed heats from the arc anodes to

balance the corresponding melting with feeding are reduced. The corresponding currents are thus reduced. Hence, both the currents are controlled by the wire feed speeds and voltage settings. However, the actual currents are not accurately controlled and also depend on other variables including the tip-to-work distance (for the main arc) and the positioning of the bypass wire in relation to the main wire (for the bypass arc).

There are three major parameters that determine the resultant welds from DE-GMAW: base metal current, heat input, and mass input. Ideally, one needs a certain amount of metal be deposited on the joint to form a weld with the desired shape and penetration. When the mass input and joint geometry are given, the weld shape and penetration are primarily determined by the penetration capability of the arc. For DE-GMAW, this penetration capability is determined by the heat input and the force of the main arc. The heat input consists of the heat input from the droplets and the heat input directly imposed on the work-piece. When the mass input is given, the heat input from the droplets is approximately fixed. The heat input directly imposed on the work-piece is due to the cathode heat of the main arc determined by $V_{cathode}I_1$ and is thus controlled by the base metal current I_1 since $V_{cathode}$ is a constant. On the other hand, the force of the main arc is proportional to the square of the base metal current I_1. Hence, when the mass input is given such that the heat input is approximately given, the resultant weld is controlled by the base metal current. However, while the mass input can be controlled, the CV power supply based system shown in Fig. 2.10 does not provide an accurate control on the base metal current.

2.7 Control of Consumable DE-GMAW

A method to produce desired welds is to control the base metal current and bypass current at desired levels such that the heat input determined by the total current (their sum) and penetration capability determined by the base metal current and heat input are accurately controlled. When CV power supplies are used, these two currents may be adjusted by their corresponding wire feed speeds in large ranges. The adjustments on the wire feed speeds affect the total mass input but it may be acceptable as long as the required minimal mass be deposited.

Fig. 2.11 shows a method which feedback controls the base metal current by adjusting the main wire feed speed such that the base metal current may be adjusted in a large range. This is needed because the base metal current not only contributes to the total heat input but also is the most critical parameter to control the penetration capability when the mass and heat input are in a certain range. The bypass voltage is feedback controlled using the CV mode bypass power supply which adjusts the bypass current. The bypass current is changed such that the heat input is changed. However, the adjustment range for the bypass current, thus the heat input, is relatively small because the bypass wire feed speed is not changed. For open arc (rather than submerged arc) consumable DE-GMAW, the stability of the bypass arc relies on its arc length. Hence, the control system provides an accurate control on the arc pressure, an accurate control on the bypass arc stability which is critical for consumable DE-GMAW especially when the bypass arc is open, and approximate controls on the mass and heat input.

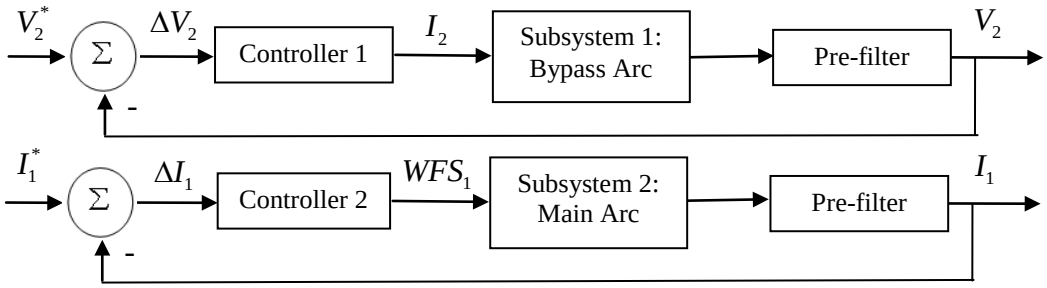

Fig. 2.11 A control for two CV power supply based consumable DE-GMAW system [23]

The design of the control system in Fig. 2.11 needs the process being controlled to be modeled. As in conventional GMAW, the main arc voltage V_1 is also automatically feedback controlled in the DE-GMAW process by the CV welder, and the location of the main wire tip is approximately fixed. The length of the bypass arc (l_2), i.e., the distance from the bypass wire tip to the main wire, is determined by the balance between the melting and feeding of the bypass wire:

$$\frac{dl_2}{dt} = (v_{m2} - WFS_2)sin\theta \tag{2.12}$$

where v_{m2} is the melting speed of the bypass wire; θ is the angle between the two wires; and sinθ projects the bypass wire (length) to the direction of the bypass arc. When the given wire feeding speed WFS_2 is balanced by the melting speed v_{m2}, $\frac{dl_2}{dt} = 0$.

The melting speed v_{m2} is determined by the bypass arc cathode power $IV_{cathode}$ and the resistive heating power rI_2^2, where r is the resistance of the wire extension carrying the bypass current I_2. The resistance r is proportional to the length of the wire extension (E_2). It has been proved [24, 25] that the melting speed of a wire in GMAW can be expressed as $k_1 I + k_2 E I^2$ where k_1 and k_2 are constants and E is the length of the wire extension. Hence, the melting speed for the bypass wire is

$$v_{m2} = a_1 I_2 + a_2 E_2 I_2^2 \tag{2.13}$$

where a_1 and a_2 are constants. When the welding arc is stable, the melting speed is equal to the wire feed speed:

$$WFS_2 = v_{m2} = a_1 I_2 + a_2 E_2 I_2^2 \tag{2.14}$$

If the bypass current (the control variable in subsystem 1) is changed to $I_2 + \Delta I_2$ from I_2, the equilibrium will be broken and the melting speed becomes

$$\begin{aligned} v_{m2} &= a_1(I_2 + \Delta I_2) + a_2(E_2 + \Delta E_2)(I_2 + \Delta I_2)^2 \\ &\cong (a_1 I_2 + a_2 E_2 I_2^2) + (a_1 + 2a_2 E_2 I_2)\Delta I_2 + a_2 I_2^2 \Delta E_2 \\ &= WFS_2 + (a_1 + 2a_2 E_2 I_2)\Delta I_2 + a_2 I_2^2 \Delta E_2 \end{aligned} \tag{2.15}$$

where high order deviations have been omitted. Thus, Eq. (2-12) can be written as

$$\frac{dl_2}{dt} = (a_1 + 2a_2 E_2 I_2)\Delta I_2 \sin\theta + a_2 I_2^2 \Delta E_2 \sin\theta \tag{2.16}$$

after the bypass current is changed. Because the arc voltage is a linear function of the arc length and $\Delta V_2 \propto -\Delta E_2 \sin\theta$ where ΔV_2 is the deviation of the bypass arc voltage from its previous value V_2 at the equilibrium, model (2-16) can thus give

$$\frac{d(V_2 + \Delta V_2)}{dt} = \frac{d\Delta V_2}{dt} = \lambda \frac{dl_2}{dt} = k\Delta I_2 - \alpha \Delta V_2 \tag{2.17}$$

where k, λ, and α are coefficients. Hence

$$\frac{d\Delta V_2}{dt} + \alpha \Delta V_2 = k\Delta I_2 \tag{2.18}$$

Subsystem 1 can thus be approximated as a first order model but the model parameters depend on the manufacturing condition parameters, such as E_2, I_2, θ, etc. as can be seen from Eq. (2-16). Using the control system, satisfactory welds have been made [23].

2.8 Variants of DE-GMAW and Double-electrode Arc Welding

A few variants have been proposed to extend the DE-GMAW concept or beyond the exact definition of DE-GMAW. The indirect arc method [26] has been independently

proposed and developed at Shandong University, which establishes an arc between two consumable rods without the work-piece to be a part of the arc, either anode or cathode, will not be discussed below. It reduces the heat input to a minimum and shares a certain similarity with DE-DMAW but lacks the mechanism to adjust the heat input as the DE-GMAW and its variants do.

2.8.1 Dual-Bypass GMAW

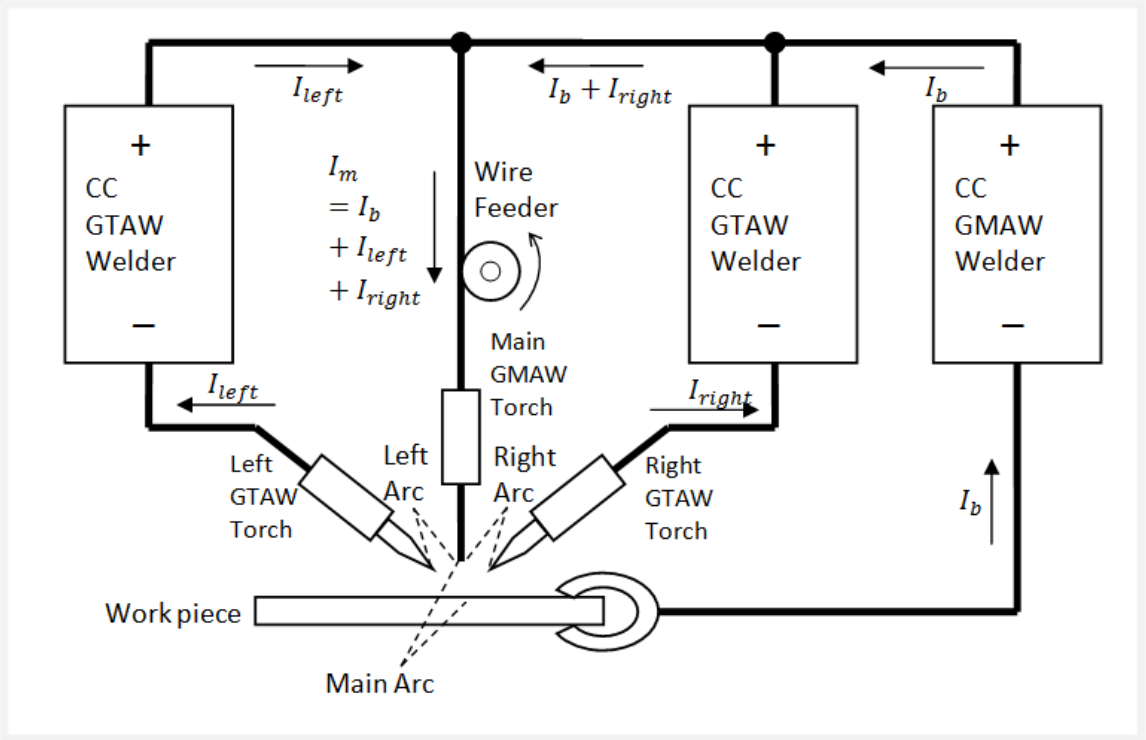

Fig. 2.12 Principle of DB-GMAW

Dual-bypass GMAW process (DB-GMAW) is a variant of DE-GMAW [27-30] which, as can be seen from Fig. 2.12, is established from a conventional GMAW system by adding two GTAW torches to provide two bypass loops for the melting current. The main loop is the path that the base metal current (I_b) flows through, and the two bypass loops are the

paths that the two bypass current (I_{right} and I_{left}) flow through. As illustrated in Fig. 2.12, the positive terminals of the three power supplies are connected together as a common positive terminal, and all of them are working in CC mode although CV may also be possible. The main torch is connected to the common positive terminal. The work-piece (or base metal) is connected with the negative terminal of the GMAW power supply. Each bypass GTAW torch is connected separately to the negative terminal of its corresponding GTAW power source. After the main arc is established between the tip of the electrode of the main GMAW torch and the surface of the work-piece, each bypass arc is established separately between the tip of the main electrode wire and the tip of its corresponding bypass electrode. The base metal current flows from the main electrode wire to the work-piece. The melting current for the main wire equals the sum of the base metal current and the two bypass currents:

$$I_m = I_b + I_{left} + I_{right} \tag{2.19}$$

where,

I_m is the total welding current;

I_b is the base metal current that flows through the work-piece;

I_{left} is the bypass current that flows through the left bypass torch;

I_{right} is the bypass current that flows through the right bypass torch.

Similar to DE-GMAW, DB-GMAW is also able to reduce the heat input of the welding process without reducing the deposition speed. As a result, the heat affected zone (HAZ) and the distortion of the work-piece can be reduced without affecting the productivity. Compared to DE-GMAW, more power supplies must be provided and the configuration of the system is more complicated to a certain extent.

For the metal transfer in DB-GMAW, the following has been found:

- The electromagnetic forces generated by the two bypass arcs (left and right) enhance the shrinking of the droplet neck and increase the anode area on the bottom of the droplet. The resultant influence of the neck shrinkage and the anode enlargement increase the detaching forces of the droplet.
- By changing the arc size and plasma flow speed, the bypass arcs increase the aerodynamic drag force of the droplet. As a result, the detachment of the droplet from the electrode wire is accelerated.

2.8.2 Arc Assisted Hot-Wire GTAW

In conventional gas tungsten arc welding (GTAW), the process often requires adding filler metals to produce desired welds. Currently, there are two primary approaches for filling the wire: cold wire GTAW and hot wire GTAW. In the cold wire GTAW process [31], the filler wire is added directly into the weld pool as is. In order to melt the wire faster, in the hot wire GTAW [32] as shown in Fig. 2.13, the filler wire is pre-heated by a resistive heat while it is being fed into the weld pool. This resistive heat is generated from a separate current (typically an alternating-current (AC)) supplied to the filler wire that flows from the wire directly into the weld pool. The current is properly adjusted so that ideally the temperature of the filler wire can reach its melting point as soon as it enters the weld pool.

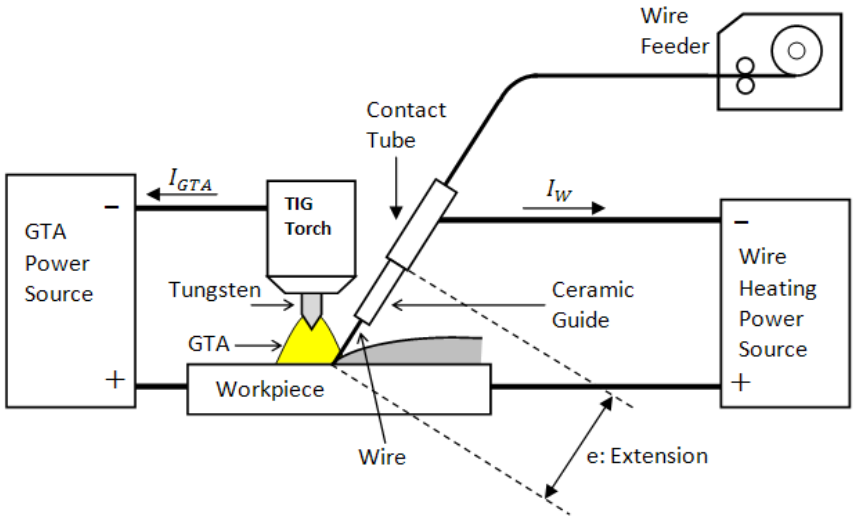

Fig. 2.13 Principles of hot wire GTAW system [33]

However, even if hot wire GTAW is applied, its deposition speed is still limited especially when the electric resistivity of the wire material is relatively low. To resolve this issue, researchers at the Harbin Institute of Technology invented an Arc Assisted Hot Wire GTAW system. In this system, a second arc is added to increase the pre-heat temperature of the wire using the system as shown in Fig. 2.14 [34, 35]. Although two arcs have been established on the surface of the filler wire in the arc assisted hot wire GTAW system, there is no arc between the two electrodes of GTAW torches. Therefore, the principle of the arc assisted hot wire GTAW is completely different from that of double-electrode based methods which are being discussed.

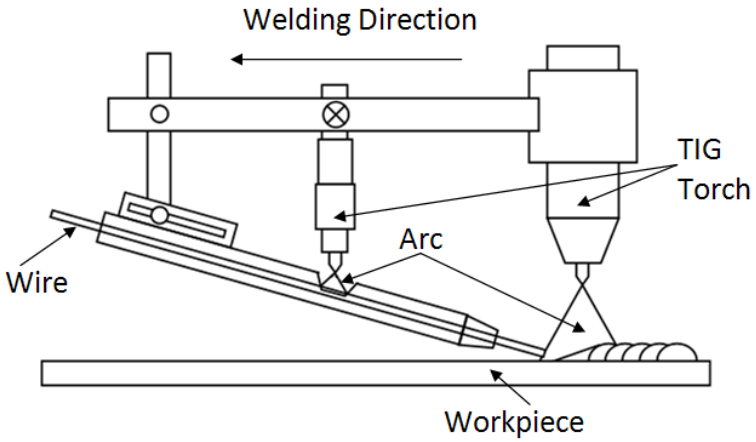

Fig. 2.14 Arc assisted hot-wire GTAW [35]

2.8.3 Arcing-Wire GTAW and Double-Electrode Arc Welding

To increase the deposition speed without increasing the weld puddle and freely control the penetration and mass input in GTAW, the arcing-wire GTAW [36] as shown in Fig. 2.15 has been developed at the Adaptive Intelligent Systems LLC [47] as a modification of GTAW by adding an arc (referred to as the side arc), established between the tungsten electrode and a filler, into the existing gas tungsten arc (GTA). It shares a similarity with the DE-GMAW in the sense that the current in the main electrode equals the base metal current and the current in an added electrode. However, the purpose is changed from melting the main electrode to melting the added electrode only and the main electrode is changed from consumable to non-consumable. For convenience, the authors propose the double-electrode arc welding (DE-AW) as a new category of arc welding processes which includes DE-GMAW, together with its variants, arcing-wire GTAW and other possible variants which use a main electrode to establish an arc with the work-piece and arcs with an added electrode or added electrode group.

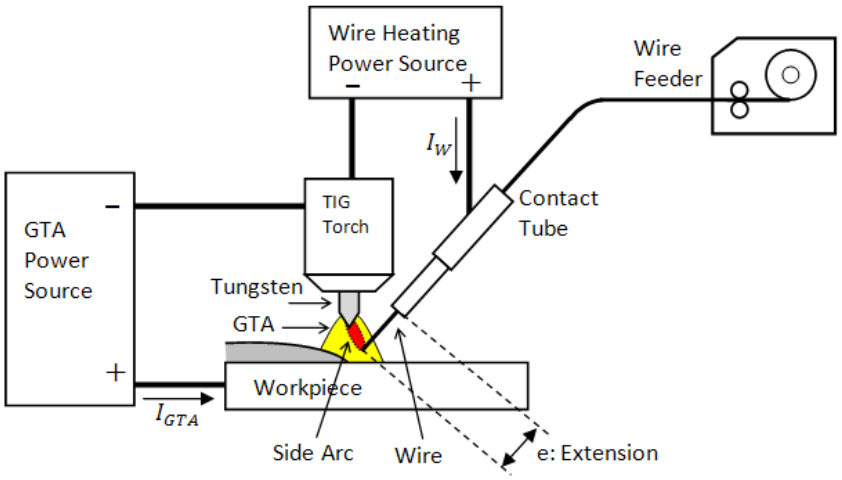

Fig. 2.15 Principle of arcing-wire GTAW [36]

As shown in Fig. 2.15, the arcing-wire GTAW system also needs two power sources. The GTA power supply is used to generate the GTA between the tungsten electrode and base metal; the wire heating power supply is used to generate the side arc between the tungsten electrode and filler wire. Because the negative terminals of the two power sources are connected together onto the tungsten electrode as a common point, a GTA current loop and wire heating current loop are both formed. The wire is melted not only by the resistance heat but also the side arc. The melting efficiency of the filler wire is thus much higher than that in the conventional hot wire GTAW especially for highly conductive filler such as copper and aluminum wires. Analysis suggests that the deposition speed achievable by and the wire melting mechanism for arcing-wire GTAW are similar with those for GMAW but the arcing-wire GTAW offers the arc controllability similar as conventional GTAW.

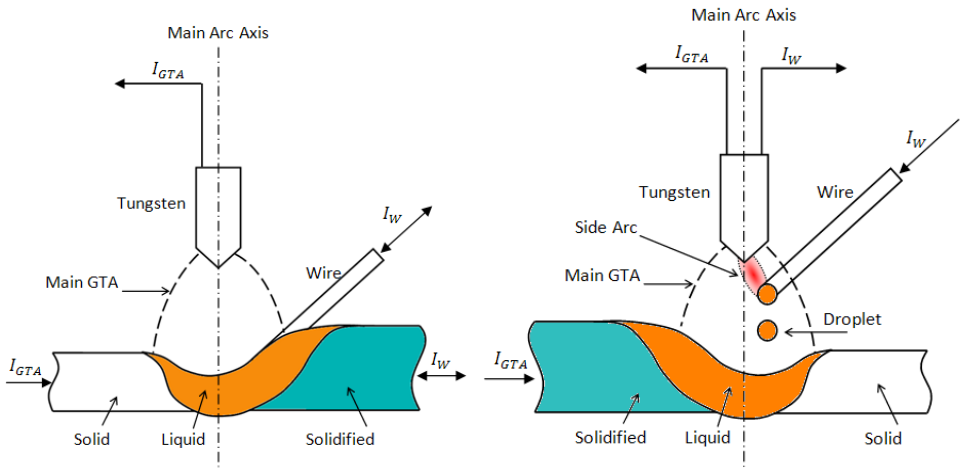

(a) (b)

Fig. 2.16 Comparison of hot wire GTAW with arcing-wire GTAW process
(a) Left: Arc and weld pool in hot wire GTAW;
(b) Right: Arcs and weld pool in arcing-wire GTAW

The primary difference between the hot-wire and arcing-wire GTAW lies in the melting mechanism for the filler wire. As can be seen in Fig. 2.16 (a), in the hot wire GTAW process, the filler wire is pre-heated at first by the resistance heat generated by the current flowing through the wire, and then melted within the weld pool by absorbing heat from the liquid metal in the weld pool. Similarly as in cold wire GTAW, the heat that finishes the melting of the filler wire is still the heat absorbed from the weld pool. There is thus no gap between the filler wire and the weld pool. However, in the arcing-wire GTAW process shown in Fig. 2.16 (b), the wire is actually completely melted by the side arc established between the tungsten and the wire before transferring into the weld pool. The wire can thus be melted similarly as in GMAW process at high speeds despite possible low resistivity of the wire. Further, this melting process does not depend on the weld puddle. The coupling between the deposition speed and arc energy is thus decoupled.

The Beijing University of Technology studied the metal transfer [37] on the arcing-wire GTAW and found that the metal melted from the filler may transfer into the weld pool in three modes: free transfer, touching transfer and bridging transfer. In free transfer, the metal detaches from the filler wire before it touches the weld pool. In touching transfer, the droplet of the melted metal starts to form with a gap to the weld pool surface and transfers into the weld pool after it touches the surface periodically. In bridging transfer, the wire enters the weld pool when it is still solid. The melting of the filler wire becomes similar as in the hot-wire GTAW with the resistive heat as the pre-heating source and the heat form liquid metal in the weld pool to finish the melting. The desirable free and touching transfer may be achieved from the given wire feed speed by adjusting the melting current and the wire position in relation to the tungsten appropriately [37].

Chapter 3 DE-SAW and Use of Root Opening

Similar to GMAW or any other consumable electrode arc welding, the electrode of submerged arc welding (SAW) process is also consumable. Therefore, it is natural and reasonable to transplant the Double-Electrode technology to the SAW process from the GMAW environment so that the good characteristics of DE-GMAW such as high deposition rate and low heat input can be borrowed from.

3.1 Submerged Arc Welding (SAW)

Submerged arc welding (SAW) is a widely used arc welding process. The American Welding Society (AWS) defines SAW as follows [38]:

> *"An arc welding process which produces coalescence of metals by heating them with an arc or arcs between a bare metal electrode or electrodes and the work. The arc and molten metal are shielded by a blanket of granular, fusible material on the work. Pressure is not used, and filler metal is obtained from the electrodes and sometimes from a supplemental source (welding rod, flux or metal granules)."*

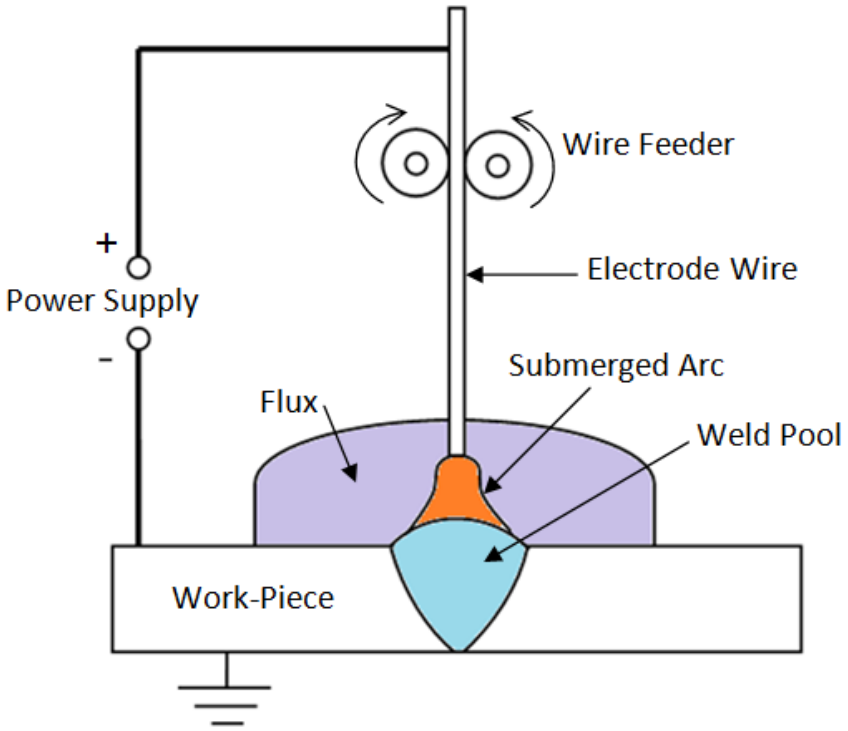

Fig. 3.1 General SAW Process

Fig. 3.1 illustrates a general simplified SAW process. Similarly as conventional gas metal arc welding (GMAW) [21, 39, 40] and flux-cored arc welding (FCAW) [41, 42], it melts a continuously fed consumable solid or flux cored electrode wire [38, 43, 44] to deposit metal into the work-piece. In SAW process, however, the consumable wire (electrode) and the arc zone are better shielded from atmospheric contamination because of being "submerged" under a blanket of granular, fusible flux [45]. SAW has many significant advantages [38, 44-46] over most open arc welding processes (e.g. GMAW, SMAW and FCAW) such as higher productivity, more stable arc, no spatters, and no harmful ultraviolet radiation. Since the losses from radiation, convection and spatter are minimal in SAW, the efficiency of energy transfer from the electrode source to the work-piece is very high; usually this transfer rate can be over 90% [47]. Moreover, the molten metal is

effectively protected by the fused flux, which together with the un-fused flux can be recovered again before the cooling process. SAW is thus the most commonly used process for down-hand mechanical welding in the shipbuilding industry, especially in joining plates for ship shells, decks, and bulkheads [48].

3.2 Double-Electrode SAW (DE-SAW)

Due to the requirement with regard to the weld size, a sufficient amount of metal must be melted. In conventional SAW, the heat input is proportional to the amount of metal melted and deposited in the process. As a result, the excessive heat can cause the unwanted distortions to the welded work-pieces whose follow-up straightening is highly costly. Now that both SAW and GMAW are using consumable electrode wires, then it is natural and reasonable to think about transplanting the Double-Electrode technology to the SAW process from the GMAW environment so that the good characteristics of DE-GMAW such as high deposition rate and low heat input can be borrowed. That is the how and why the DE-SAW is created.

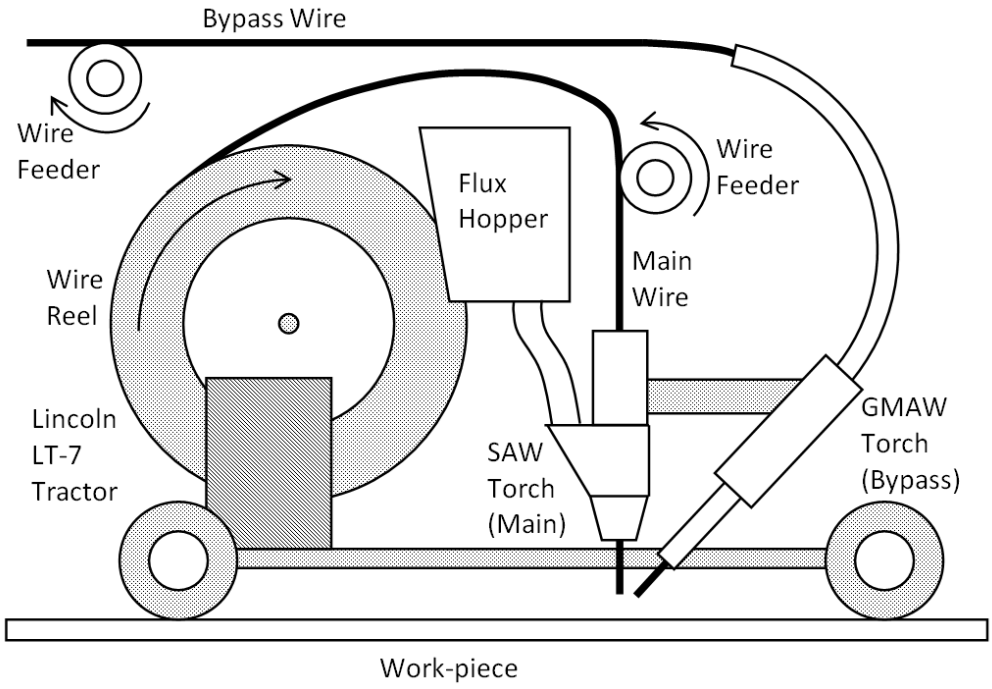

Fig. 3.2 Diagrammatic Sketch of DE-SAW Configuration

Fig. 3.2 shows the experimental platform of DE-SAW process. DE-SAW is established on a conventional SAW process by adding another GMAW torch next to the SAW torch of Lincoln LT-7 tractor [49] to provide a second/bypass loop for the welding current. The main wire feeder is combined with the tractor itself; the bypass wire needs an additional wire feeder. The relationship of the welding currents in DE-SAW can be explained clearly by Fig. 3.3.

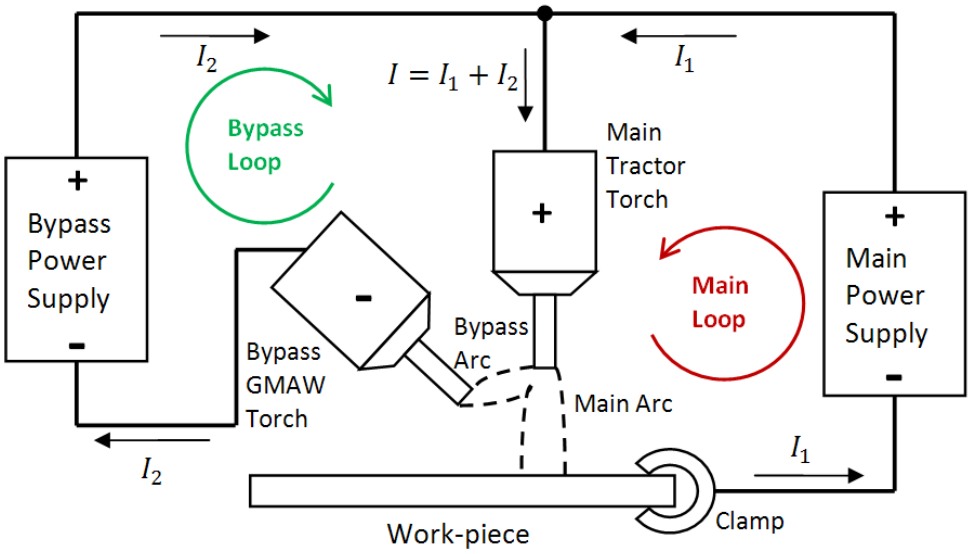

Fig. 3.3 Current Relationships in DE-SAW Process

As shown in Fig. 3.3, the main loop represents the path through which the base metal current (I_1) flows, and the bypass loop represents the path through which the bypass current (I_2) flows. The positive terminals of the two power supplies (both of them are working in CV or constant-voltage mode) are connected together as a common positive terminal. The main torch is connected to the common positive terminal. The work-piece (or base metal) is connected with the negative terminal of the main power supply. This kind of connection is based on the direct current positive polarity (DCEP) mode. Namely, the wire electrode is connected to the anode terminal of the direct current (DC) power supply, and the work-piece is connected to the cathode. For most of the applications, DCEP mode is used due to its benefits to the arc stability, metal transfer and deep penetration [50]. The bypass GMAW torch is connected to the negative terminal of the bypass power supply. In DE-SAW, there are two cathodes: one is the base metal, and the other is the bypass wire electrode, which forms the bypass arc with the main wire [18]. After the power supplies are turned on, the main arc is established between the tip of the

electrode of the main torch and the surface of the work-piece, and the bypass arc is established between the tip of the main electrode and the tip of the bypass electrode.

Similar to the consumable DE-GMAW process, the base metal current (I_1) flows from the main electrode to the work-piece; the bypass current (I_2) flows from the main electrode to the bypass electrode. Because both the base metal current and the bypass current flow through the main wire electrode, the current inside the electrode of the main SAW torch equals the total welding current (I). This fundamental current relationship can be expressed by Equation (3-1). This relationship represents the essence of Double-Electrode technology and DE-SAW as well.

$$I = I_1 + I_2 \tag{3.1}$$

Where,

I is the total welding current;

I_1 is the base metal current that flows through the work-piece;

I_2 is the bypass current that flows through the bypass wire.

Since part of the total welding current is bypassed without flowing into the work-piece, the heat input into the work-piece is reduced. When the metal from the bypass wire melted by the bypass arc is added into the work-piece, the reduced heat input is added back but the metal deposition is increased. DE-SAW is thus capable of depositing the same amount of metal at reduced heat input or depositing more metal at the same heat input.

3.3 Fillet DE-SAW and Use of Root Opening

Fillet welding, as shown in Fig. 3.4, is a type of joint used for welding pieces of plates in which the angle between them (between the tee and the panel) varies from zero to 180 degrees [51]. SAW for fillet joints is one of the major applications in modern shipbuilding industry. A great number of complicated internal structures inside the hulls of ships have to rely on the fillet welding of SAW. In a typical 150,000 DWT (Deadweight Tonnage) tanker, the length of the horizontal fillet welding (a kind of down-hand welding) can reach more than 70% of the whole welding length of the bottom shell block at the assembly stage [52].

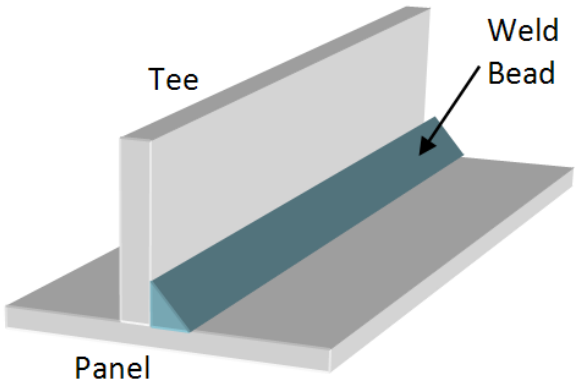

Fig. 3.4 Example of Fillet Joint

Similar to other SAW process, a sufficient amount of metal must be melted due to the requirement for the weld size. In conventional SAW, the heat input is proportional to the amount of metal melted and deposited in the process. As a result, any excessive heat used may cause unwanted distortions to the welded work-pieces whose follow-up straightening is highly costly. In solving these problems in SAW for fillet joints, it is the key to find an effective way that can deposit the same amount of metal at reduced heat

input and at the same time allow the reduced heat input to produce welds meeting other requirements in addition to the weld size. DE-SAW is apparently a promising candidate for reducing the heat input, and that is how Double-Electrode combines with fillet SAW process.

However, after having the heat input reduced greatly in the fillet joints by using the DE-SAW process, the penetration capability is also reduced due to the reduction in the base metal current. The weld beads produced become convex causing the re-entrant angle (see Fig. 3.6) reduced undesirably as shown in Fig. 3.5. Decreasing the penetration capability required for producing desirable welds is thus an issue that needs to be resolved in order to effectively utilize the ability of DE-SAW in reducing the heat input to produce desirable fillet weld beads.

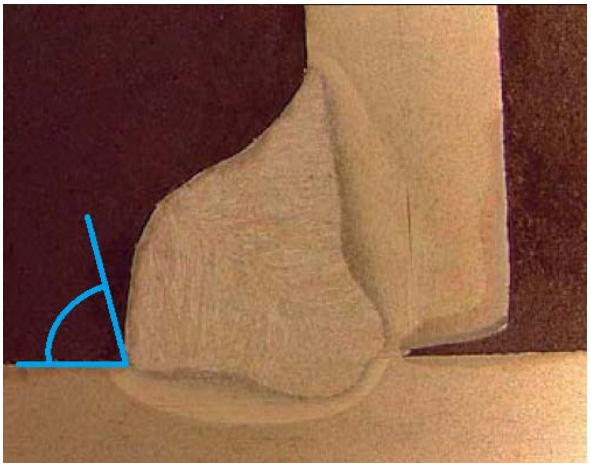

Fig. 3.5 Sharp Re-entrant Angle (Show with Blue Line) Caused by Low Penetration

In order to lower the needed penetration capability for producing desirable welds while guaranteeing the heat input at a low level at the same time, a root opening between the tee

and the panel has been introduced intentionally forming a modified fillet joint as shown in Fig. 3.6.

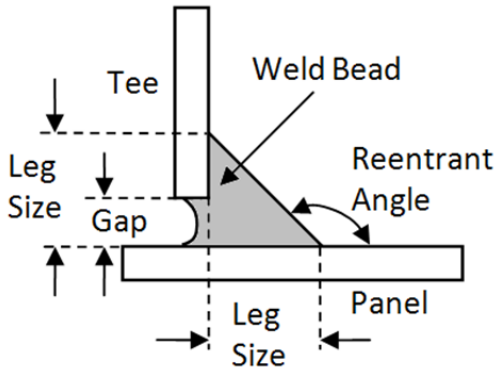

Fig. 3.6 Use of Root Opening between Tee and Panel

3.4 Necessity of Effective Control in DE-SAW for Fillet Joints

Although the fillet welding of DE-SAW with a root opening introduced above provides a potential way to adjust and reduce the ratio of heat input to metal deposition, there are still some challenges before applying it to the practice directly.

At first, the existence of a root opening between the tee and the panel introduces certain complexities to fillet DE-SAW as shown in Fig. 3.7.

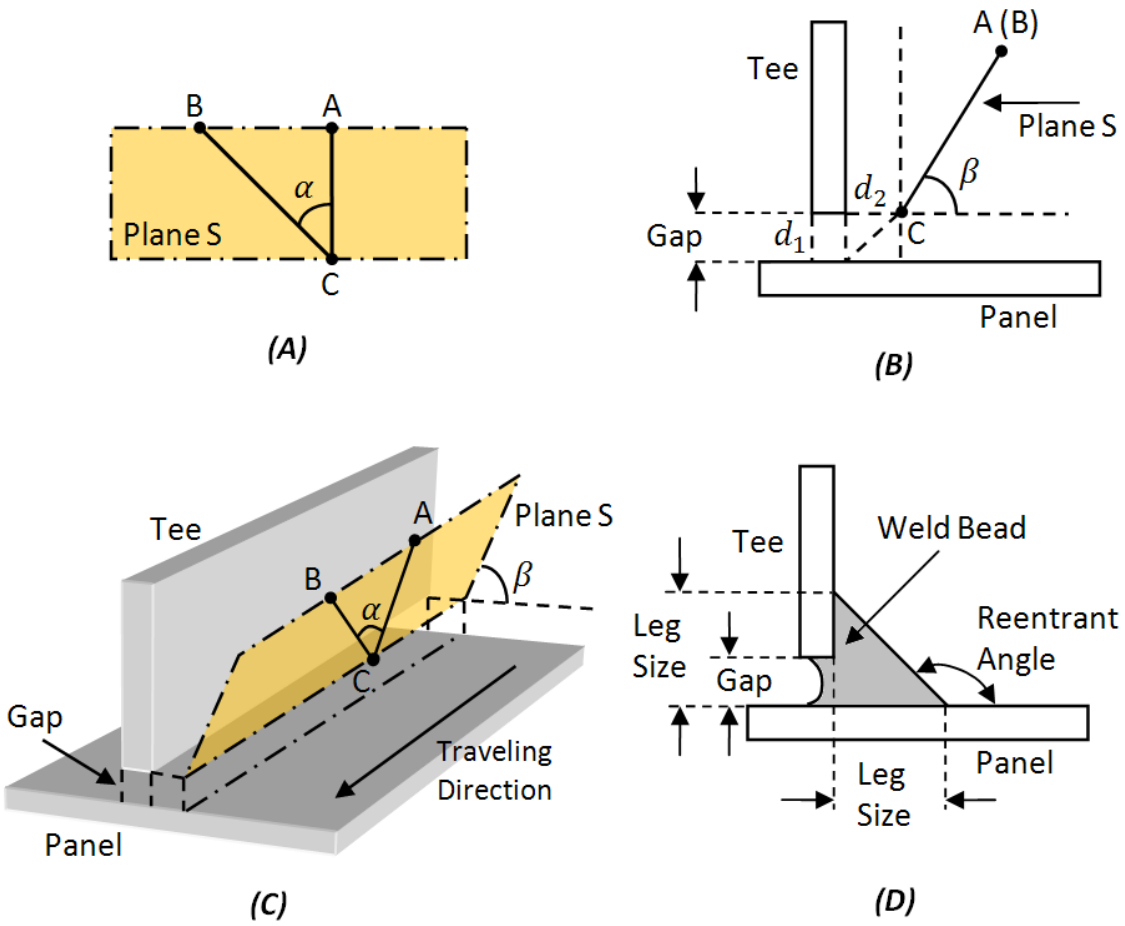

Fig. 3.7 Relative Positions of Wires and Work-Pieces in DE-SAW for Fillet Joints

In Part (A) of Fig. 3.7, the line segment $\overline{AC}$ represents the extension (stick-out) of the main wire electrode; the line segment $\overline{BC}$ stands for the extension of the bypass wire electrode. The main wire and the bypass wire (or their extensions) intersect at point C. ∠α represents the angle between the two wires. Generally, ∠α should be around 45° based on the previous experience. The plane in which the two wires are located is called plane S.

Part (B) of Fig. 3.7 displays the cross-section of the fillet welding of DE-SAW. Because viewed with 90° difference, plane S, shown in Part (A), becomes a line segment in Part

(B), and point A and B overlap into one point. From this view, a gap or root opening, d_1, between the tee and the panel plate can be seen. For fillet joints, previous experiments had been done without a root opening between the panel and tee. It was found that reducing the heat input and base metal current significantly causes the weld bead to be convex because of the reduced penetration capability determined by the base metal current, and a large convexity may produce unacceptable weld beads (The reentrant angle as shown in Fig. 3.7 (D) is less than 90°). Further reduction in heat input and distortion is thus limited. Hence, a key to effectively using the DE-SAW process to reduce the heat input and distortion is to reduce the needed heat input and penetration capability. Analysis suggests that this reduction may be achieved by redesigning the fillet joints with a certain root opening. Feedback from shipyards confirmed that the root opening between the panel and tee can be up to 3/16" and it is not uncommon to have a root opening around 1/16". Hence, a joint design with a root opening has been proposed as shown in Part (B). In this paper, a 1.5 mm root opening was tested. The point of intersection (Point C) of the two wires is equidistant from the tee and the panel. In this paper, these two distances are also equal to 1.5 mm. The angle $\angle\beta$ represents the angle between plane S and the surface of the panel. Because of gravity, the melted metal will flow downwards. In order to make sure both of the leg sizes (see Fig. 3.7 (D)) of the weld bead are equal, the angle $\angle\beta$ should be greater than 45°. In this paper, the angle $\angle\beta$ was tested on 60° approximately.

In Part (C) of Fig. 3.7, the process of DE-SAW for fillet joints is shown three-dimensionally. Along the traveling direction pointed by the arrow, both the main wire

and the bypass wire are moving together on the plane S. The bypass wire is ahead of the main wire along the traveling direction. During the entire welding process, the main wire (line segment $\overline{AC}$) is vertical to the traveling direction; the relative position of main wire and bypass wire does not change; and the point of intersection (Point C) of the two wires is equidistant from the tee and the panel at any time.

By following the standards and rules demonstrated by Part (A), (B) and (C) in Fig. 3.7, the expected shape of the weld bead is shown in Part (D) of Fig. 3.7. The two leg sizes, the re-entrant angle and the flatness of the weld bead are the main concern for the quality. In reality, the ratio of the root opening size to the leg size should be much smaller than the illustration sketch.

However, Fig. 3.7 just shows an extremely ideal case, and maintaining such an ideal case is not easy. First of all, in fillet welding of DE-SAW, there are two wires (main wire and bypass wire) melting simultaneously. Accordingly, the distance between the tips of the two electrodes and the distances between the electrodes to the work-pieces (d_1 and d_2 in Part (B) of Fig. 3.7) will keep changing from time to time. Meanwhile, the electric arc is not as stable as that in the single wire (conventional) SAW. Secondly, owing to the presence of the bypass arc, the process becomes a coupled two-input-two-output multivariable system which cannot be approximated simply through decoupling. It means the base metal current (I_1) will be determined not only by the main wire speed (W_1), but also by the bypass wire speed (W_2). As a result, those decoupling based algorithms about Double-Electrode processes in previous researches cannot be used [23, 53] here. Last but

not least, the control concerning the SAW for fillet joints which is different from that in butt joint or bead-on-plate has not been previously studied. Moreover, in order to decrease the required heat input in the fillet joint process itself, a root opening between the tee and the panel has been introduced. Because of this root opening, the arcing condition becomes more sensitive to the relative positions among the tee, the panel and the wires. All above variations affect the melting of the wires such that given wire feed speeds may not achieve the desired total and base metal currents. Because the heat input is determined by the total current and the penetration capability is determined by the base metal current [25], a feedback control may be used to control the total current ($I_1 + I_2$) and the base metal current (I_1). This equals a feedback of I_1 and I_2. Hence, overcoming the variations aforementioned is converted into a feedback control problem in which the main and bypass wire feed speeds are adjusted to maintain I_1 and I_2 at desired levels despite possible variations. To this end, an effective multivariable predictive control system based on an accurate model of the physical process which cannot be approximated via decoupling should be designed and applied.

Chapter 4 Parameters Selection

In chapter 2 and 3, it has been discussed that after having the heat input reduced greatly in the fillet joints by using DE-SAW, the penetration capability is also reduced due to the reduction in the base metal current. That is why the root opening between the tee and the panel of the fillet joint has to be introduced. However, the appearance of the root opening brings much more complications to the process stability. Therefore, the process control is necessary, and the root opening size as well as some important welding parameters which cannot be controlled with the algorithm must be selected and optimized carefully.

In this chapter, the root opening size and the travel speed of the tractor are selected and optimized in that they cannot be changed during the welding process by using any control algorithm, so that a complete solution for the DE-SAW, i.e. the fillet DE-SAW with a root opening, can be provided before applying any advanced control algorithm to improve the system stability.

Meanwhile, the proper heat input or actually main wire feed speed should be selected based on the principle of minimizing the heat input and guaranteeing the welding quality simultaneously. The appropriate main wire feed speed confirmed in this chapter will be used in chapter 7 as the initial main wire feed speed when the advanced control algorithm is being applied.

4.1 Experimental Conditions

The experimental conditions here refer primarily to the materials of the wire electrodes, the materials of the steel plates used for the tees as well as the panels, and the model number of the flux powder. The specifications of experimental conditions are listed in Table 4.1. All the experiments in this chapter were conducted under these conditions.

Table 4.1 Experimental Conditions

	Model Number	Size
Tee Plate	C1018 Cold Rolled Steel Plate	Thickness: 3/16 inch (4.763 mm) Width: 1 inch (25.4 mm)
Panel Plate	C1018 Cold Rolled Steel Plate	Thickness: 3/16 inch (4.763 mm) Width: 4 inch (101.6 mm)
Main Wire	Lincoln Weld L-61	Diameter: 3/32 inch (2.381 mm)
Bypass Wire	Kobelco MG-51T	Diameter: 0.045 inch (1.14 mm)
Flux Powder	Lincoln Weld 882	N/A

4.2 Root Opening Effect and Selection

With the purpose of illustrating the effect of the root opening, different root opening sizes have been tested in this section: “No Root Opening”, “Small Root Opening”, and “Large Root Opening”. In order to decouple from the effect of the mass, all the experiments are conducted using open-loop controls, i.e., using constant wire feed speeds without feedback control, that would adjust the wire feed speeds such that the mass would change also. Because the major concern is if the root opening may reduce the convexity/increase the reentrant angle, analysis will first be done in this section qualitatively without exact readings/measurements of the reentrant angles or leg sizes.

4.2.1 “No Root Opening” Experiment

In the “No Root Opening” experiment, the fillet joint is prepared without an intentional root opening. This experiment serves as a reference to illustrate the effect of the root opening in later experiments with root openings. The welding parameters used in the “No Root Opening” as well as the following experiments with root openings in this section are listed in Table 4.2. Due to 1.5 mm is the minimal thickness of the washer used to create the root opening between the tee and the panel, this thickness (1.5 mm) has been used as the increment unit in the root opening effect experiments.

Table 4.2 Welding Parameters for Root Opening Experiments

	Value	Unit
Main Wire Speed (W1)	90 (288.6)	IPM (cm/min)
Bypass Wire Speed (W2)	300 (762)	IPM (cm/min)
Travel Speed (v)	50 (127)	IPM (cm/min)
Main Voltage (V1)	28	Volt
Bypass Voltage (V2)	28	Volt
Root Opening between Tee & Panel	0, 1.5, 3	mm

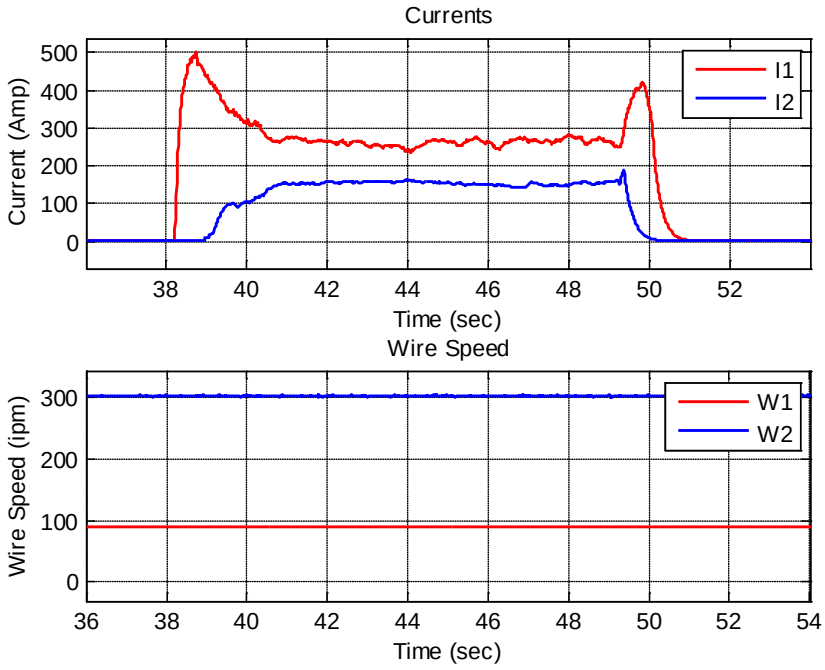

Fig. 4.1 Currents and Wire Speeds Plot in No-Root Opening Experiment

Fig. 4.1 shows the welding currents and wire feed speeds recorded from the data-acquisition (DAQ) system. In the legend of the plots, I_1 and I_2 represent the base metal and bypass currents and W_1 and W_2 stand for the main and bypass wire feed speeds hereafter. As can be seen from the experimental data, after the process reaches its steady-state, the average base metal current is 262 Amp approximately; the average bypass current is around 154 Amp. Hence, the average total welding current within the steady-state period is 416 Amp. Because the panel and tee plates are relatively straight, the welding process is relatively stable although there is no feedback control used.

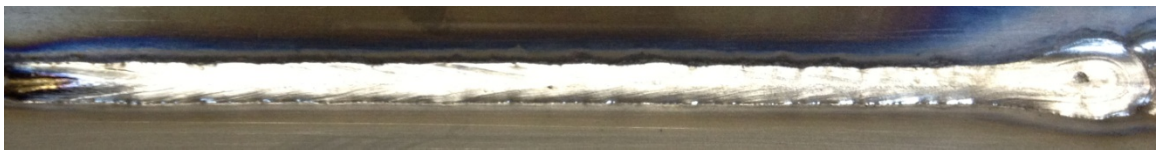

Fig. 4.2 Weld Bead in No-Root Opening Experiment (Direction: Right to Left)

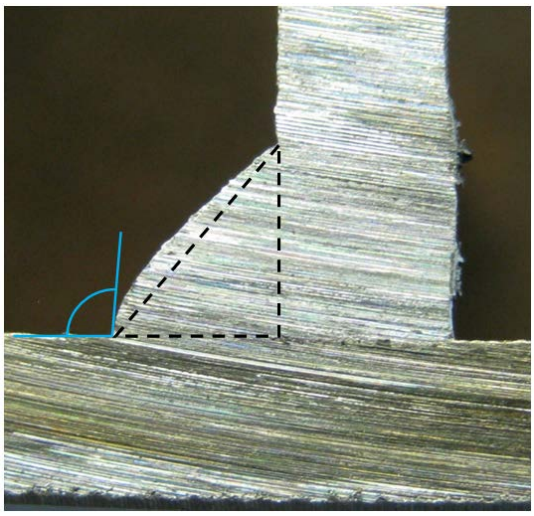

Fig. 4.3 A Cross Section of Weld Bead in No-Root Opening Experiment

Fig. 4.2 shows the photo of the weld bead in the “No Root Opening” experiment; Fig. 4.3 shows a typical cross section of the welded joint. It can be seen that the weld bead is convex (shown with the dashed lines in Fig. 4.3). Also, the reentrant angle (shown with the blue lines in Fig. 4.3) is already close to 90°.

4.2.2 “Small Root Opening” Experiment

In section 4.2.2, a 1.5 mm root opening is tested. Except for the root opening, all other conditions and parameters are unchanged from the “No Root Opening” experiment (shown in Table 4.1 and Table 4.2).

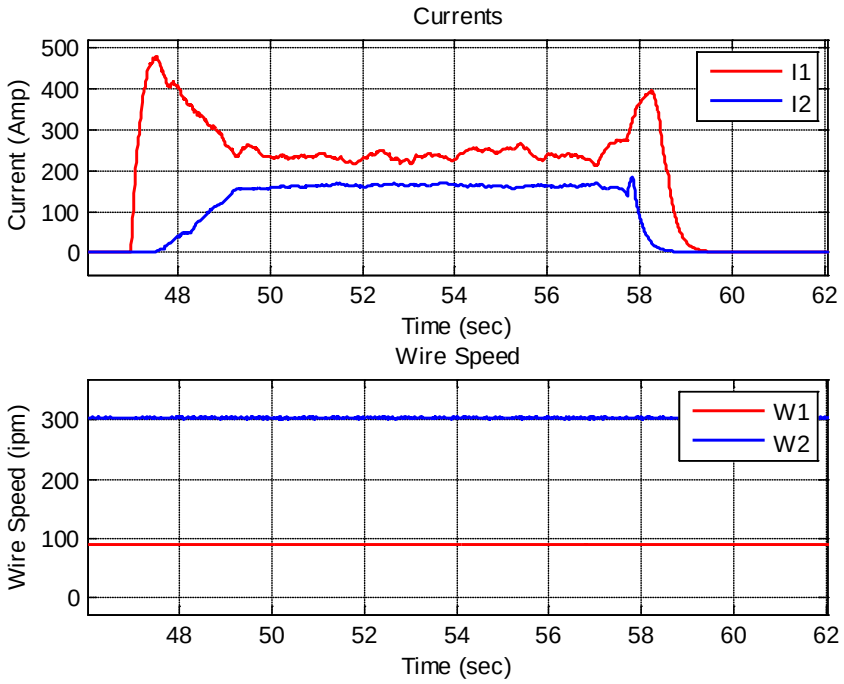

Fig. 4.4 Currents and Wire speeds Plot in "Small-Root Opening" Experiment

As can be seen from the recorded experimental data shown in Fig. 4.4, after reaching the steady-state, the average base metal current is 238 Amp approximately; the bypass current is around 164 Amp. Hence, the total welding current in steady-state period is 402 Amp. The welding process is relatively stable with only insignificant fluctuations within acceptable ranges.

Due to the existence of the root opening between tee and panel, the relative position among the electrodes and the work-pieces are different from that in "No Root Opening" experiments. As a result, the values of welding currents in the experiment with a root opening are not exactly the same as those in "No Root Opening" condition although the wire feed speeds and the welding voltages are the same.

Fig. 4.5 Weld Bead in “Small-Root opening” Experiment (Direction: Right to Left)

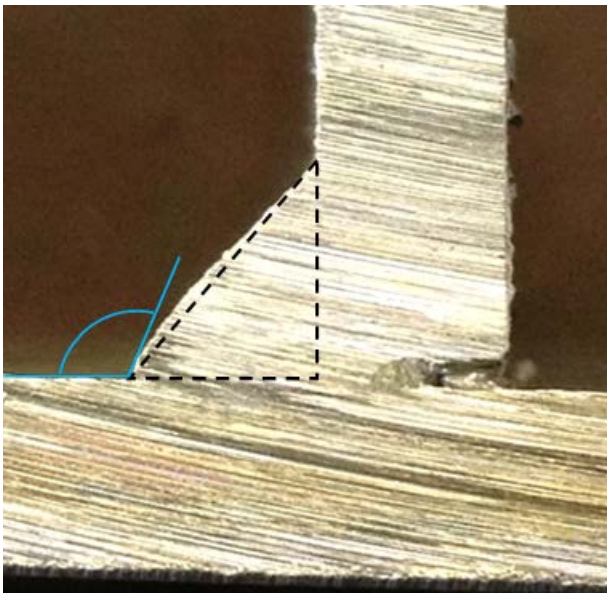

Fig. 4.6 A Cross Section of Weld Bead in “Small-Root opening” Experiment

As can be seen from the photo of the weld bead (Fig. 4.5) and a typical cross section of the weld bead (Fig. 4.6), the convexity on the weld bead (shown with the dashed lines in Fig. 4.6) has been reduced by 50% approximately after the introduction of the root opening despite the reduction in the actual heat input (total current). At the same time, the reentrant angle (shown with the blue lines in Fig. 4.6) has also been increased accordingly. The effect of the root opening on the convexity and reentrant angle is clearly demonstrated.

4.2.3 “Large Root opening” Experiment

In section 4.2.3, the root opening is further increased to 3 mm while other parameters and conditions are unchanged.

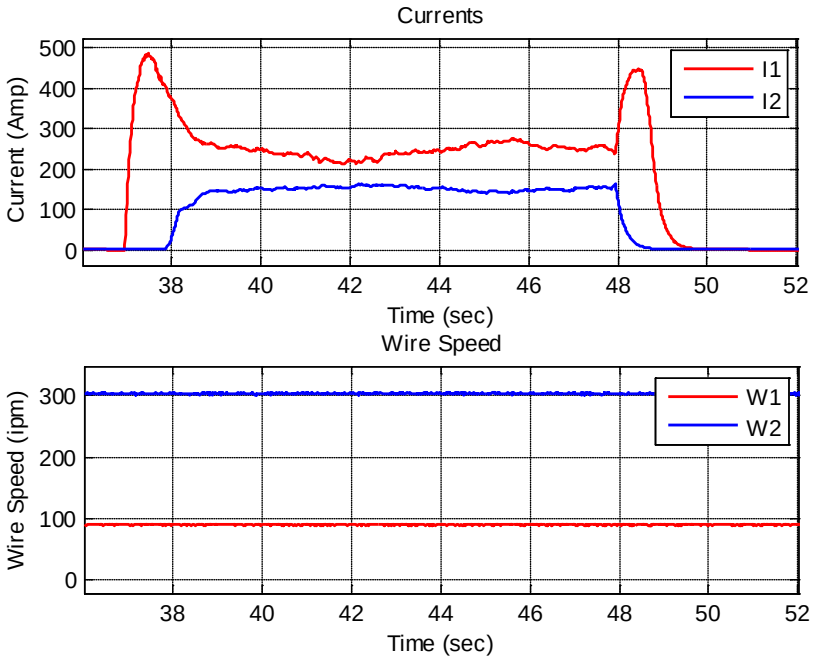

Fig. 4.7 Currents and Wire Speeds Plot in “Large-Root opening” Experiment

As can be seen from Fig. 4.7, after reaching the steady-state, the average base metal current is 244 Amp approximately; the bypass current is around 152 Amp. Hence, the total welding current within the steady-state period is 396 Amp. The welding currents drifted more significantly than those in “No Root opening” and “Small Root opening” experiments. The weld appears to be wider in the second half of the weld where the base metal current is greater (Fig. 4.8).

Fig. 4.8 Weld Bead in “Large-Root opening” Experiment (Direction: Right to Left)

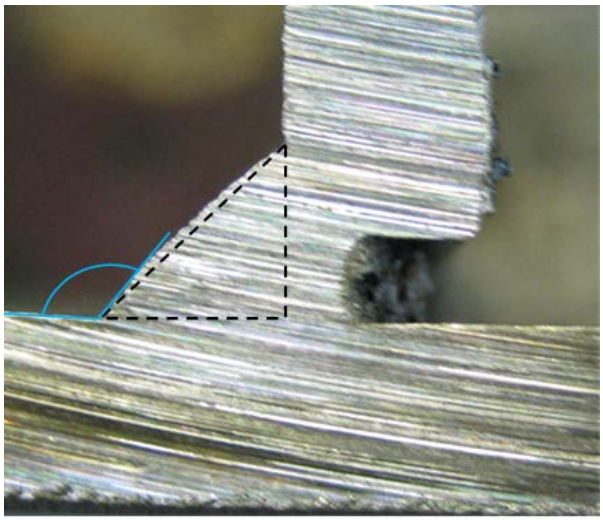

Fig. 4.9 A Cross Section of Weld Bead in “Large-Root opening” Experiment

As can be seen, the convexity on the weld bead (shown with the dashed lines in Fig. 4.9) in the “Large Root opening” experiment has also been reduced greatly than that in the “No Root opening” experiment. However, the difference with that in “Small Root opening” is not significant. The reentrant angle in the “Large Root opening” becomes greater.

4.2.4 Remarks on Root Opening Effect

Results in the three “Root opening” experiments clearly demonstrate the effectiveness of root opening in reducing the convexity and increasing the reentrant angle for desirable weld bead geometry. The penetration capability required to produce desirable weld bead

is thus reduced by the root opening. To determine which root opening is more appropriate (1.5 mm or 3.0 mm), it has been noted that the vertical leg size of the weld bead in the "Large Root opening" experiment is 6 mm approximately. However, the largest root opening allowed in production is 3/16" (4.76 mm) and for every 1/16" (1.59 mm) root opening (over 1/16"), the weld size must be increased by 1/16" accordingly. For example, if ¼" weld is needed and there is a 1/8" root opening between the tee and the panel, then the required leg size will become into 5/16". (Root opening 1/8" less the permitted initial 1/16" equals to 1/16", this 1/16" is added to the ¼" size required, resulting in 5/16"). As a result, the required leg size will become 1/4" (6.35 mm) for the 3/16" work-piece thickness if 3 mm root opening is used. Consequently, the heat input will be increased due to the increase in the required mass. On the other hand, for the "Small Root opening" (1.5 mm, smaller than the permitted 1/16"), the leg size can still be equal to the thickness of the plate (3/16"). Hence, the small root opening, namely 1.5 mm, is a more appropriate root opening size. Meanwhile, the drifts on the welding currents after introducing the root opening between the tee and the panel further illustrate the necessity of the feedback control to the currents in the fillet DE-SAW process.

4.3 Travel Speed Optimization

Once the root opening is selected such that the modified joint design is given, the travel speed of the tractor and the wire feed speeds can be optimized. Such optimization will be conducted using quantitative analysis in addition to qualitative comparison/analysis method used for the root opening study in section 4.2. Before the optimization is performed, the methods for quantitative analysis need to be specified first.

4.3.1 Analysis Method

The leg sizes (vertical and horizontal) will be measured for each of the weld beads as shown in Fig. 4.10. Specifically, for any weld bead, in order to assure the accuracy of the measurement, the beginning adjustment section for arc-establishing period (2 inch long approximately) and the ending section (1 inch long approximately) for turning off the contactors of the two power supplies individually are skipped from being measured. Then, along the welding direction, the full length of the rest weld in the steady section will be divided into N short sections with a 10 mm interval except for the last section left that may not be exactly 10 mm long. Within each of these short sections (section i for example), one maximum leg size (max_i) and one minimum leg size (min_i) can be measured using a Vernier caliper on both the horizontal (on the panel) and the vertical (on the tee) directions. In this way, a series of Max-Min pairs can be obtained for each weld bead.

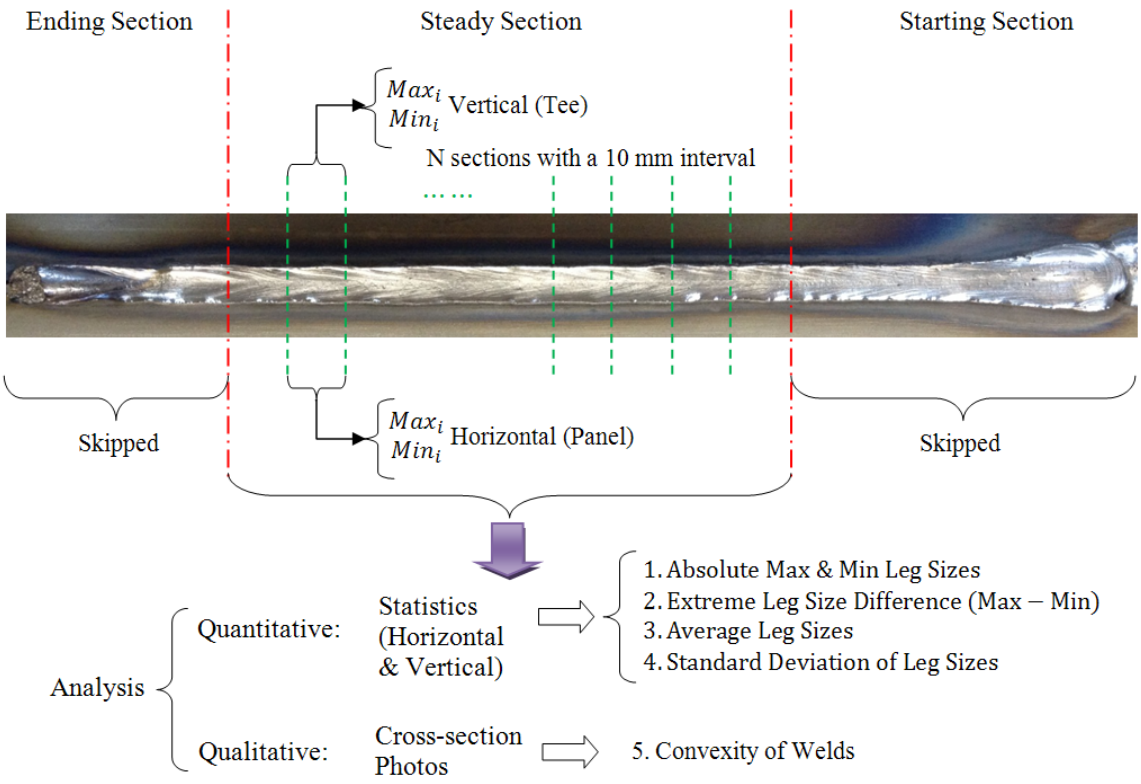

Fig. 4.10 Measurement and Analysis Approach

After obtaining the raw data pairs as specified above, analyses for travel speed optimization and heat input minimization can be conducted quantitatively. To this end, four major performance indices can be calculated as shown in Fig. 4.10. The specific calculations are as follows using one weld bead as example:

First, after comparing the Max-Min pairs, two extreme values - the absolute maximum and minimum leg sizes - can be found for both horizontal and vertical directions respectively. Then, the difference between these two extreme values gives the extreme difference of the leg size. Third, within the steady section, the average leg sizes can be calculated by Equation (4-1).

$$\bar{x} = \frac{1}{N}\sum_{i=1}^{N}\left(\frac{max_i + min_i}{2}\right) \quad (4.1)$$

Here, $\bar{x}$ represents either the horizontal or the vertical average leg size. The horizontal and vertical average leg sizes can give the average leg size that averages the leg sizes in two directions together. At last, the standard deviation of the leg sizes can be calculated by Equation (4-2).

$$\sigma = \sqrt{\frac{1}{N}\sum_{i=1}^{N}(x_i - \bar{x})^2} \quad (4.2)$$

where, $x_i = \begin{cases} \max_i & \text{abs}(\max_i - \bar{x}) > abs(\min_i - \bar{x}) \\ \min_i & \text{abs}(\max_i - \bar{x}) \leq \text{abs}(\min_i - \bar{x}) \end{cases}$

In the same way, these four quantitative performance indices will be obtained on the horizontal and vertical directions individually for all weld beads. By plotting these four indices, the resultant plots will show the changing tendency of the statistical data, and thereby quantitatively illustrate the influence of the parameters being studied.

The quantitative analysis will be conducted together with the qualitative analysis. In particular, by comparing and contrasting the cross-sections photos of the weld beads, the changes of the convexity with the parameter being examined will be demonstrated clearly. This qualitative analysis can provide a useful complimentary to the quantitative statistical analysis. By summarizing the indices and convexity of the welds, the parameter value that maximizes the leg sizes and minimizes the deviation of the leg sizes with acceptable convexity is selected as the optimal value for this parameter.

4.3.2 Experiment Design and Study Approaches

In section 4.3.2, a series of experiments have been conducted using different travel speeds. In particular, the travel speed is increased progressively at the 5 IPM increment within the attainable range from 30 IPM to 60 IPM. The wire feed speeds (main wire and bypass wire) are adjusted proportionally with the travel speed, as shown in Table 4.3, to maintain the linear deposition speed (mass deposition) unchanged. The "Incremental Ratio" in Table 4.3 represents the ratio of the travel speed relative to the lowest travel speed in the series of experiments, and certainly also the ratio of the wire feed speed to the lowest wire feed speed.

Table 4.3 Experimental Conditions for Travel Speed Study Experiments

	Travel Speed IPM (cm/min)	Incremental Ratio	Main Wire Speed IPM (cm/min)	Bypass Wire Speed IPM (cm/min)
Exp 5.1	30 (76.2)	1.0	60 (152.4)	150 (381)
Exp 5.2	35 (88.9)	1.17	70 (177.8)	175 (444.5)
Exp 5.3	40 (101.6)	1.33	80 (203.2)	200 (508)
Exp 5.4	45 (114.3)	1.5	90 (228.6)	225 (571.5)
Exp 5.5	50 (127)	1.67	100 (254)	250 (635)
Exp 5.6	55 (139.7)	1.83	110 (279.4)	275 (698.5)
Exp 5.7	60 (152.4)	2.0	120 (304.8)	300 (762)

4.3.3 Experimental Results and Analysis

Seven experiments, under the same basic conditions (Table 4.1) as designed and unchanged linear deposition speed, have been conducted following the sequence listed in Table 4.3. Fig. 4.11 shows the plots of the welding currents and wire feed speeds recorded from the data-acquisition system.

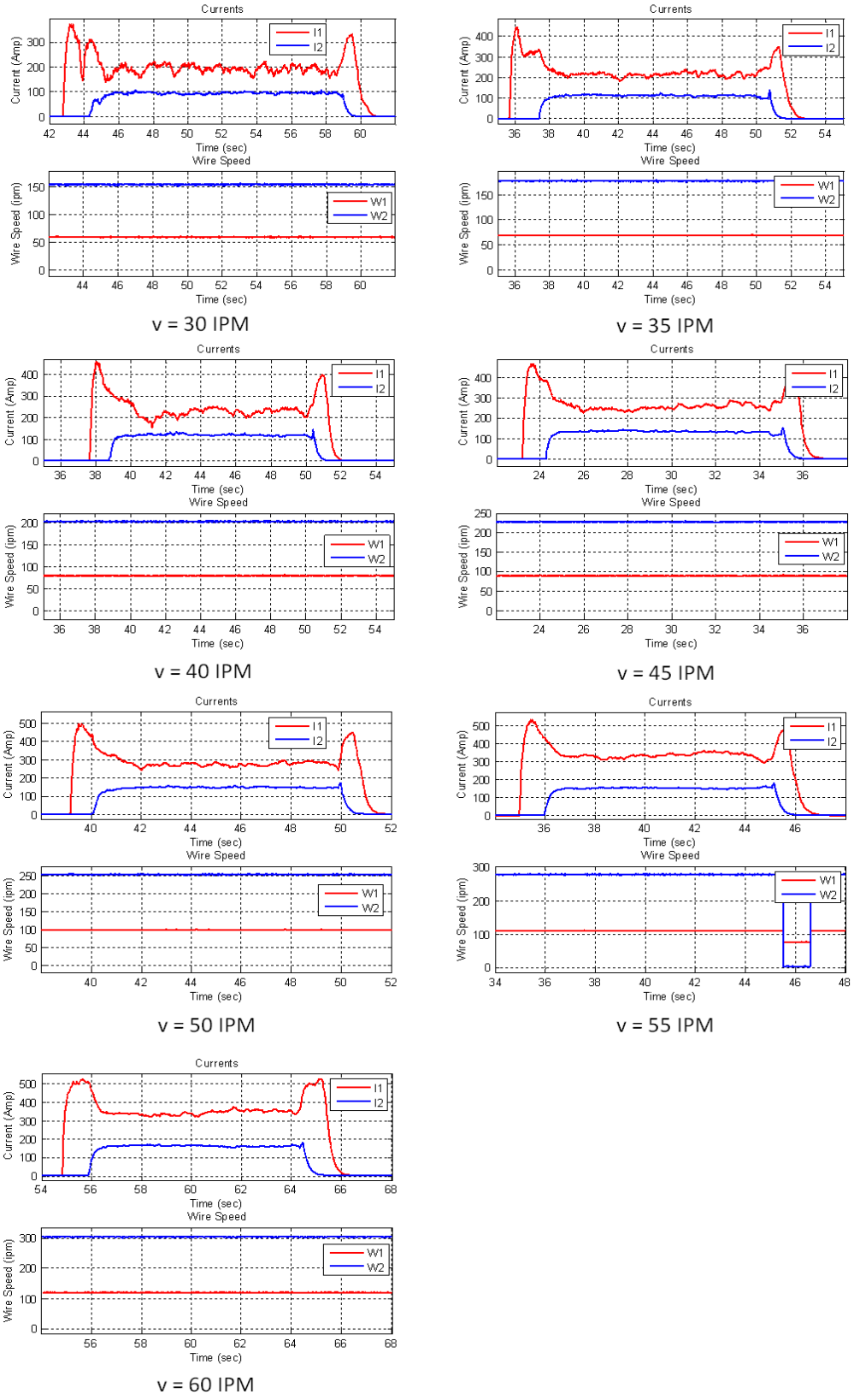

Fig. 4.11 Currents and Wire Speeds in Travel Speed Study Experiments

As shown in Fig. 4.11, the welding currents are relatively stable after the establishment of the bypass arcs. Careful observation to Fig. 4.11 shows that the fluctuation on the base metal currents are relatively strong when the travel speed equals 30 IPM, 35 IPM and 40 IPM (the first three plots in Fig. 4.11); when the travel speed, however, is equal to and greater than 45 IPM, then the base metal current becomes much smoother.

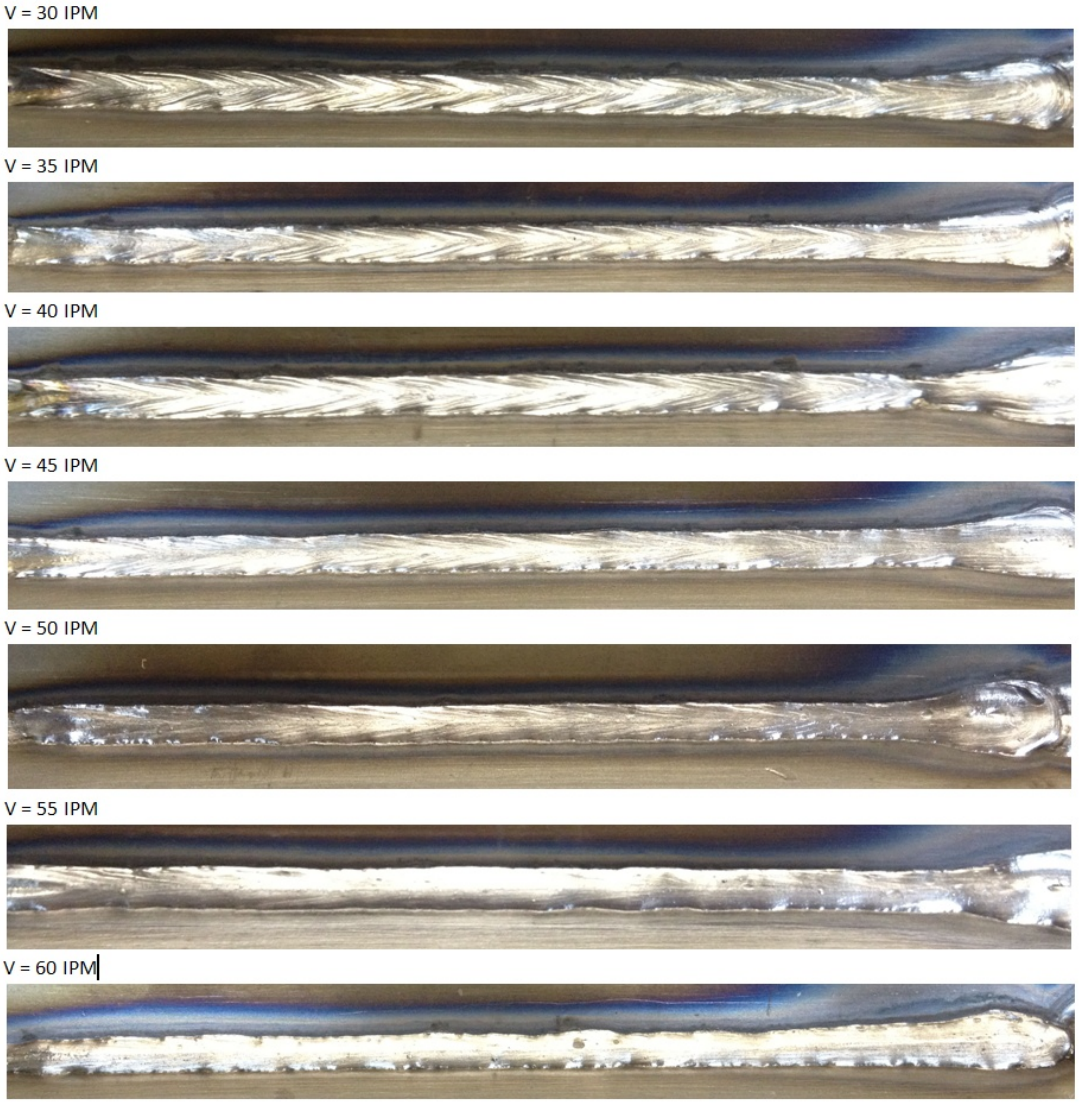

Fig. 4.12 Weld Beads from Travel Speed Study Experiments

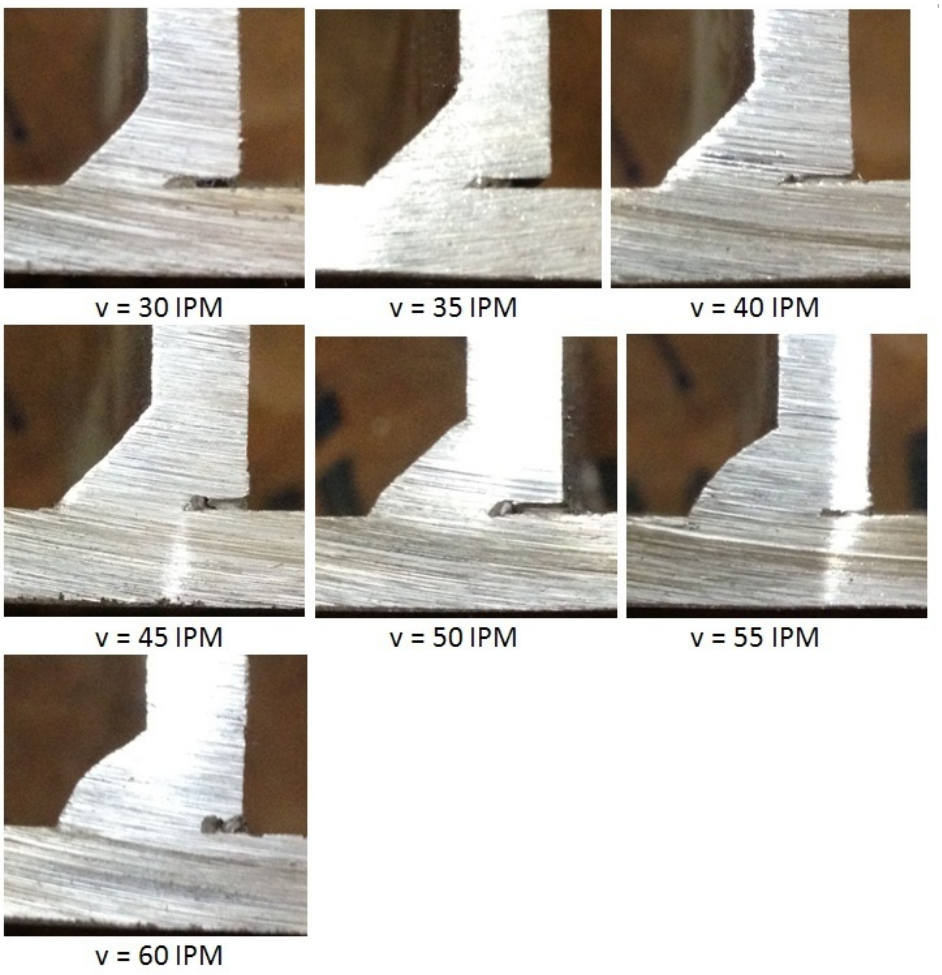

Fig. 4.13 Cross Sections of Weld Beads in Travel Speed Study Experiments

Fig. 4.12 and 4.13 give the weld beads and typical cross sections in the travel speed study experiments respectively. From these photos, it can be seen that when the travel speed is equal to and lower than 45 IPM, there is no obvious difference among the convexity of the weld beads. All of them are fairly flat. However, when the travel speed is equal to and greater than 50 IPM, the convexity phenomenon on the surface of the weld beads begins to appear; and with the increase in the travel speed, the convexity of the weld beads is getting greater and greater noticeably. In particular, the convexity of the weld beads is approximately proportional to the travel speed.

4.3.4 Standard Deviation and Extreme Difference Analysis

Standard deviation and extreme difference are two important performance indices in statistics that are used to describe the spread of the distribution of a group of experimental data [54-56]. Using the statistical data of the seven experiments with different travel speeds, Fig. 4.14 shows the changing tendency of the standard deviation and extreme difference of the leg sizes.

It is not difficult to see that when the travel speed is at 30 IPM (lowest travel speed), the standard deviation and the extreme difference of the leg sizes are both largest. The high standard deviation and extreme difference are actually coherent to the fluctuating base metal current (see the first plot in Fig. 4.11) and the rough surface and uneven edges of the weld bead with 30 IPM travel speed (see the first photo in Fig. 4.12) because fluctuations in base metal current increase the fluctuations in the penetration capability and thus evenness of the welds produced. Then, as the travel speed increases (from 35 IPM to 45 IPM), the standard deviation and extreme difference both become smaller, reaching their lowest points at 45 IPM, and then rise a little bit as the travel speed continues to increase (from 45 IPM to 60 IPM).

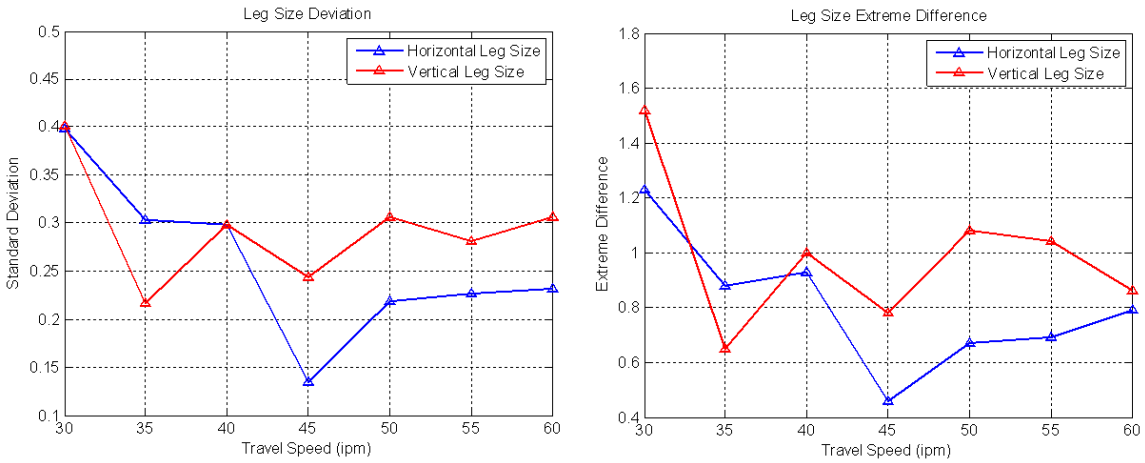

Fig. 4.14 Standard Deviation (Left) and Extreme Difference (Right) of Leg Sizes in Travel Speed Study Experiments

From 35 IPM to 60 IPM, however, the deviations and the extreme differences are all relatively small. Hence, 35 IPM to 60 IPM can be considered as an acceptable range for the travel speed. Although in the vertical direction the deviation and extreme difference are very low at 35 IPM, the speed of 45 IPM should still be a better choice because both directions should be equally important.

4.3.5 Average and Minimum Leg Sizes Analysis

In addition to the standard deviation and extreme difference, the average leg sizes and minimum leg sizes are two other important indices that can be used to evaluate the welding performance for fillet joints. In practice, the average and minimum leg sizes of the weld beads are more concerned.

Fig. 4.15 shows the changing tendency of the average and minimum leg sizes. It can be seen that, with the increase in the travel speed, the average and minimum leg sizes

increase gradually at the beginning, reach their largest sizes between 35 IPM and 45 IPM, and then decrease gradually. Because making weld beads absolutely symmetrical on both the vertical and horizontal directions is relatively difficult in laboratory but it may not in shipyards, the average leg size, i.e. the average between the weld sizes in the two directions as given by the black line in Fig. 4.15, may be a better measurement for the weld size. Considering the average leg sizes together with the vertical and horizontal minimum sizes, 45 IPM is optimal.

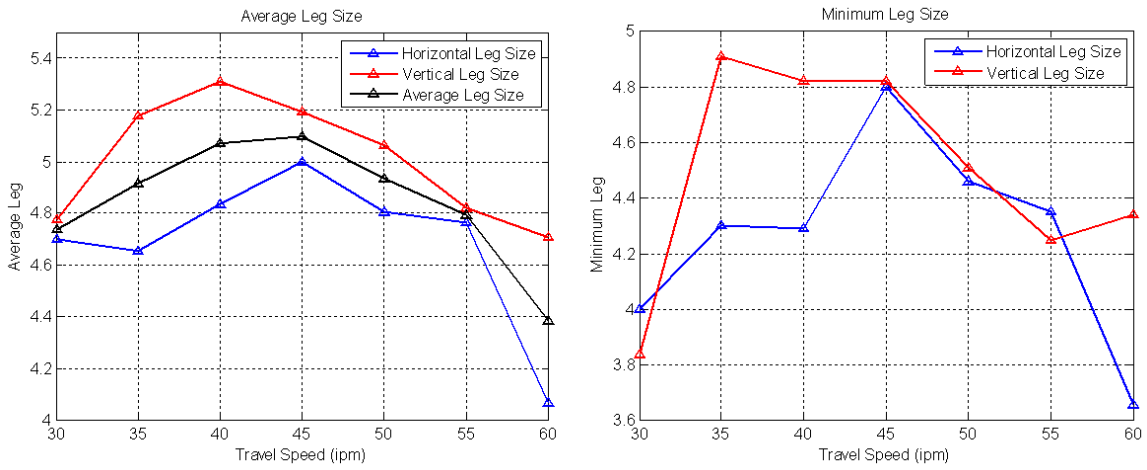

Fig. 4.15 Changing Tendency of Average Leg Sizes (Left) and Minimum Leg Sizes (Right) in Travel Speed Study Experiments

4.3.6 Remarks on Travel Speed Optimization

From the changing tendencies of all the four important performance indices, it is apparent that, both the leg sizes and their distributions are undesirable if the travel speed is too slow or too fast. The travel speed from 35 IPM to 50 IPM is considered most appropriate to produce welds meeting size and smoothness requirements.

Specifically, the changing tendencies of the quantitative indices are coherent to the changes on the convexity and shapes of the weld beads, and can be explained through the physical process. When the travel speed is relatively slow, the wire feed speeds (main and bypass wire) have to be reduced accordingly due to the limit on the constant linear deposition speed (mass deposition). Naturally, the welding currents will be relatively low because of the reduced wire feed speeds. Unfortunately, the welding currents are more fluctuating in their low ranges (see Fig. 4.11). As a result, the fluctuating welding currents lead to the relatively large standard deviation and extreme difference. On the contrary, if the travel speed is too fast, the formation of the even welds at high speed becomes an issue resulting in large standard deviations and extreme differences of the leg sizes as well as the uneven narrow and convex weld beads. Therefore, the quantitative statistical results and the qualitative analysis on the convexity of the welds both suggest the moderate 45 IPM the optimal travel speed for the DE-SAW process for fillet joints.

4.4 Heat Input (Initial Main Wire Feed Speed) Selection

With the root opening and travel speed selected/optimized, the initial main wire feed speed should also be selected properly. Even if some advanced control algorithm is applied, the total heat input must be chosen wisely as the initial condition to the control system. Otherwise, the welding currents will start from an improper value and lots of time and energy will be wasted to bring the system back to the steady status once the control gets started. Due to the total heat input is primarily determined by the main wire feed speed, the selection of the proper heat input is actually a process of selecting the main wire feed speed.

4.4.1 Experiment Design

Different from the constant ratio used in the travel speed optimization, if the ratio between the main and bypass wire feed speeds can be adjusted, then the same linear deposition rate can be achieved at reduced/increased main wire feed speed (thus the total current that determines the heat input fundamentally) but higher/lower bypass wire feed speed (that does not affect the heat input directly) so that the heat input can be adjusted.

Hence, a series of experiments are conducted in this section with the parameters shown in Table 4.4 to optimize the wire feed speeds, i.e., to determine the minimal heat input (with corresponding welding parameters) needed to produce acceptable welds. In particular, the main wire feed speed has been increased progressively at the 10 IPM increment within the attainable range from 70 IPM to 110 IPM. Simultaneously, the bypass wire speed (from 382 IPM to 206 IPM) has been adjusted accordingly to maintain the linear deposition rate unchanged. When viewing Table 4.4, one should note that the diameter of the main wire and that of the bypass wire are different (2:1 approximately, see Table 4.1). The adjustment on the bypass wire speed is exactly calculated based on this diameter ratio.

Table 4.4 Experimental Parameters

	Root opening Size mm	Travel Speed IPM (cm/min)	Main Voltage volt	Bypass Voltage volt	Main Wire Speed IPM (cm/min)	Bypass Wire Speed IPM (cm/min)
Exp 6.1	1.5	45 (114.3)	28	28	70 (177.8)	382 (970.28)
Exp 6.2	1.5	45 (114.3)	28	28	80 (203.2)	338 (858.52)
Exp 6.3	1.5	45 (114.3)	28	28	90 (228.6)	294 (746.8)
Exp 6.4	1.5	45 (114.3)	28	28	100 (254)	250 (635)
Exp 6.5	1.5	45 (114.3)	28	28	110 (279.4)	206 (523.2)

After conducting these five experiments, the leg sizes (vertical and horizontal) are measured for each of the five weld beads with the same method shown Fig. 4.10. Similarly, the analysis as to the welding performances will be qualitative and quantitative. In addition, the heat input is now added as another measurement. If the weld sizes are all acceptable within a certain range of the linear deposition, then the lower heat input resulted from the lower main wire feed speed should be selected to maximally minimize the heat input.

4.4.2 Experimental Results and Analysis

Under the same basic conditions (Table 4.1) and unchanged linear deposition speed as designed, five experiments have been conducted following the sequence listed in Table

4.4. Fig. 4.16 shows the plots of the experimental data recorded from the data-acquisition system.

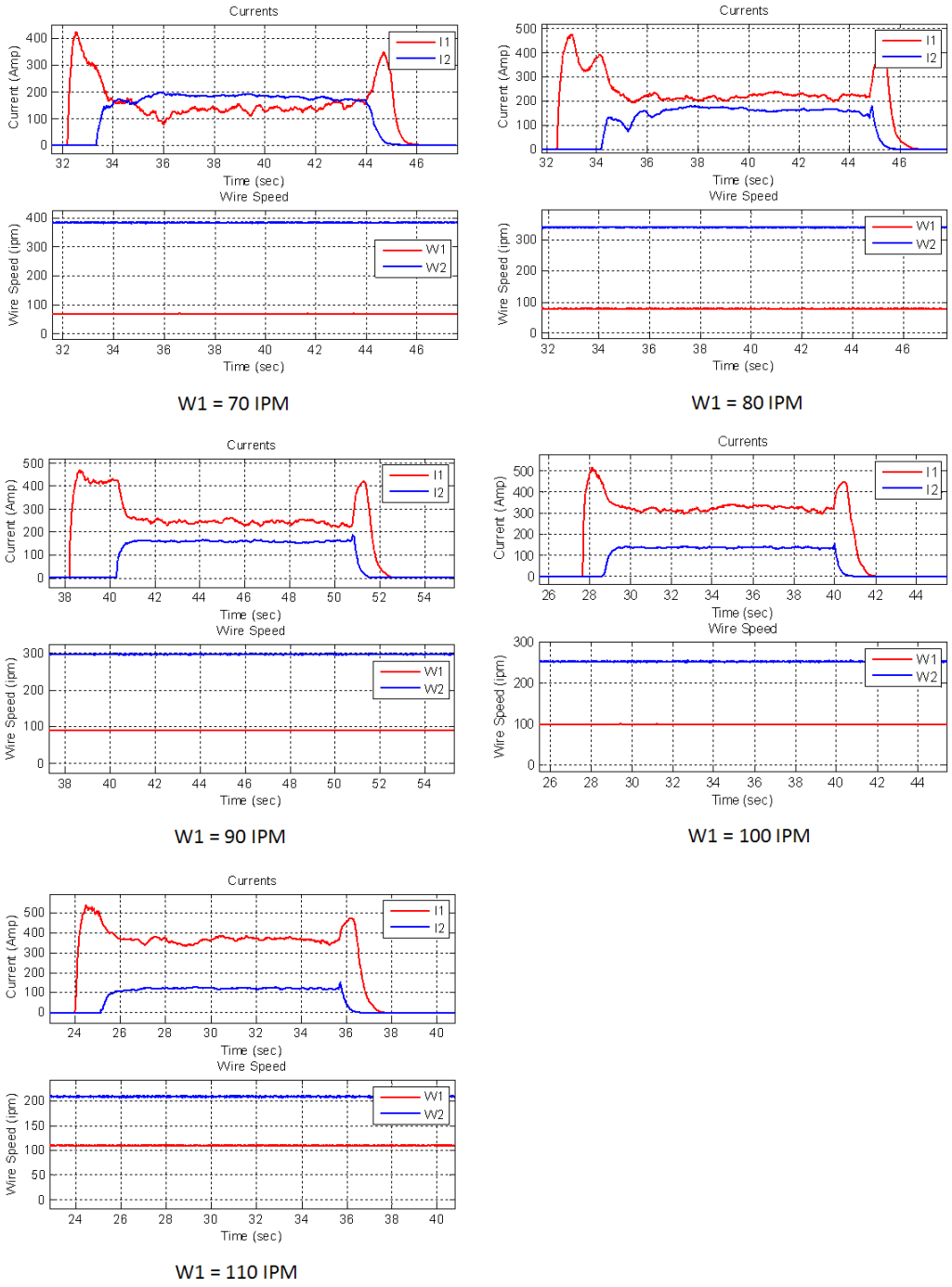

Fig. 4.16 Currents and Wire Speeds Plots in Heat Input Experiments

As shown in Fig. 4.16, with the increase of the main wire speed (from 70 IPM to 110 IPM) and the decrease of the bypass wire (from 382 IPM to 206 IPM), the heat input consequently has been increased, and the average steady-state base metal current (red lines in Fig. 4.16) has been increased accordingly. Careful observation on Fig. 4.16 also shows that the fluctuation on the base metal current is relatively strong and obvious when the wire feed speed is set at 70 IPM. Apart from this, the welding processes in the rest four experiments are quite stable.

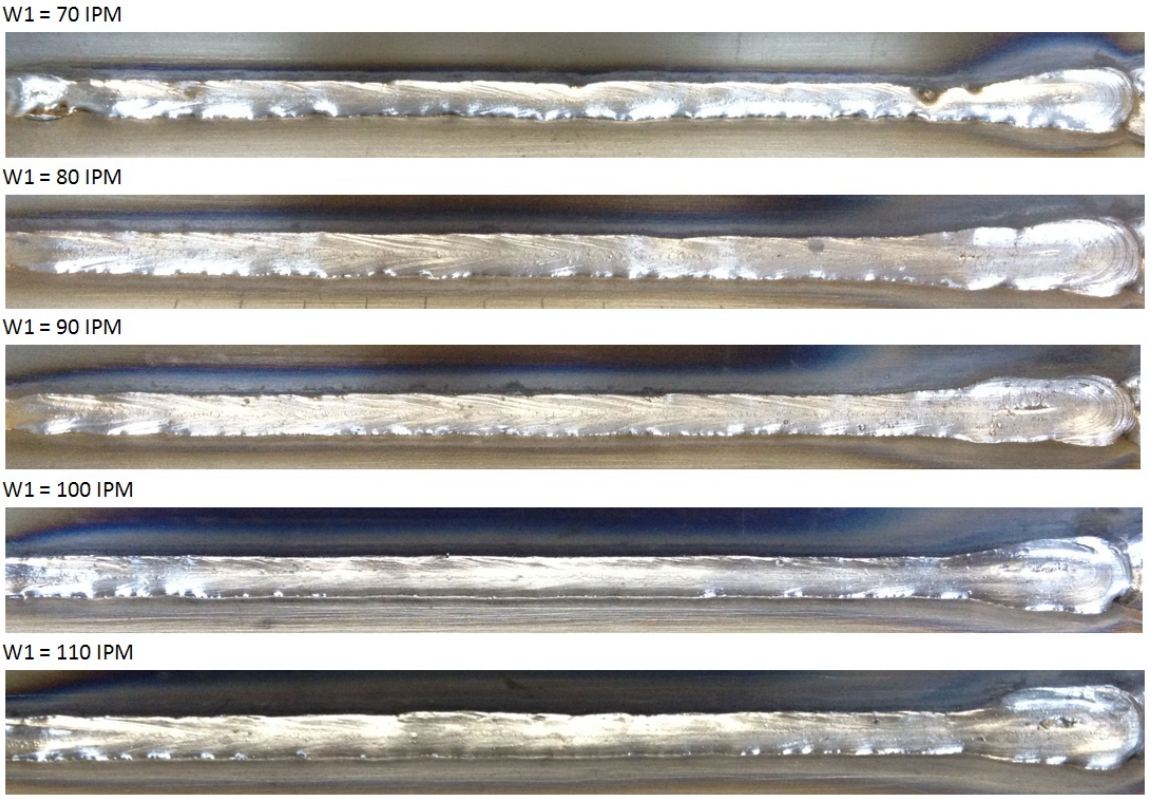

Fig. 4.17 Weld Beads in Heat Input Experiments

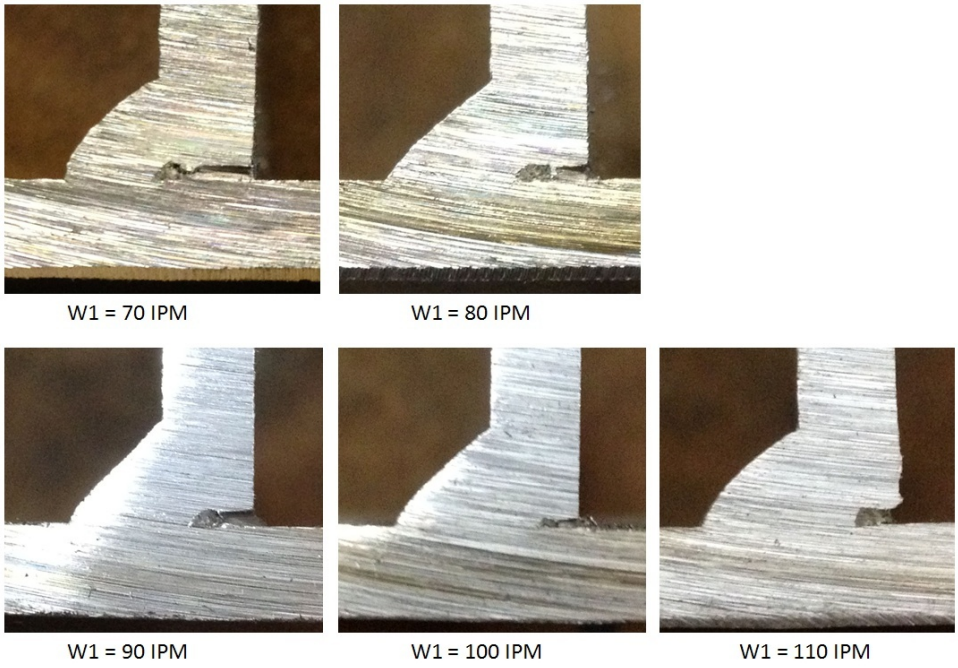

Fig. 4.18 Cross-sections of Weld Beads in Heat Input Experiments

Fig. 4.17 and 4.18 give the weld beads and typical cross sections in the heat input optimization study respectively. From these photos, it can be seen that when the main wire feed speed equals 70 IPM and 110 IPM (two extreme settings in this series), the weld beads appear to be convex. Additionally, at 70 IPM, the edges of the weld bead are quite rough and uneven. However, when the main wire speed is between 80 IPM and 100 IPM, the quality of the weld beads is quite satisfactory. Especially, when viewing the typical cross-sections, the surface and reentrant angle of the weld beads within this range are all fairly acceptable.

4.4.3 Standard Deviation and Extreme Difference Analysis

Similar to the quantitative analysis used in the travel speed optimization, four performance indices are calculated. According to the statistical data from the five

experiments with different heat input, Fig. 4.19 shows the changing tendency of the standard deviation and extreme difference on the leg sizes.

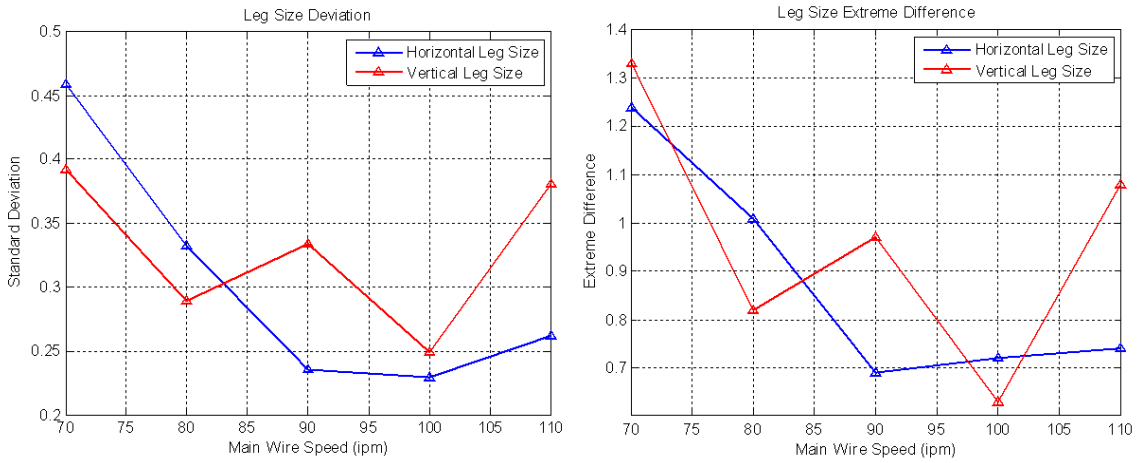

Fig. 4.19 Standard Deviation and Extreme Difference of Leg Sizes in Heat Input Experiments

After taking the data on both horizontal and vertical directions into consideration, it can be seen that when the main wire feed speed is at 70 IPM (lowest heat input in the series of experiments), the standard deviation and extreme difference of the leg sizes are both the largest. Then, from 80 IPM to 100 IPM, the standard deviation and extreme difference of the leg sizes are both on the declining trend. Actually, the deviation and the extreme difference are all relatively small within this range. Hence, 80 IPM to 100 IPM can be considered as an acceptable range for the heat input. Comparatively, the heat input when $W_1 = 100$ IPM gives the best performance. At last, when the main wire feed is close to 110 IPM (the highest wire feed speed in the series of experiments), both the standard deviation and extreme difference rise up rapidly.

The changing tendencies on deviation and extreme difference are coherent to the welds shown in Fig. 4.17 and 4.18. From $W_1 = 80$ IPM to $W_1 = 100$ IPM, the surfaces of the weld beads are relatively smooth, and the edges of the welds are quite uniform. However, when the heat input is either too high or too low, the surfaces of the welds appear to be convex and the edges of the welds are relatively rough and uneven. Hence, simply from the standard deviation and extreme difference of the leg sizes, the appropriate range of the main wire feed speed (represents the range of heat input) should be between 80 IPM and 100 IPM.

4.4.4 Average and Minimum Leg Sizes Analysis

In addition to the deviation and the extreme difference, Fig. 4.20 shows the changing tendencies of average and minimum leg sizes. By referring to the statistical data on both horizontal and vertical direction, it can be seen that the average and minimum leg sizes are all on the rising trend at the beginning. After reaching their largest sizes when the main wire speed equals 90 IPM respectively, the leg sizes become shorter instead of keeping increasing with the continuing rising of the heat input. This decreasing phenomenon is different from our previous expectation. The excessive penetration appeared following the high heat input should be the major reason leading to the narrow and uneven welds.

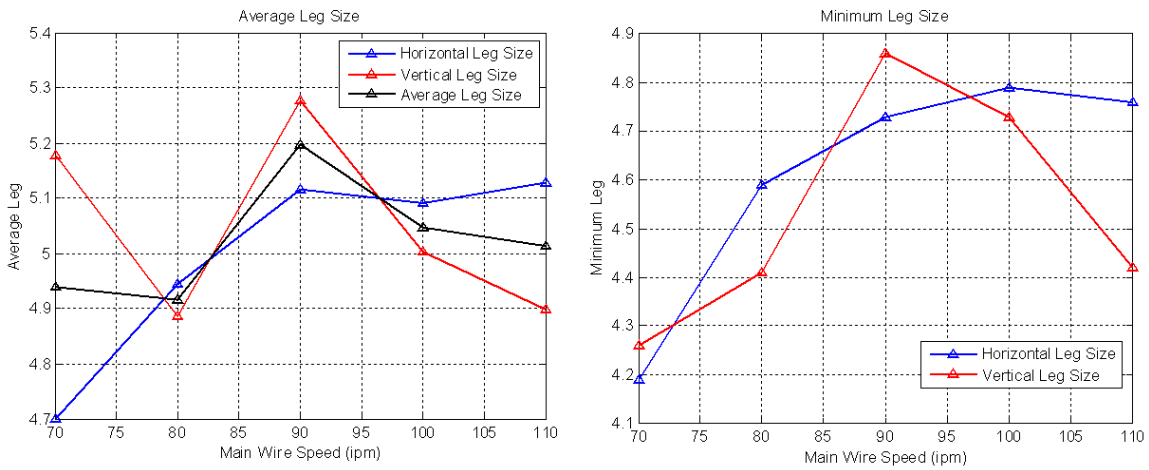

Fig. 4.20 Changing Tendency of Average and Minimum Leg Sizes in Heat Input Experiments

In typical applications, the vertical and horizontal leg sizes must be greater than the thickness of the work-pieces (4.7 mm approximately). From this point of view, only the leg sizes resulted from the heat inputs when $W_1 = 90$ IPM and $W_1 = 100$ IPM are fully qualified. At 80 IPM and 110 IPM, although the average leg sizes are acceptable, the minimum leg sizes are excessively undersized. And after observing the weld beads at 80 IPM and 110 IPM, there are more than one spot appeared along the welds with the leg size lower than 4.7 mm. Hence, considering the average leg sizes together with the vertical and horizontal minimum sizes, only the heat inputs when the main wire feed speed equals 90 IPM and 100 IPM can be accepted.

4.4.5 Heat Input Comparison

Heat input reduction is the primary purpose to use the DE-SAW process. Table 4.5 shows the heat input comparison among the five heat input optimization experiments and

shipyard single-wire SAW benchmark. “Heat Input Ratio” in Table 4.5 represents the heat input in relation to that of the benchmark.

Table 4.5 Heat Input Comparison

	Main Wire Speed (IPM)	Total Current (Amp)	Travel speed (IPM)	Heat Input (J/inch)	Heat Input Ratio
Single Wire	75	400	30	22400	100%
Exp 5.1	70	320	45	11947	53%
Exp 5.2	80	380	45	14187	63%
Exp 5.3	90	420	45	15680	70%
Exp 5.4	100	465	45	17360	78%
Exp 5.5	110	510	45	19040	85%

Table 4.5 clearly shows that the DE-SAW process with 1.5 mm root opening lowers the heat input. Meanwhile, as analyzed in the quantitative comparison, the welding sizes at $W_1 = 90$ IPM and $W_1 = 100$ IPM are all satisfactory.

4.4.6 Remarks on Heat Input Optimization

From the changing tendencies of all the four important performance indices and the convexity of the welds, it is apparent that both the leg sizes and their distributions are undesirable if the heat input is too low or too high. Meanwhile, on the premise of minimizing the heat input and guaranteeing the weld quality, it is reasonable to say that

the heat input when the main wire feed speed equals from 90 IPM to 100 IPM is optimal with a 30% reduction approximately on the heat input relative to the conventional SAW process for fillet joints. On the premise of guaranteeing the weld quality, 100 IPM main wire feed speed has been chosen as the initial value when an advanced control algorithm is applied. After all, the welding quality is more important than 8% reduction on the heat input. Due to the diameter of the bypass wire is much thinner than that of the main wire, the adjustment range of the bypass wire would be larger. Thus, for security reason, the initial bypass wire speed is lowered by 100 IPM from 250 IPM to 150 IPM when 100 IPM initial main wire feed speed is applied.

4.5 Chapter Summary

The use of a root opening between the tee and the panel provides an effective way to reduce the penetration capability required to produce desirable weld beads. The heat input reduction capability of the DS-SAW can thus be effectively utilized to produce desirable fillet welds with minimized heat input. 1.5 mm is recommended for fillet welding on 3/16” thick plates.

Quantitative and qualitative analysis methods have been used to optimize the welding parameters for minimized heat input. The resultant optimized practice for DE-SAW of 3/16” fillet joints is to use 1.5 mm root opening, 45 IPM travel speed and 100 IMP initial main wire feed speed for 3/32 inch” (2.381 mm) diameter main wire.

The appropriate heat input or initial main wire speed confirmed in this chapter will be used in chapter 7 as the initial condition when the advanced control algorithm is being applied. Of course, in terms of the requirement of the advanced control as well as the security needs, the initial bypass wire feed speed might be reduced to some extent when 100 IPM initial main wire feed speed is being used.

Chapter 5 Process Modeling

After having the root opening size, travel speed and the initial wire feed speeds selected and optimized, as well as confirming the necessity of feedback control in DE-SAW for fillet joints, the design of the control system can be started. In this chapter, the process model of DE-SAW has been analyzed based on the study to the physical process, so that the advanced control algorithm can be applied easily and effectively.

5.1 Physical Process

The melting process of the two wires in DE-SAW is the starting point of the model analysis. In Fig. 5.1, the two arcs have been abstracted and described in an ideal way.

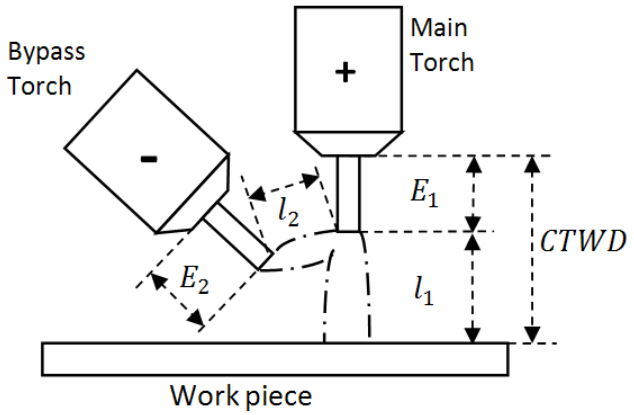

Fig. 5.1 Wire extensions and arc lengths in DE-SAW

where,

E_1 is the extension (stick-out) of main wire;

l_1 is the length of main arc;

E_2 is the extension (stick-out) of bypass wire;

l_2 is the length of bypass arc;

CTWD is the contact tip to work distance.

It can be seen that when the ideal dynamic balance of the arcs is established, the main arc is formed between the tip of the main electrode and the surface of the work-piece (in fillet joints, the root of the main arc should be located on the surface of the panel or that of the tee or both); the bypass arc is established between the tips of the two wires. The long dash dot curves in the Fig. 5.1 represent the edges of arcs in this ideal case.

5.2 Basic Equations

In DE-SAW, the bypass loop melting heat consists of two parts, cathode heat and the bypass electrical resistance heat. In that case, the melting speed of the bypass wire (v_{m2}) is determined by two terms in Equation (5-1):

$$v_{m2} = \lambda_1 V_c I_2 + \lambda_2 E_2 {I_2}^2 \tag{5.1}$$

where,

v_{m2} is the melting rate of bypass wire;

V_c is the cathode voltage;

λ_1 and λ_2 are coefficients.

When the DE-SAW process is established steadily, v_{m2} is considered to be equal to the bypass wire feed speed W_2 such that

$$W_2 = \lambda_1 V_c I_2 + \lambda_2 E_2 {I_2}^2 \tag{5.2}$$

The main wire melting process is similar to the bypass wire melting process. In DE-SAW, the main loop melting heat primarily consists of the anode heat and the main electrical resistance heat that are both determined by the total current (Sum of the base and bypass currents). Hence, the melting speed of the main wire (v_{m1}) is

$$v_{m1} = \lambda_3 V_a I + \lambda_4 E_1 I^2 \tag{5.3}$$

where,

v_{m1} is the melting rate of main wire;

V_a is the anode voltage.

Similarly,

$$W_1 = \lambda_3 V_a I + \lambda_4 E_1 I^2 \tag{5.4}$$

where,

W_1 is the main wire feed speed.

Generally, the main power supply in DE-SAW works in the constant voltage (CV) mode. The output voltage of the power supply is thus controlled at its setting voltage V_1 by adjusting the current outputted by the power supply, i.e. the base metal current I_1 such that

$$\begin{aligned} V_1 &= V_c + V_a + R_{11} I_1 + R_{12} I \\ &= V_c + V_a + (\rho_{11} l_1) I_1 + (\rho_{12} E_1) I \end{aligned} \tag{5.5}$$

can be derived from the main loop shown in Fig. 3.3. Where,

V_1 is the voltage of the main power supply;

R_{11} is the resistance of main arc column;

R_{12} is the resistance of main wire extension.

The second part in Equation (5-5) is obtained by assuming the resistance is linear to the length of the arc length [57, 58].

The bypass power supply in DE-SAW system also works in the constant voltage (CV) mode such that the follows can be obtained from the bypass loop in Fig. 3.3:

$$V_2 = V_c + V_a + R_{21}I_2 + R_{22}I_2 + R_{12}I$$
$$= V_c + V_a + (\rho_{21}l_2)I_2 + (\rho_{22}E_2)I_2 + (\rho_{12}E_1)I \quad (5.6)$$

Where,

V_2 is the voltage of the bypass power supply;

R_{21} is the resistance of bypass arc column;

R_{22} is the resistance of bypass wire extension.

In summary, (3-1), (5-2), (5-4), (5-5) and (5-6) are the basic equations that govern the DE-SAW process. The process model will be established based on these equations.

5.3 Linearization and Static Incremental Model

Four equations obtained in section 5.2 can be differentiated below:

$$\Delta W_2 = \lambda_1 V_c \Delta I_2 + 2\lambda_2 E_2 I_2 \Delta I_2 + \lambda_2 {I_2}^2 \Delta E_2$$

$$= (\lambda_1 V_c + 2\lambda_2 E_2 I_2)\Delta I_2 + \lambda_2 {I_2}^2 \Delta E_2 \quad (5.7)$$

$$\Delta W_1 = \lambda_3 V_a(\Delta I_1 + \Delta I_2) + (\lambda_4 I^2)\Delta E_1 + 2\lambda_4 E_1 I(\Delta I_1 + \Delta I_2)$$

$$= (\lambda_3 V_a + 2\lambda_4 E_1 I)\Delta I_1 + (\lambda_3 V_a + 2\lambda_4 E_1 I)\Delta I_2 + (\lambda_4 I^2)\Delta E_1 \quad (5.8)$$

$$0 = \rho_{11} l_1 \Delta I_1 + \rho_{11} I_1 \Delta l_1 + \rho_{12} E_1(\Delta I_1 + \Delta I_2) + \rho_{12} I \Delta E_1$$

$$= (\rho_{11} l_1 + \rho_{12} E_1)\Delta I_1 + (\rho_{12} E_1)\Delta I_2 + (\rho_{11} I_1)\Delta l_1 + (\rho_{12} I)\Delta E_1 \quad (5.9)$$

$$0 = \rho_{21} l_2 \Delta I_2 + \rho_{21} I_2 \Delta l_2 + \rho_{22} E_2 \Delta I_2 + \rho_{22} I_2 \Delta E_2 + \rho_{12} E_1 \Delta I + \rho_{12} I \Delta E_1$$

$$= (\rho_{12} E_1)\Delta I_1 + (\rho_{21} l_2 + \rho_{22} E_2 + \rho_{12} E_1)\Delta I_2 + (\rho_{21} I_2)\Delta l_2 + (\rho_{12} I)\Delta E_1 + (\rho_{22} I_2)\Delta E_2 \quad (5.10)$$

V_1 and V_2 are considered constant in this differentiation due to the use of the CV mode. These four equations described the relationships among wire feed speeds, welding currents, arc lengths, and wire extensions in the DE-SAW process.

When the positions of the two torches in relation to the work-piece surface are fixed, the following process constraints can be obtained:

$$\Delta l_1 = -\Delta E_1 \quad (5.11)$$

$$\Delta l_2 = -(\Delta E_1 + \Delta E_2) = -\Delta E_1 - \Delta E_2 \quad (5.12)$$

Substituting Equation (5-11) and (5-12) into Equation (5-9) and (5-10) gives:

$$0 = (\rho_{11} l_1 + \rho_{12} E_1)\Delta I_1 + (\rho_{12} E_1)\Delta I_2 + (\rho_{12} I - \rho_{11} I_1)\Delta E_1 \quad (5.13)$$

$$0 = (\rho_{12}E_1)\Delta I_1 + (\rho_{21}l_2 + \rho_{22}E_2 + \rho_{12}E_1)\Delta I_2 +$$

$$(\rho_{12}I - \rho_{21}I_2)\Delta E_1 + (\rho_{22}I_2 - \rho_{21}I_2)\Delta E_2 \quad (5.14)$$

Solving the Equation (5-13) gives,

$$\Delta E_1 = \sigma_1 \Delta I_1 + \sigma_2 \Delta I_2 \quad (5.15)$$

Where,

$\sigma_1 = \frac{\rho_{11}l_1 + \rho_{12}E_1}{\rho_{11}I_1 - \rho_{12}I}$;

$\sigma_2 = \frac{\rho_{12}E_1}{\rho_{11}I_1 - \rho_{12}I}$.

Substituting Equation (5-15) into Equation (5-14), and then solving the Equation (5-14) gives,

$$\Delta E_2 = \sigma_3 \Delta I_1 + \sigma_4 \Delta I_2 \quad (5.16)$$

Where,

$\sigma_3 = \frac{\rho_{12}E_1 + \sigma_1(\rho_{12}I - \rho_{21}I_2)}{\rho_{21}I_2 - \rho_{22}I_2}$;

$\sigma_4 = \frac{\rho_{21}l_2 + \rho_{22}E_2 + \rho_{12}E_1 + \sigma_2(\rho_{12}I - \rho_{21}I_2)}{\rho_{21}I_2 - \rho_{22}I_2}$.

Then, substituting Equation (5-15) and (5-16) into Equation (5-7) and (5-8) gives,

$$\Delta I_1 = \mu_1 \Delta W_1 + \mu_2 \Delta W_2 \quad (5.17)$$

$$\Delta I_2 = \mu_3 \Delta W_1 + \mu_4 \Delta W_2 \quad (5.18)$$

Where,

μ_1, μ_2, μ_3 and μ_4 are coefficients contain σ_1, σ_2, σ_3 and σ_4 obtained before.

After applying differentiation and process constraints, the system model becomes a two-input-two-output form as shown by Equation (5-17) and (5-18). The main wire feed speed (W_1) and the bypass wire feed speed (W_2) are the two input signals; the base metal current (I_1) and the bypass current (I_2) are the two output signals. They are referred to as a static incremental model of DE-SAW. If the control period is significantly longer than the time constants in the arcing and melting processes involved, such static incremental model will be an accurate description of the DE-SAW process being controlled. Hence, the system can be schematically represented by Fig. 5.2.

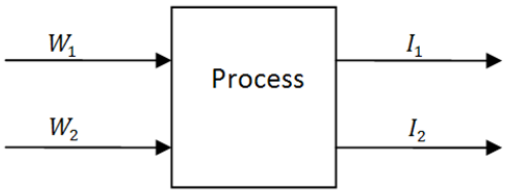

Fig. 5.2 Model of DE-SAW Process

5.4 Filter Design and Dynamic Incremental Model

In GMAW and its variant SAW, the cathode is on the work-piece. However, the cathode is mobile and continues looking for oxide films for easy electron emission [59]. As a result, the current fluctuates continuously. To control the current I_1 and I_2 in DE-SAW (still a variant of GMAW), the signals sampled from the current sensors for I_1 and I_2 should be filtered. The outputs that will be feedback controlled are thereby the filtered I_1 and I_2, denoted as y_1 and y_2, and the process to be controlled, referred to as the "controlled plant", thus consists of the DE-SAW process and the filters as shown in Fig. 5.3. The realization of the digital filters used in this paper can be illustrated by Equation (5-19) and (5-20).

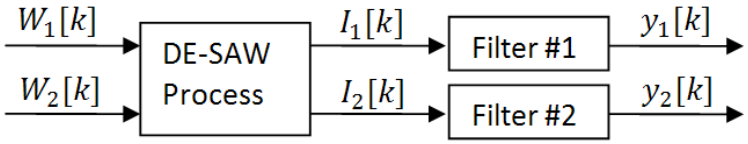

Fig. 5.3 Block Diagram of Controlled Plant

$$y_1[k] = \alpha y_1[k-1] + (1-\alpha) I_1[k] \tag{5.19}$$

$$y_2[k] = \alpha y_2[k-1] + (1-\alpha) I_2[k] \tag{5.20}$$

Where, the coefficient of the filter (α) that determines the filter's time constant needs to be designed based on current fluctuation spectrum. When the sampling period is 10 ms, it is found that $\alpha = 0.95$ can filter the fluctuated currents with a balanced responding speed and fluctuating filtering. The resultant time constant is much greater than those of the arcing and melting processes involved. Hence, when the filter is used, the static incremental model of DE-SAW can be combined with the filter forming the dynamic process being controlled:

$$y_1[k] = y_1[k-1] + h_1 \Delta W_1[k-1] + h_2 \Delta W_1[k-2] + \cdots + h_N \Delta W_1[k-N] + g_1 \Delta W_2[k-1] + g_2 \Delta W_2[k-2] + \cdots + g_N \Delta W_2[k-N] \tag{5.21}$$

$$y_2[k] = y_2[k-1] + f_1 \Delta W_1[k-1] + f_2 \Delta W_1[k-2] + \cdots + f_N \Delta W_1[k-N] + p_1 \Delta W_2[k-1] + p_2 \Delta W_2[k-2] + \cdots + p_N \Delta W_2[k-N] \tag{5.22}$$

Where, $\Delta W_i[k-j] = W_i[k-j] - W_i[k-j-1]$ $(i = 1,2; j = 1, \ldots, N)$.

System order "N" and parameters h_j, g_j, f_j, p_j ($j = 1,2, \dots, N$) can be obtained using data from welding experiments that produce sampled and filtered currents y_1 and y_2 from the applied W_1 and W_2. "k" stands for the present discrete-time instant and "$k - j$" ($j = 1, \dots, N$) are the previous instants. From the experimental data, the bypass current (y_2) has not been found to have correlation with the main wire speed (W_1). Hence, $f_1 = f_2 = \cdots = f_N = 0$, resulting in

$$y_2[k] = y_2[k-1] + p_1 \Delta W_2[k-1] + p_2 \Delta W_2[k-2] + \cdots + p_N \Delta W_2[k-N] \qquad (5.23)$$

Equations (5-21) and (5-23) together constitute the dynamic incremental model of the DE-SAW process, and this dynamic incremental model will be used to develop an advanced control algorithm for fillet DE-SAW system.

Chapter 6 Predictive Control Algorithm Design

Based on the dynamic incremental model of fillet DE-SAW obtained in chapter 5, a predictive control algorithm was developed for the DE-SAW process. The predictive control is considered as one of the most effective advanced control algorithms that has gained wide industrial applications. It functions similarly as a human operator who quickly evaluates/predicts how the system output will change if he changes the input command and optimize the change based on the prediction [60-64].

6.1 Review of Predictive Control

At the end of the seventies in the 20th century, a type of new control algorithms based on computers, such as Dynamic Matrix Control (DMC) [65-68] and Model Algorithmic Control (MAC) [69, 70], appeared in many industrial process control fields with the purpose of conquering the conflict between the traditional control theory and the industrial application. This type of control algorithms applied rolling optimal control theory; the models used in these algorithms were obtained from step or impulse responses. In 1978, Richalet and his co-workers introduced the motivation, principles and industrial applications of this type of control algorithms thoroughly for the first time [71]. Since then, “Predictive Control” was used as the uniform name of this type of control algorithms.

Aimed at the dynamic incremental model of fillet DE-SAW described with Equations (5-21) and (5-23), the basic idea of the predictive control can be explained with the following five steps:

1. Predicting the system outputs j-step-ahead ($j = 1, \dots, N$) using the dynamic incremental model given in Equations (5-21) and (5-23) as functions of the changes to be taken in the wire feed speeds for the present time, i.e., as functions of $\Delta W_1[k]$ and $\Delta W_2[k]$ without applying further future changes (constant future) in wire feed speeds;
2. Creating desired trajectories for output signals (y_1 and y_2) of the controlled plant to transit from their present values to the desired values;
3. Forming a cost function using the squared differences between the predicted outputs and the trajectories for the future "N" steps. Penalties can be added to penalize fast changes in the wire feed speeds. The cost function will be a quadratic function of $\Delta W_1[k]$ and $\Delta W_2[k]$.
4. Finding the control law by minimizing the cost function with respect to $\Delta W_1[k]$ and $\Delta W_2[k]$.
5. Moving forward to the next control cycle, and repeating the prediction and control law recursively.

6.2 Output Prediction

As shown by Equations (5.21) and (5.23), the process model contains two parts, the base metal current part and the bypass current part; in order to simplify the derivation and

avoid some redundant repetition, the bypass current part in the model is considered at first. And subsequently, the outcome of the derivation can be shared to the base metal current part in the model.

Equation (5-23) is the output expression of the bypass current at instant "k" in discrete-time domain. In terms of this expression, the output expressions at the future "N" steps ($[\mathrm{k}+1], [\mathrm{k}+2], \cdots, [\mathrm{k}+\mathrm{N}]$) are able to be predicted recursively:

$$y_2[k+1|k] = y_2[k] + p_1 \Delta W_2[k] + p_2 \Delta W_2[k-1] + \cdots + p_N \Delta W_2[k-N+1] \qquad (6.1)$$

Where, "$\mathrm{k}+1|\mathrm{k}$" stands for predicting at instant "k".

The first term on the right side of Equation (6-1), $\mathrm{y}_2[\mathrm{k}]$, is the filtered bypass current at the present time; it can be measured from the bypass current sensor. The second term, $\mathrm{p}_1 \Delta \mathrm{W}_2[\mathrm{k}]$, is the influence caused by the change of input at the present time. It is the calculating result from the single board computer (core part of the control system), so it can be recorded as well. The rest "$\mathrm{N}-1$" terms together, $\mathrm{p}_2 \Delta \mathrm{W}_2[\mathrm{k}-1] + \cdots + \mathrm{p}_\mathrm{N} \Delta \mathrm{W}_2[\mathrm{k}-\mathrm{N}+1]$, is the whole contribution caused by the previous changes of the input. They are the historical influence of the change of input.

From Equation (6-1), a brief conclusion can be summarized. Namely, the output at instant "$\mathrm{k}+1$" consists of three parts:

1) The output at present time;

2) The influence of the change of input at present;

3) The historical influence of the change of input.

If "$F_1[k-1]$" is used to represent the historical influence of the change of input, then Equation (6-1) can be simplified as:

$$y_2[k+1|k] = y_2[k] + p_1 \Delta W_2[k] + F_1[k-1] \tag{6.2}$$

Similarly,

$$\begin{aligned} y_2[k+2|k] = y_2[k+1] + p_1 \Delta W_2[k+1] + p_2 \Delta W_2[k] \\ + p_3 \Delta W_2[k-1] + \cdots + p_N \Delta W_2[k-N+1] \end{aligned} \tag{6.3}$$

Notice that the second term on the right side of Equation (6-3) is the influence caused by the change of input at instant "$k+1$". Based on the "constant future" assumption, the input signals do not change at all in the future period. In particular, all of the unknown changes of input signals are considered as no change.

$$\Delta W_1[k+1] = \Delta W_1[k+1] = \cdots = \Delta W_1[k+N] = 0 \tag{6.4}$$

$$\Delta W_2[k+1] = \Delta W_2[k+1] = \cdots = \Delta W_2[k+N] = 0 \tag{6.5}$$

In that case, Equation (6-3) can be simplified as:

$$y_2[k+2|k] = y_2[k+1] + p_2 \Delta W_2[k] + F_2[k-1] \tag{6.6}$$

Where, " $F_2[k-1] = p_3\Delta W_2[k-1] + \cdots + p_N\Delta W_2[k-N+1]$ " is the historical influence of the change of input.

Substitute "$y_2[k+1]$" in Equation (6-6) with Equation (6-2) yields:

$$y_2[k+2|k] = y_2[k] + (p_1 + p_2)\Delta W_2[k] + F_1[k-1] + F_2[k-1] \quad (6.7)$$

If "$F_1[k-1] + F_2[k-1]$" is considered together as the historical contribution caused by previous changes of input, then it can be seen that, the output at instant "$k+2$" consists of three parts as well: the output at present, the influence of the change of input at present, and the historical influence of the change of input. The only difference between the output prediction of instant "$k+1$" and that of instant "$k+2$" is the coefficient of $\Delta W_2[k]$. This substituting process is very important, because the output prediction at instant "$k+2$" can be expressed by a series of known or detectable components.

By following this pattern and using the same approach, the prediction about the system output can be continued as far as necessary until the last step (system order "N") of the dynamic process of the system response. Equation (6-8) shows the output prediction of the last step.

$$y_2[k+N|k] = y_2[k] + \sum_{i=1}^{N} p_i\,\Delta W_2[k] + \sum_{i=1}^{N} F_i[k-1] \quad (6.8)$$

Similarly, the prediction about the output of the base metal current "y_1" can use the same strategy. Equation (6-9) shows the expression of the prediction regarding the base metal current at the last step. The only difference is that this prediction contains two inputs (W_1 and W_2); and the historical influence should be caused by the previous changes of both inputs (ΔW_1 and ΔW_2);.

$$y_1[k+N|k] = y_1[k] + \sum_{i=1}^{N} h_i \, \Delta W_1[k] + \sum_{i=1}^{N} g_i \, \Delta W_2[k] + \sum_{i=1}^{N} M_i[k-1] \qquad (6.9)$$

Where, $M_i[k-1]$ represents the historical influence which should be caused by the previous changes of both inputs.

Equations (6-8) and (6-9) formed the whole output prediction of the last step (step "N"). A laconic version of the output prediction can be given by replacing the summations as shown in Equation (6-10):

$$\begin{bmatrix} y_1[k+j|k] \\ y_2[k+j|k] \end{bmatrix} = \begin{bmatrix} y_1[k] \\ y_2[k] \end{bmatrix} + \begin{bmatrix} H(j) & G(j) \\ 0 & P(j) \end{bmatrix} \Delta u[k] + \begin{bmatrix} M(j) \\ F(j) \end{bmatrix}, \quad j = 1, 2, \cdots, N \qquad (6.10)$$

Where, $\Delta u[k] = \begin{bmatrix} \Delta W_1[k] \\ \Delta W_2[k] \end{bmatrix}$;

$H(j) = \sum_{i=1}^{j} h_i$;

$G(j) = \sum_{i=1}^{j} g_i$;

$P(j) = \sum_{i=1}^{j} p_i$;

$M(j) = \sum_{i=1}^{j} M_i[k-1]$;

$$\mathrm{F(j)} = \sum_{\mathrm{i}=1}^{\mathrm{j}} \mathrm{F_i[k-1]};$$

Equation (6-10) gives the predicting expression of the system outputs at a certain instant "j". Based on this expression, if the predictions from step "1" to step "N" are combined together, a complete form about the output prediction of the controlled plant can be given in Equation (6-11) and (6-12). The capital notations in Equation (6-12) are corresponding to the vectors in Equation (6-11). The predictive expression about the system output has laid the foundation for the development of the model predictive control.

$$\begin{bmatrix} y_1[k+1|k] \\ \vdots \\ y_1[k+N|k] \\ y_2[k+1|k] \\ \vdots \\ y_2[k+N|k] \end{bmatrix} = \begin{bmatrix} y_1[k] \\ \vdots \\ y_1[k] \\ y_2[k] \\ \vdots \\ y_2[k] \end{bmatrix} + \begin{bmatrix} H(1) & G(1) \\ \vdots & \vdots \\ H(N) & G(N) \\ 0 & P(1) \\ \vdots & \vdots \\ 0 & P(N) \end{bmatrix} \Delta u[k] + \begin{bmatrix} M(1) \\ \vdots \\ M(N) \\ F(1) \\ \vdots \\ F(N) \end{bmatrix} \tag{6.11}$$

$$Y_p = Y + A\Delta u[k] + B \tag{6.12}$$

6.3 Trajectory

The purpose of creating the trajectories for the system outputs is ensuring that the system outputs can arrive at their desired settings in a smooth way instead of resulting in too much over shoot. The trajectory used in this paper is a smooth curve from the present values of the system outputs to their desired values. The realization of the trajectory used to guide the outputs are shown in Equation (6-13).

$$y_t[k+i] = y[k] + (c - y[k]) \cdot \left(1 - e^{-i\frac{T_c}{\tau}}\right), \qquad i = 1, 2, \cdots, N. \tag{6.13}$$

Where, "y_t" represents the trajectory value corresponding to each control instant in the future;

"y" is the output of the controlled plant; it can be base metal or bypass current;

"T_c" is the control cycle of the control system;

"τ" is the time constant of the trajectory;

"c" is the desired value of the output.

A vector version of the trajectory can be given by Equation (6-14) after combining the trajectory points from step "1" to step "N".

$$Y_t = \begin{bmatrix} y_{1t}[k+1|k] \\ \vdots \\ y_{1t}[k+N|k] \\ y_{2t}[k+1|k] \\ \vdots \\ y_{2t}[k+N|k] \end{bmatrix} \tag{6.14}$$

Where, y_{1t} represents the trajectory of base metal current;

y_{2t} represents the trajectory of bypass current.

6.4 Cost Function and Control Law

Predictive control is also a kind of optimal control in that the control law needs to be given by minimizing the cost function which is the sum of squared differences between the predicted outputs and the trajectories for the future "N" steps with respect to the system inputs. The primary improvement of the predictive control to the general optimal control is that the control law does not have to be given only once at the beginning;

alternatively, the control law will be calculated real-time with respect to the updating of the cost function. Equation (6-15) shows the cost function used in this research.

$$J(\Delta u) = \left\|Y_t - Y_p\right\|_Q^2 + \|\Delta u\|_R^2$$

$$= \left[Y_t - Y_p\right]^T Q\left[Y_t - Y_p\right] + \Delta u[k]^T R \Delta u[k] \quad (6.15)$$

Where, "Q" and "R" are weight matrices for different outputs and changes in different inputs. Due to the two outputs (base metal and bypass currents) are important equally, the diagonal elements in "Q" matrix are set to 1. Because the diameter of the main wire is 3/32 inch (2.38 mm), and the diameter of the bypass wire is 0.045 inch (1.2 mm), then the two wire speeds must be weighted. Experiments show that "10: 1" is an acceptable/ideal ratio for the penalty "$R = \begin{bmatrix} r_1 & 0 \\ 0 & r_2 \end{bmatrix}$", that is, the penalty to the main wire speed is 10 while the penalty to the bypass wire speed is 1.

Substitute "Y_p" in Equation (6-15) with Equation (6-12) yields:

$$J(\Delta u) = \|Y_t - Y - B - A\Delta u[k]\|_Q^2 + \|\Delta u[k]\|_R^2 \quad (6.16)$$

By this substitution, the cost function becomes a function with respect to "Δu[k]". As mentioned earlier, the control law, or the change of the system input Δu[k] specifically, should be given by minimizing the cost function. Obviously, when the value of the quadratic cost function is minimal, the derivative of the cost function expression with respect to "Δu[k]" should be equal to zero. Consequently, the quadratic cost function leads to an analytical solution for the predictive control below:

$$\Delta u = (A^T Q A + R)^{-1} A^T Q (Y_t - Y - B) = D(Y_t - Y - B) \quad (6.17)$$

Where, $\Delta \mathrm{u}[\mathrm{k}] = [\Delta \mathrm{W}_1[\mathrm{k}], \Delta \mathrm{W}_2[\mathrm{k}]]^{\mathrm{T}}$.

The wire feed speeds to be applied into the DE-SAW system are thus $\mathrm{W_i}[\mathrm{k}] = \mathrm{W_i}[\mathrm{k}-1] + \Delta \mathrm{W_i}[\mathrm{k}]$ $(\mathrm{i} = 1, 2)$, where the previous wire feed speeds $\mathrm{W_i}[\mathrm{k}-1]$ $(\mathrm{i} = 1, 2)$ are known.

It is apparent that the matrix "$\mathrm{D} = (\mathrm{A^T Q A} + \mathrm{R})^{-1} \mathrm{A^T Q}$" can be calculated off-line in advance because A is known already from identification experiments; "Q" and "R" are from the design. The rest of the computation in Equation (6-17) can thus be easily implemented by an embedded system in real-time. Equation (6-17) is the control law of the advanced model predictive control algorithm used in this research for fillet DE-SAW.

Chapter 7 Experiments and Analysis

In chapter 2 and 3, the reason of using root opening and the necessity of fillet DE-SAW control have been illustrated clearly. After that, the size of root opening and the important welding parameters have been selected/optimized in chapter 4; the advanced control algorithm for DE-SAW has been developed in chapter 6 based on the dynamic incremental model obtained in chapter 5. In this chapter, in order to examine the effectiveness of the predictive control algorithm for DE-SAW, bead-on-plate experiment is conducted prior to the practical applications. Then, the predictive control algorithm has been applied onto the fillet work-pieces with a root opening to see if the performance of the control satisfies the expectation. At last, the weld bead and heat input comparisons have been conducted between the fillet welding of DE-SAW with predictive control and the conventional (single wire) SAW process to see the advantages of the control algorithm as well as the use of root opening.

7.1 Experimental Conditions

The experimental conditions here refer primarily to the materials of the wire electrodes, the materials of the steel plates used for the tees as well as the panels, and the model number of the flux powder. The specifications of experimental conditions are listed in Table 7.1.

Table 7.1 Experimental Conditions

	Model Number	Size
Tee Plate	C1018 Cold Rolled Steel Plate	Thickness: 3/16 inch (4.763 mm) Width: 1 inch (25.4 mm)
Panel Plate	C1018 Cold Rolled Steel Plate	Thickness: 3/16 inch (4.763 mm) Width: 4 inch (101.6 mm)
Main Wire	Lincoln Weld L-61	Diameter: 3/32 inch (2.381 mm)
Bypass Wire	Kobelco MG-51T	Diameter: 0.045 inch (1.14 mm)
Flux Powder	Lincoln Weld 882	N/A

7.2 Bead-On-Plate Experiment

The main SAW torch of the Lincoln LT-7 tractor was set vertically to the surface of the work-piece (3/16” C1018 cold rolled steel plates). All of the major parameters in the bead-on-plate experiment are listed in Table 7.2. Due to the purpose of this experiment is just examine the feasibility and stability of the predictive control algorithm, instead of obtaining good welds, the travel speed used here is relatively fast (60 IPM); the wire feed speeds applied as well as the desired welding currents (base metal and bypass) are just chosen randomly within the acceptable range as a demonstrating example, instead of selecting based on the heat-input research conducted in chapter 4.

Table 7.2 Parameters in Bead-On-Plate Experiment

	Value	Unit
Initial Main Wire Speed (W1)	165.1 (65.0)	cm/min (IPM)
Initial Bypass Wire Speed (W2)	330.2 (130.0)	cm/min (IPM)
Desired Base Metal Current (I1)	260	Amp
Desired Bypass Metal Current (I2)	90	Amp
Travel Speed (v)	152.4 (60.0)	cm/min (IPM)
Main Voltage (V1)	28	Volt
Bypass Voltage (V2)	28	Volt

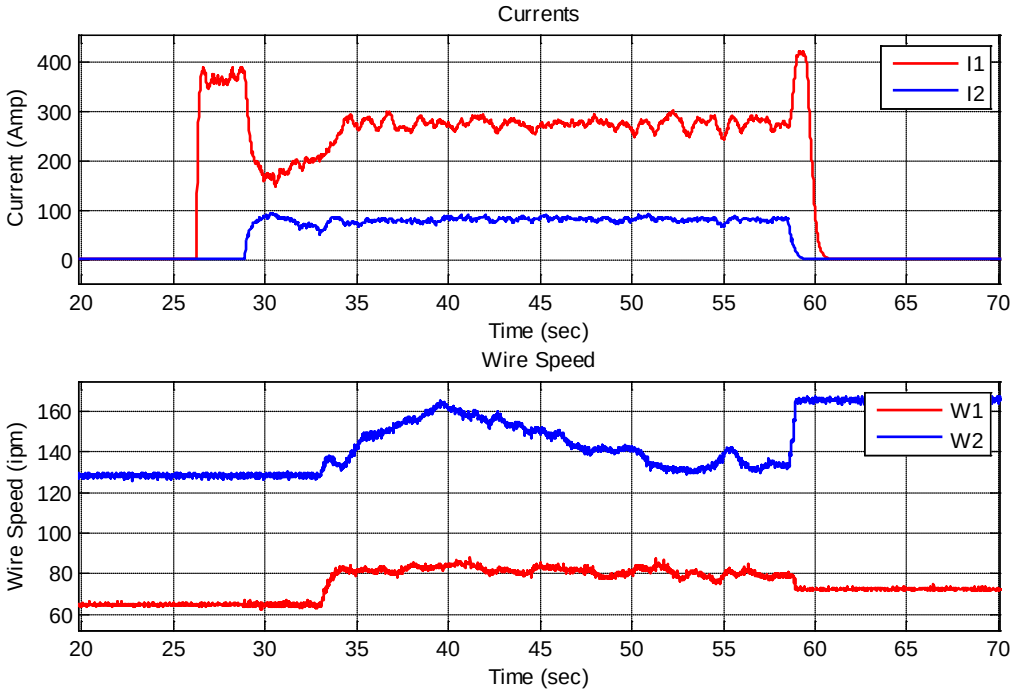

Fig. 7.1 Currents and Wire Speeds of Bead-On-Plate SAW Experiment

Fig. 7.1 plots currents vs. wire feed speeds from the bead-on-plate DE-SAW experiment. It can be seen that both the base metal current and bypass current reached and then stabilized around their desired settings. The fluctuations in the currents are slight and were due to the process. Because of the use of appropriate penalties, the changes in the

bypass wire were more active than those in the main wire. From the performance of the bead-on-plate DE-SAW experiment, it can be seen that the predictive control functions as expected.

Fig. 7.2 Weld Bead in Bead-On-Plate SAW Experiment. (Direction: L to R; the narrower weld bead was produced before the predictive feedback control starts and shows the need for feedback control)

7.3 Fillet Welding Experiments

With the proved effectiveness of the predictive control for the DE-SAW process, this predictive control algorithm can be applied to practical fillet joint SAW to feedback control the heat input and penetration in the process. The predictive control had been started after the advent of the bypass current. Different from the bead-on-plate experiment, the important welding parameters used here are all selected carefully in terms of the optimization results obtained in chapter 4 (1.5 mm root opening, 45 IPM travel speed, 100 IPM initial main wire speed). Due to the adjusting range of the bypass wire is relatively large, the initial bypass wire feed speed used here has been reduced by 100 IPM (from 250 IPM to 150 IPM) when 100 IPM initial main wire speed is using.

In order to verify the repeatability of the DE-SAW process for fillet joints, the fillet welding experiments have been repeated four times (Experiment (A), (B), (C) and (D)) with the same parameters listed in Table 7.3. The materials (tee and panel) used for fillet welding experiments are also C1018 cold rolled steel plates.

Table 7.3 Parameters in Fillet Welding Experiments

	Value	Unit
Initial Main Wire Speed (W1)	254 (100)	cm/min (IPM)
Initial Bypass Wire Speed (W2)	381 (150)	cm/min (IPM)
Desired Base Metal Current (I1)	330	Amp
Desired Bypass Metal Current (I2)	100	Amp
Travel Speed (v)	114.3 (45.0)	cm/min (IPM)
Main Voltage (V1)	28	Volt
Bypass Voltage (V2)	28	Volt
Root opening between Tee & Panel	1.5	mm
Width of Tee	4.7	mm
Width of Panel	4.7	mm

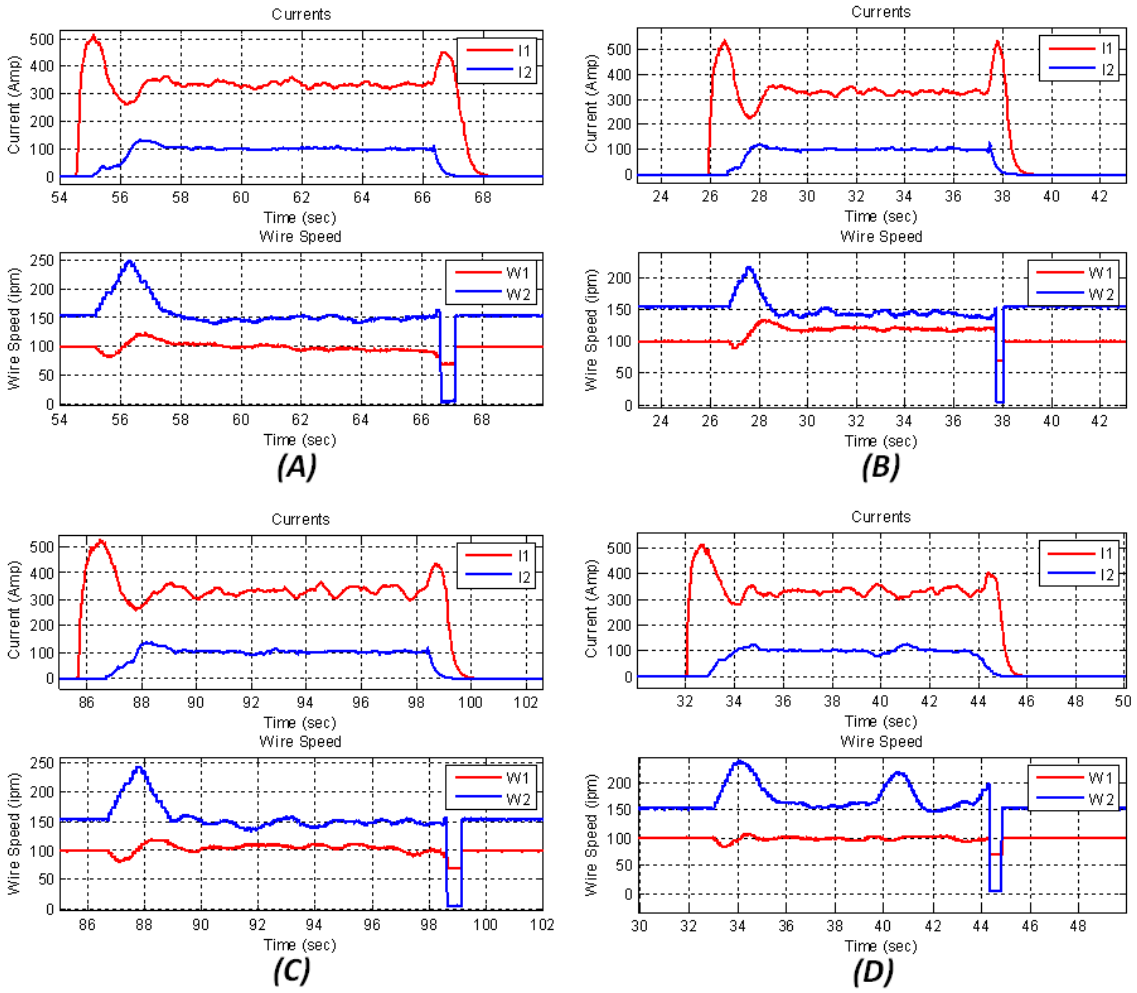

Fig. 7.3 Currents & Wire Speeds Plots of Fillet Welding Experiments

Fig. 7.3 shows the four groups of experimental data recorded from the data-acquisition (DAQ). It can be seen that all of the four processes are stable. Both of the base metal and bypass currents can be effectively kept around their desired values after the processes enter their steady states. The slight fluctuations on the currents came from the processes themselves primarily. The adjusting time for the predictive control system was about 1.8 seconds corresponding to 1 inch long welds. This adjusting time appears to be acceptable.

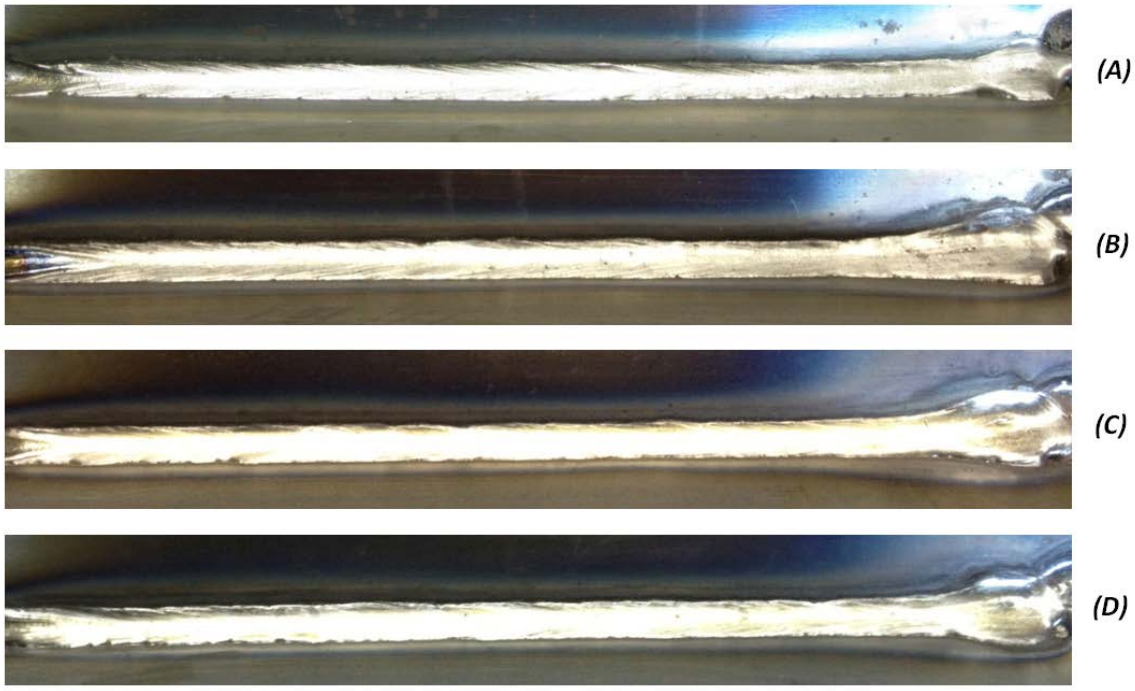

Fig. 7.4 Weld Beads of Fillet Welding Experiments (Direction: R to L)

Examined from the photos (Fig. 7.4) of weld beads in the fillet welding experiments, the widths of the weld beads in the four experiments are all uniform, and the surfaces of all the weld beads are quite flat and smooth. There is no obvious flaw found on the weld beads.

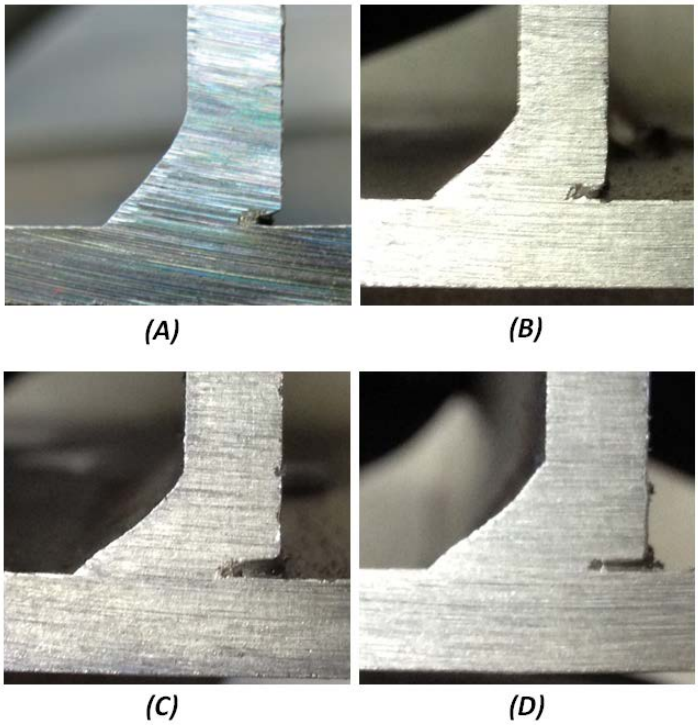

Fig. 7.5 Cross-sections of Fillet Welding Experiments

The cross-sections in Fig. 7.5 provide a clearer direct-view of the shaping of the weld beads. The re-entrant angles are large enough, greater than 90° required; the surfaces of the beads are relatively flat instead of convex or concave; and the leg-sizes of the weld beads comply with the industrial standards. Especially, the experimental results of the DE-SAW for fillet joints were accepted by shipyards.

In the shipbuilding welding industry, the heat input into the work-piece is calculated by means of the product of total welding current and welding voltage divided by the traveling speed. Thus in the DE-SAW experiments, the average heat input is:

$$\frac{430\ Amp \times 28\ V}{45\ IPM} = 267.6\ W/IPM \tag{7.1}$$

7.4 Weld Bead and Heat Input Comparison

After the predictive control based DE-SAW for fillet joints had been proven to be reliable and repeatable, the conventional SAW for fillet joints is conducted as a reference to compare with the good performance of DE-SAW. According to the industrial standard provided by the shipyards, the general traveling speed of the tractor is 30 IPM and the total welding current used for fillet welding is 400 Amp approximately. Then, based on the mapping relationship between wire speed and welding current, 76 IPM was chosen as the constant wire speed of the tractor. All of the important parameters in conventional SAW experiment are listed in Table 7.4. Owing to the conventional SAW process has a long history already, it is unnecessary to prove its repeatability.

Table 7.4 Parameters in Conventional SAW Experiment

	Value	Unit
Original Main Wire Speed (W1)	193 (76)	cm/min (IPM)
Travel Speed (v)	76.2 (30)	cm/min (IPM)
Main Voltage (V1)	28	Volt
Width of Tee	4.7	mm
Width of Panel	4.7	mm

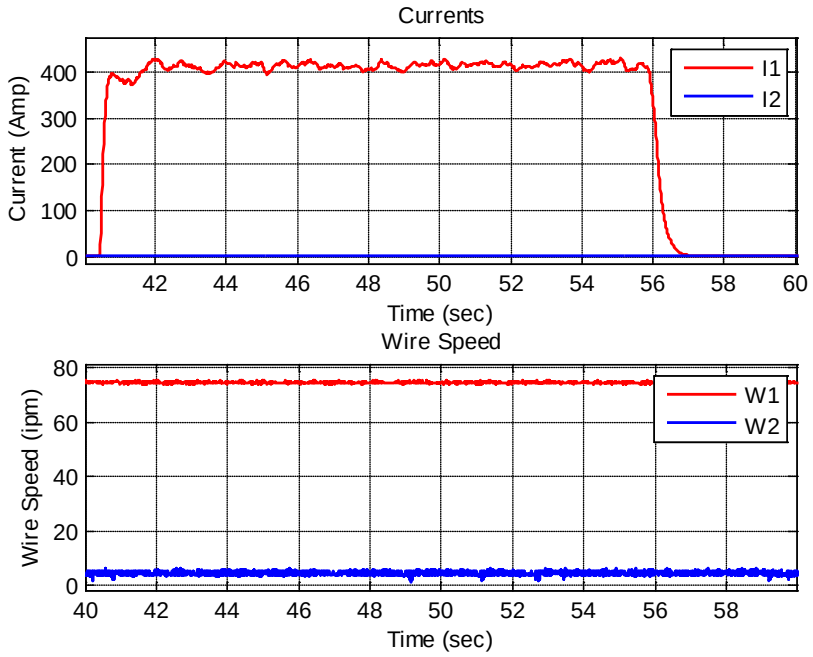

Fig. 7.6 Currents and Wire Speeds Plot in Conventional SAW Experiment

It can be seen from the DAQ record (Fig. 7.6) that the total welding current is 400 A approximately as expected. The bypass current equals zero because there is no bypass loop in conventional SAW.

Fig. 7.7 Weld Bead of Conventional SAW Experiment (Direction: R to L)

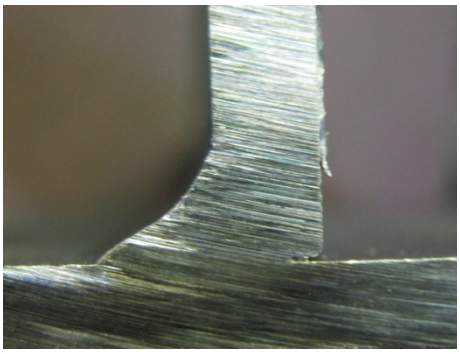

Fig. 7.8 Cross-section of Conventional SAW Experiment

Fig. 7.7 and 7.8 illustrate the shaping of the weld bead in the conventional SAW experiment. Compared with the weld beads of DE-SAW shown in Fig. 7.4 and 7.5, the shaping of weld bead in conventional SAW shows slightly concave due to the excessive heat. Same as in DE-SAW, the heat input in the conventional SAW experiment can be calculated as well:

$$\frac{400\ Amp \times 28\ V}{30\ IPM} = 373.3\ W/IPM \tag{7.2}$$

Summarizing the calculating results in Equations (7-1) and (7-2), it can be computed that the heat input in DE-SAW is about 72% of that in conventional SAW process. Therefore, by applying the predictive control based DE-SAW and the root opening between the tee and the panel, the decrease of heat input in the fillet welding, on the basis of guaranteeing the amount of metal deposition, is successful and remarkable.

7.5 Experiments and Analysis on Large Panels

In section 7.3,

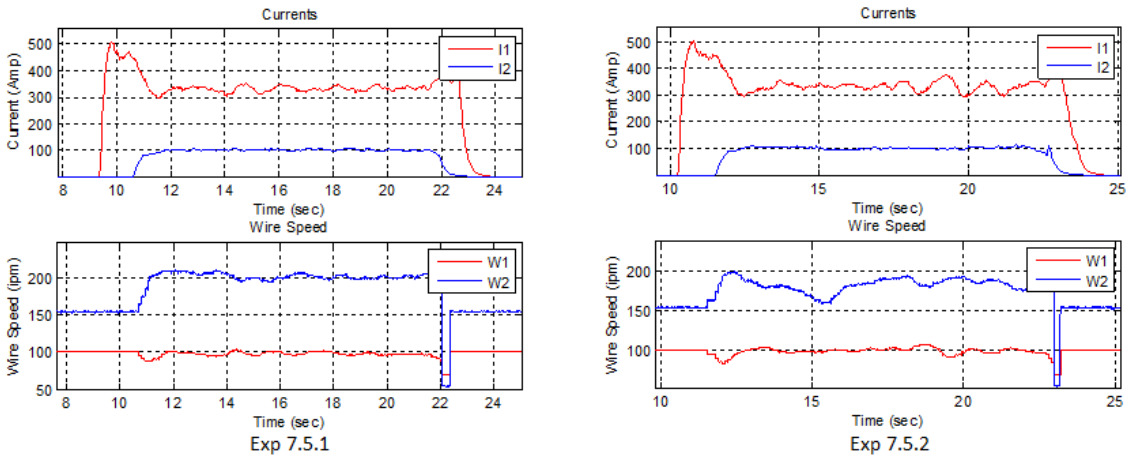

Fig. 7.9 Currents and Wire Speeds

Fig. 7.9 shows the recorded raw experimental data of experiment 7.5.1 and 7.5.2. It is not difficult to find that the wire feed speeds finished their dynamic adjustments swiftly and entered the steady state within 2 seconds approximately; both the base metal current and bypass current became quite stable, and maintained around their desired settings. Although the fluctuations of the welding currents in experiment 7.5.2, the process stability was still satisfied and the current fluctuations were within acceptable ranges.

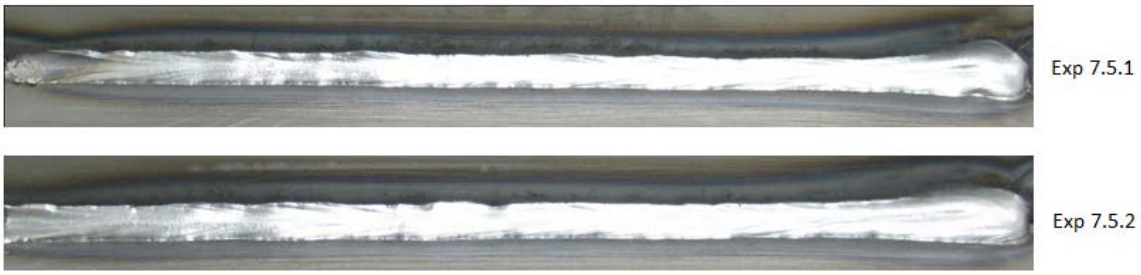

Fig. 7.10 Weld Beads

Fig. 7.10 illustrates the photos of the weld beads of experiment 7.5.1 and 7.5.2. It can be seen that the surfaces of the beads are flat and smooth. The shapes of the beads are quite uniform. No obvious flaws are found along the weld bead.

From the two experiments on larger weld-pieces (4 inch tee and 6 inch panel), the good parameters for the predictive control algorithm verified with smaller work-pieces (1 inch tee and 4 inch panel) also work for the larger work-pieces (4 inch tee and 6 inch panel).

Chapter 8 Simplified Version of Predictive Control

8.1 Background

In the previous chapters, the predicative control system of the DE-SAW fillet process with root opening have been established based on the model analysis and proved to be effective experimentally. In order to real-time adjust the main wire feed speed coming from the tractor and the bypass wire feed speed simultaneously, however, the inner structure of the LT-7 tractor (or any other welding devices used in the workshop of Ingalls) has to be altered which is challenging to be accepted by the customers. If merely the bypass wire feed speed needs to be real-time adjusted while the predictive control algorithm can still be inherited, then it would be more convenient to transplant the control system from the laboratory to the actual welding environment in shipyards. Based on this requirement, a simplified version of the predictive control, i.e. namely the bypass wire predictive control algorithm, has been developed in this chapter.

8.2 Algorithm Simplification

Owing to the good control performance, the algorithm design of the predictive control introduced in Chapter 6 is still inherited in the simplified version system. The only drawback of the previous predictive control is that the adjustment on the main wire feed speed sending out from the LT-7 tractor is difficult to be realized in the real workshop. Unfortunately, the practical DE-SAW process must be treated as a two-input-two-output system (see Fig. 5.3) when using the predictive model. Thus, the model structure of the

DE-SAW process brings a lot of challenges for combining the predictive control with the simplified hardware experimental platform.

Equation (6-17) shows the control law of the full version (two wires) predictive control. In that equation, the matrix "$\mathrm{D} = (\mathrm{A}^{\mathrm{T}}\mathrm{QA} + \mathrm{R})^{-1}\mathrm{A}^{\mathrm{T}}\mathrm{Q}$" can be calculated off-line in advance because A is known already from identification experiments; "Q" and "R" are from the design. Now that the adjustment of the input signals (wire feed speeds) and the importance of the changes of the inputs are determined completely by the weight matrices "Q" and "R", then the control algorithm can be approximated to a single-input-single-output control process as long as the weight of the inputs and the weight of the outputs are adjusted reasonably.

In particular, in matrix "Q" as shown in Eq. (8-1), the diagonal entries in sub-matrix "Q_1" determines the weights (importance) of the filtered base metal current values at each instants (from "k" to "k+N-1"); and the diagonal entries in sub-matrix "Q_2" determines the weights (importance) of the filtered bypass current values at each instants (from "k" to "k+N-1").

$$Q = \begin{bmatrix} Q_1 & 0 \\ 0 & Q_2 \end{bmatrix} \tag{8.1}$$

In the full version predictive control discussed in Chapter 6, because the two outputs (base metal and bypass currents) are important equally, all the diagonal elements in "Q" matrix are set to 1. Now, if the sub-matrix "Q_2" is set to a zero matrix, it means that the importance of the bypass current is completely ignored. In another word, only the base

metal current will be feedback controlled and the number of the process output has been simplified to one.

For the process inputs (wire feed speeds), the weight matrix R is a 2 by 2 diagonal matrix as shown in Eq. (8-2). When using the full version predictive control algorithm previously, the penalty to the main wire (r_1) is 10 and the penalty to the bypass wire (r_2) is 1.

$$R = \begin{bmatrix} r_1 & 0 \\ 0 & r_2 \end{bmatrix} \tag{8.2}$$

The larger the penalty value is, the smaller the adjustment of the input will be. Therefore, if the penalty to the main wire (r_1) is large enough, then the adjustment to the main wire would be approaching towards zero. As a result, only the bypass wire can be adjusted effectively as the process input.

The calculation shows that when the penalty to the main wire (r_1) is enlarged to 100000 while the weight of the bypass current is set to zero, then the adjustment of the main wire speed would be zero until the fourth figures after the decimal point. That accuracy is high enough to consider that the base metal current is actually feedback controlled completely by the bypass wire speed merely and the main wire feed speed is sent out constantly. Therefore, the knob of the main wire speed on the panel of the tractor can be fixed at an appropriate position by the human operator. That is the simplified or bypass wire predictive control law.

By using the new weight coefficients, the control is approximated to a single-input-single-output control process. The bypass wire feed speed will be the system input; the base metal current is the output signal. Thus, the new control law is coherent with the simplified version hardware platform. Meanwhile, the strategic decision of the predictive control algorithm has been inherited, so the good performance of the predictive control should be saved. In fact, the control logic is still the predictive control used in the full version control, but the decision of the control law performs as the simplified version apparently.

8.3 Experiment and Analysis on Small Panels

In order to test the feasibility of the new predictive control algorithm, a series of practical fillet DE-SAW experiments have been conducted. The small work pieces (1 inch tee and 4 inch panel) are used first.

Experiment 8.3.1 and 8.3.2:

In the first two experiments, the desired welding current is set a little bit lower than that in the full version predictive control. Due to the main wire feed speed is uncontrollable, it has been set with the knob on the panel of the tractor (unit: gauge). Experiment 8.3.1 and 8.3.2 are using the same parameters shown in Table 8.1.

Table 8.1 Experimental Conditions

	Value	Unit
Original Main Wire Speed (W1)	4.25	gauge
Original Bypass Wire Speed (W2)	381 (150)	cm/min (IPM)
Desired Base Metal Current (I1)	305	Amp
Travel Speed (v)	114.3 (45.0)	cm/min (IPM)
Main Voltage (V1)	28	Volt
Bypass Voltage (V2)	28	Volt
Root opening between Tee & Panel	1.5	mm

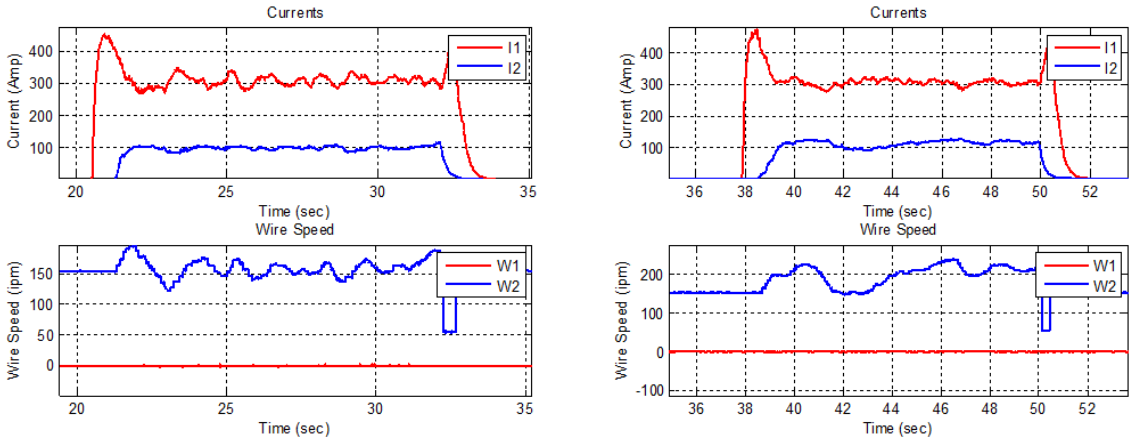

Fig. 8.1 Currents and Wire Feed Speeds

Fig. 8.1 shows the recorded experimental data from experiment 8.3.1 and 8.3.2. It is not difficult to find that the bypass wire feed speed has being changed in real-time to maintain the base metal current around its desired setting. And the main wire feed speed is not changed at all due to the large penalty used in the simplified predictive control algorithm. The entire welding process is quite stable.

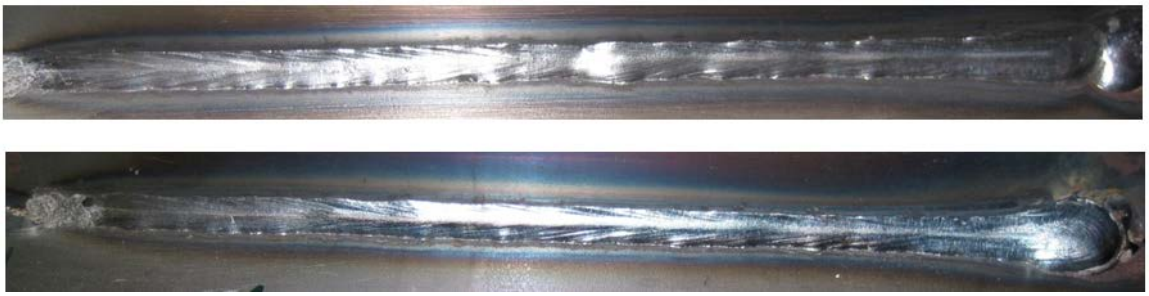

Fig. 8.2 Weld Bead Photos

From the weld bead photo (Fig. 8.2), it can be seen that the welding performance is acceptable basically. The penetration of the two experiments is relatively low resulting in the slight uneven of the shapes and the convex of the beads. The performance of experiment 8.3.2 is similar to the first experiment. The stable process proves the feasibility of the new predictive control, but the penetration of the process needs to be increased properly.

Experiment 8.3.3, 8.3.4 and 8.3.5:

In experiment 8.3.3, the desired base metal current is increased by 5 Amp from 305 Amp to 310 Amp so that the penetration of the process can be increased a little bit. All the important parameters are listed in Table 8.2. Also, in order to prove the repeatability of the good performance, the same parameters have been repeated twice in Experiment 8.3.4 and 8.3.5.

Table 8.2 Experimental Conditions

	Value	Unit
Original Main Wire Speed (W1)	4.25	gauge
Original Bypass Wire Speed (W2)	381 (150)	cm/min (IPM)
Desired Base Metal Current (I1)	310	Amp
Travel Speed (v)	114.3 (45.0)	cm/min (IPM)
Main Voltage (V1)	28	Volt
Bypass Voltage (V2)	28	Volt
Root opening between Tee & Panel	1.5	mm

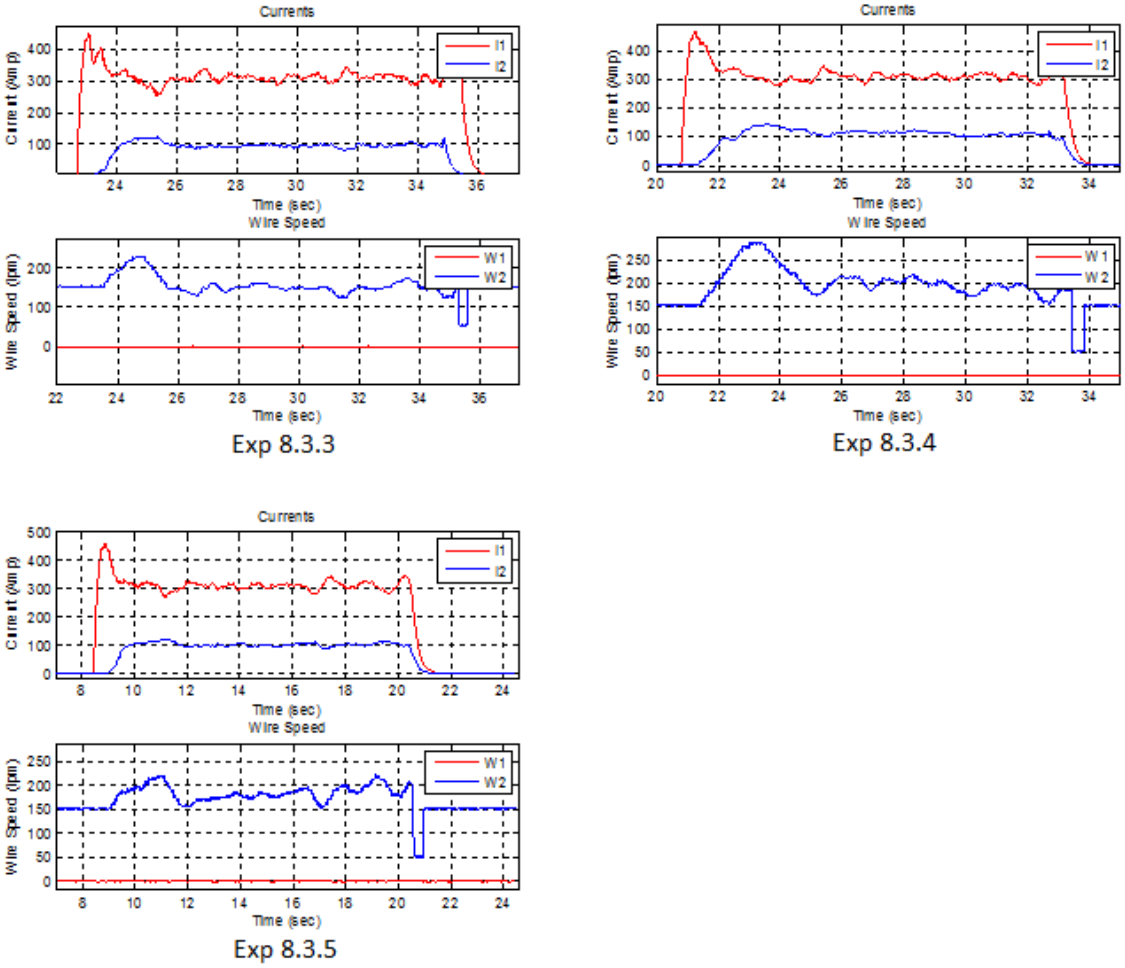

Fig. 8.3 Currents and Wire Feed Speeds

Fig. 8.3 shows the recorded experimental data from experiment 8.3.3, 8.3.4 and 8.3.5. It can be seen that the bypass wire feed speed in these three experiments has being changed

in real-time to maintain the base metal current around its desired setting. The entire welding process is still quite stable.

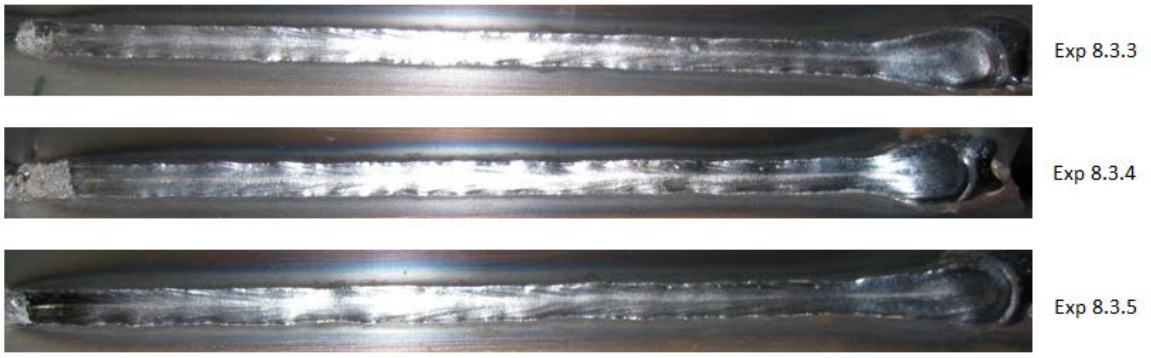

Fig. 8.4 Weld Beads

Fig. 8.4 illustrates the photo of the weld beads for Experiment 8.3.3, 8.3.4 and 8.3.5. It can be seen that the surface of the beads are flat and smooth after appropriately increasing the penetration. The shapes of the beads are uniform. No obvious flaws are found along the weld bead. From the experimental data recorded by the data acquisition and the photos of the weld beads, it can be seen that all the processes are stable. And the weld performances are satisfactory. Also, experiment 8.3.4 and 8.3.5 proved that the good performance by using the simplified predictive control algorithm is repeatable.

8.4 Experiment and Analysis on Large Panels

After confirming the good parameters for the simplified predictive control algorithm in section 8.3, and also proving the repeatability, the experiments are conducted on the large work pieces (4 inch tee and 6 inch panel) to simulate a more practical condition in the Ingalls shipyards. The welding parameters used in Experiment 8.4.1 and 8.4.2 are the same to those in Table 8.2.

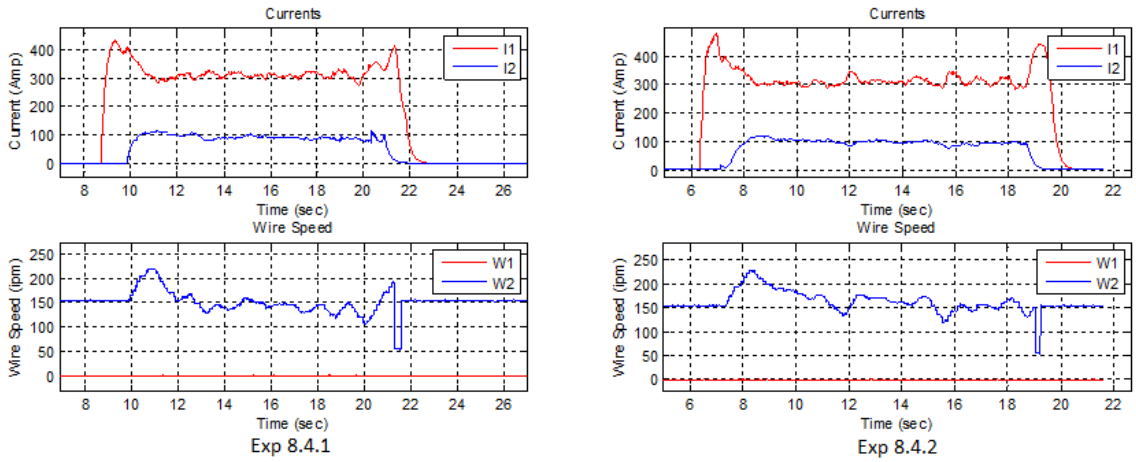

Fig. 8.5 Currents and Wire Feed Speeds

Fig. 8.5 shows the recorded raw experimental data. It is not difficult to find that the base metal current became stable after entering the stable status, and maintained around its desired setting. Also, the adjustment of the bypass wire is coherent to the expectation. Although the fluctuations of the welding currents in experiment 8.4.2 were a little more pronounced than those in the experiment 8.4.1, the process stability was still satisfied and the current fluctuations were within acceptable ranges.

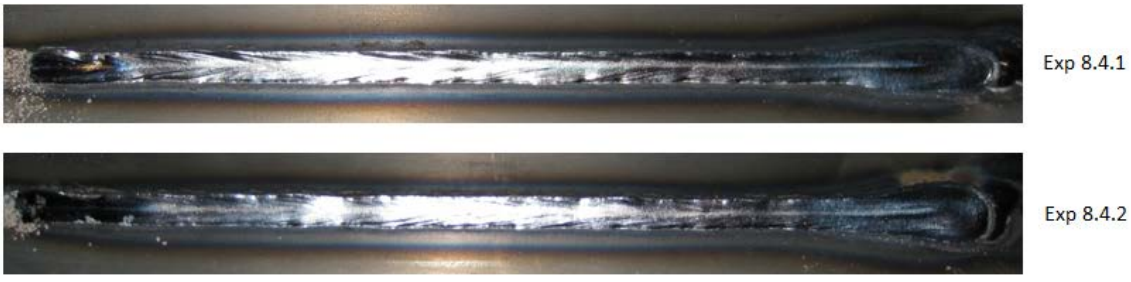

Fig. 8.6 Weld Beads

Fig. 8.6 illustrates the photos of the weld beads for experiment 8.4.1 and 8.4.2. It can be seen that the surfaces of the beads are flat and smooth. The shapes of the beads are quite uniform. No obvious flaws are found along the weld bead.

From the two experiments on larger weld-pieces (4 inch tee and 6 inch panel) for practical condition simulation, the good parameters for the simplified predictive control algorithm verified with smaller work-pieces (1 inch tee and 4 inch panel) also work for the larger work-pieces (4 inch tee and 6 inch panel).

Chapter 9 Conclusion and Future Work

9.1 Conclusion

In this dissertation research, the major achievements could be summarized as:

1. Double Electrode technology has been applied on the Submerged Arc Welding (SAW) process for the first time.
2. DE-SAW provides an effective technology for fillet joints in shipbuilding that can reduce the heat input/energy consumption and assure the amount of metal deposition; this technology can be readily transferred to shipyards.
3. Predictive control played a critical role in successfully developing the fillet welding of DE-SAW technology and the challenges existed in the realization process of DE-SAW for fillet joints have been systematically solved.
4. The use of a root opening between the tee and the panel provides an effective way to reduce the penetration capability required to produce desired weld beads. The heat input reduction capability of the DS-SAW can thus be effectively utilized to produce desirable fillet welds with minimized heat input. 1.5 mm is recommended for fillet welding on 3/16” thick plates.
5. Quantitative and qualitative analysis methods have been used to optimize the welding parameters for minimized heat input. The resultant optimized practice for DE-SAW of 3/16” fillet joints is to use 1.5 mm root opening, 45 IPM travel speed and 100 IPM initial main wire feed speed for 3/32 inch” (2.381 mm) diameter main wire.

6. By using the predictive control and the root opening between the tee and the panel, the fillet DE-SAW process results in 30% reduction approximately on the heat input from the shipyard single-wire benchmark.
7. The simplified predictive control algorithm cooperating with the simplified hardware platform has been proved experimentally to be feasible. By using this algorithm, the simplified experimental platform can be used without changing the inner structure of the tractor. And it would be easier to transplant the control system to the practical on-site welding environment in the shipyards.
8. The experiments on the larger work-pieces (4" tee and 6" panel) proved the repeatability of the two controls (full version predictive control and simplified predictive control) and as well as their robustness with respective to the work-piece size.
9. The simplified control algorithm/method can be considered as an alternative plan to the full version predictive DE-SAW control algorithm. In particular, if the internal structure of the LT-7 tractor or other SAW welding tractors using in shipyards is allowed to be reorganized, then the predictive DE-SAW control algorithm should still have the priority to be used; otherwise, the simplified control algorithm/method can be applied alternatively cooperating with the DE-SAW control system.

9.2 Future Work

To improve the performance of the predictive control system for the fillet joint DE-SAW process with root opening, some possible future developments are listed below:

1. In the process model analysis of DE-SAW, the main wire and bypass wire feed speeds are chosen as the input signals that can be adjusted real-time to maintain the welding currents. Actually, when the wire feed speeds are fixed constantly, the welding voltages (main and bypass power supplies) can also be used as the adjusting variables to realize the control of the welding currents. This idea is well worth trying.
2. In order to transplant the success of the predictive control algorithm of DE-SAW to the practical environment in the shipyards, the terminals, ports and cables of the entire control system might need to be redesigned according to the devices used in the shipyards.
3. The simplified predictive control system illustrated in Chapter 8 can be tested in the shipyards in the future, so that improvement suggestions can be obtained from the human operators.

References

1. Ueyama, T., et al., Effects of torch configuration and welding current on weld bead formation in high speed tandem pulsed gas metal arc welding of steel sheets. Science and Technology of Welding and Joining, 2005. 10(6): p. 750-759.
2. Tsushima, S. and M. Kitamura, Tandem electrode AC-MIG welding - development of AC-MIG welding process (report 4). Welding Research Abroad, 1996. 42(2): p. 26-32.
3. Talkington, J.E., Variable Polarity Gas Metal Arc Welding, in Welding Engineering 1998, Ohio State University: Columbus, Ohio.
4. Cary, H. and W. Chaisson, Variable Polarity Plasma Arc Welding, 1986, Metairie, LA, USA: Aluminum Assoc: Washington, DC, USA.
5. Ueyama, T., et al., AC pulsed GMAW improves sheet metal joining. Welding Journal (Miami, Fl), 2005. 84(2): p. 40-46.
6. Tong, H., et al., Quality and productivity improvement in aluminum alloy thin sheet welding using alternating current pulsed metal inert gas welding system. Science and Technology of Welding and Joining, 2001. 6(4): p. 203-208.
7. HARWIG, D.D., et al., Arc behavior and melting rate in the VP-GMAW process. Welding Journal, 2006. 85(3): p. 52S-62S.
8. HARWIG, D.D., Arc Behavior and Melting Rate in the VP-GMAW Process, 2003, Cranfield University.
9. Mahrle, A. and E. Beyer, Hybrid laser beam welding-classification, characteristics, and applications. Journal of Laser Applications 2006. 18(3): p. 169-180.
10. Liu, L., X. Hao, and G. Song, A new laser-arc hybrid welding technique based on energy conservation. Materials Transactions 2006. 47(6): p. 1611-1614.
11. Seyffarth, P. and I.V. Krivtsun, Laser-Arc Processes and Their Applications in Welding and Materials Treatment, 2002, Taylor & Francis: New York.
12. Bagger, C. and F.O. Olsen, Review of laser hybrid welding. Journal of Laser Applications, 2005. 17(1): p. 1-14.
13. Steen, W.M. and M. Eboo, Arc augmented laser welding. Metal Construction, 1979. 11(7): p. 332-333.
14. Walduck, R.P. and J. Biffin, Plasma arc augmented laser welding. Welding and Metal Fabrication, 1994. 62(4): p. 3.
15. Reutzel, E.W., M.J. Sullivan, and D.A. Mikesic, Joining pipe with the hybrid laser-GMAW process: Weld test results and cost analysis. Welding Journal (Miami, Fla), 2006. 85(6): p. 66-71.
16. Sullivan, M., Laser pipe welding project, in National Shipbuilding Research Program Welding Panel Meeting 2006: Provo, UT.
17. Zhang, Y.M., M. Jiang, and W. Lu, Double electrodes improve GMAW heat input control. Welding Journal (Miami, Fla), 2004. 83(11): p. 39-41.
18. Li, K.H., J.S. Chen, and Y.M. Zhang, Double-electrode GMAW process and control. Welding Journal (Miami, Fla), 2007. 86: p. 231s-237s.
19. Amin, M., Pulse Current Parameters for Arc Stability and Controlled Metal Transfer in Arc Welding. Metal Construction, 1983(15): p. 272-278.

20. Li, K.H. and Y.M. Zhang, Metal transfer in double-electrode gas metal arc welding. Journal of Manufacturing Science and Engineering, Transactions of the ASME, 2007. 129: p. 991-999.
21. Wu, C.S., et al., Numerical analysis of double-electrode gas metal arc welding process. Computational Materials Science, 2007. 39: p. 416-423.
22. Li, K.H. and C.S. Wu, Mechanism of metal transfer in DE-GMAW. Journal of Materials Science and Technology, 2009. 25: p. 415-418.
23. Li, K.H. and Y.M. Zhang, Interval model control of Consumable Double-Electrode Gas Metal Arc Welding process. IEEE Transactions on Automation Science and Engineering, 2010. 7: p. 826-839.
24. Waszink, J.H. and G.P.M.V.d. Heuvel, Heat generation and heat flow in the filler metal in GMAW welding. Welding Journal 1982. 61: p. 269s-282s.
25. Li, X.R., Y.M. Zhang, and L. Kvidahl, Penetration Depth Monitoring and Control in Submerged Arc Welding. Welding Journal, 2013. 92(2): p. 48s-56s.
26. Zhang, S.S., et al., Effect of magnetic field on twin-wire indirect arc shape. Transactions of The Chian Welding Institute, 2010. 31(7): p. 87-90.
27. Liu, X., et al. Dual bypass GMAW of aluminum. in 35th North American Manufacturing Research Conference, NAMRC 35, May 22, 2007 - May 25, 2007. 2007. Ann Arbor, MI, United states: Society of Manufacturing Engineers.
28. Xue, C., et al., Edge extraction algorithm and analysis for dual bypass GMAW metal transfer. Shanghai Jiaotong Daxue Xuebao/Journal of Shanghai Jiaotong University, 2008. 42(SUPPL. 1): p. 90-92+96.
29. Xue, C., et al., Edge extraction algorithm for dual bypass GMAW weld pool. Shanghai Jiaotong Daxue Xuebao/Journal of Shanghai Jiaotong University, 2010. 44(SUPPL. 1): p. 4-7.
30. Xue, C., et al. High speed weld control system of dual-bypass MIG based on LabVIEW. in 2010 International Conference on Manufacturing Engineering and Automation, ICMEA2010, December 7, 2010 - December 9, 2010. 2010. Guangzhou, China: Trans Tech Publications.
31. Meng, L., et al. Research and development of high energy pulse precision cold-welding technology. in 2011 International Conference on Advanced Engineering Materials and Technology, AEMT 2011, July 29, 2011 - July 31, 2011. 2011. Sanya, China: Trans Tech Publications.
32. Shinozaki, K., et al., Melting phenomenon during ultra-high-speed GTA welding method using pulse-heated hot-Wire. Yosetsu Gakkai Ronbunshu/Quarterly Journal of the Japan Welding Society, 2009. 27: p. 22s-26s.
33. Hori, K., et al., Development of hot wire TIG welding methods using pulsed current to heat filler wire - Research on pulse heated hot wire TIG welding processes (report 1). Yosetsu Gakkai Ronbunshu/Quarterly Journal of the Japan Welding Society, 2003. 21: p. 362-373.
34. Lv, S.X., et al., Arc heating hot wire assisted arc welding technique for low resistance welding wire. Science and Technology of Welding and Joining, 2007. 12(5): p. 431-435.
35. Lv, S.X., et al., Investigation on TIG cladding of copper alloy on steel plate. Science and Technology of Welding and Joining, 2008. 13(1): p. 10-16.

36. Chen, J.S., et al., Gas Tungsten Arc Welding Using an Arcing Wire. Welding Journal, 2012. 91: p. 9.
37. Chen, S.J., et al., Droplet Transfer in Arcing-Wire GTAW. Accepted for Publication in 7th Asia Pacific IIW International Congress 2013 July 8-10: Singapore.
38. Submerged Arc Welding1982: Miller Electric MFG. CO.
39. Holliday, D.B., Gas-Metal Arc Welding. 10 ed. ASM Handbook. Vol. 6. 1993: ASM International.
40. Wang, G., P.G. Huang, and Y.M. Zhang, Numerical analysis of metal transfer in gas metal arc welding. Metallurgical and Materials Transactions B: Process Metallurgy and Materials Processing Science, 2003. 34: p. 345-354.
41. Meyer, D.W., Flux-Cored Arc Welding. 10 ed. ASM Handbook. Vol. 6. 1993: ASM International.
42. The Welding Handbook for Maritime Welders. 10 ed: Barwil Unitor Ships Service.
43. Welding Handbook. 8 ed, ed. R.L. O'Brien. Vol. 2: Welding Processes. 1991: American Welding Society.
44. Su, H., J. Hu, and H. Guo. Submerged arc welding procedure improvement based on human-machine operation analysis. in 3rd International Conference on Information Management, Innovation Management and Industrial Engineering, ICIII 2010, November 26, 2010 - November 28, 2010. 2010. Kunming, China: IEEE Computer Society.
45. Ogborn, J.S., Submerged Arc Welding. 10 ed. ASM Handbook. Vol. 6. 1993: ASM International.
46. Yang, X., et al., Twin-wire submerged arc welding process of a high-strength low-alloy steel. Journal Wuhan University of Technology, Materials Science Edition, 2011. 26: p. 114-117.
47. Li, Z. and S. Cheng. Torque ripple reduction in brushless DC motors based on model predictive control. in International Conference on Electrical and Control Engineering, ICECE 2010, June 26, 2010 - June 28, 2010. 2010. Wuhan, China: IEEE Computer Society.
48. Bruce, G.J. and D.J. Eyres, Ship Construction. 7 ed 2012: Butterworth-Heinemann.
49. LT-7 Lightweight Tractor Service Manual2010: Lincoln Global Inc.
50. Key, J.F., Arc Physics of Gas-Tungsten Arc Welding. 10 ed. ASM Handbook. Vol. 6. 1993: ASM International.
51. Fillet Welding Technical Sheets, 2007, European Federation for Welding, Joining and Cutting (EWF)
52. The National Shipbuilding Research Program: Proceedings of the REAPS Technical Symposium Paper No. 14: Shipbulding Equipment at Mitsubishi, 1976.
53. Li, K.H. and Y.M. Zhang, Consumable double-electrode GMAW part II: Monitoring, modeling, and control. Welding Journal, 2008. 87: p. 44-s-50-s.
54. Moore, D.S. and W.I. Notz, Statistics - Concepts and Controversies. 7 ed2009, New York: W. H. Freeman and Company.
55. Shanmugan, K.S. and A.M. Breipohl, Random Signals: Detection, Estimation and Data Analysis. 1 ed1988: Wiley.

56. Ziemer, R.E. and W.H. Tranter, Principles of Communications. 6 ed2008: Wiley.
57. Serway, R.A. and J.W. Jewett, Physics for Scientists and Engineers 6ed2003: Brooks Cole.
58. Tipler, P., Physics for Scientists and Engineers: Electricity, Magnetism, Light, and Elementary Modern Physics. 5 ed2003: W. H. Freeman.
59. Zhang, Y.M., Arc Physics of Gas Tungsten and Gas Metal Arc Welding. In ASM Handbook, ed. T. Lienert, et al. Vol. 6A: Welding Fundamentals and Processes. 2011: ASM.
60. Clarke, D.W., C. Mohtadi, and P.S. Tuffs, GENERALIZED PREDICTIVE CONTROL - PART II. EXTENSIONS AND INTERPRETATIONS. Automatica, 1987. 23: p. 149-160.
61. Clarke, D.W., C. Mohtadi, and P.S. Tuffs, GENERALIZED PREDICTIVE CONTROL - PART I. THE BASIC ALGORITHM. Automatica, 1987. 23: p. 137-148.
62. Clarke, D.W., APPLICATION OF GENERALIZED PREDICTIVE CONTROL TO INDUSTRIAL PROCESSES. IEEE Control Systems Magazine, 1988. 8: p. 49-55.
63. Maciejowski, J.M., Modelling and predictive control: Enabling technologies for reconfiguration. Annual Reviews in Control, 1999. 23: p. 13-23.
64. Maciejowski, J.M., Predictive Control with Constraints. 1 ed2000: Prentice Hall.
65. Rodrigues, J.A.D. and R. Maciel Filho. Application of a novel approach for DMC predictive controller design by response surface analysis in a fed-batch bioreactor. 1999. Langford Lane, Kidlington, Oxford, OX5 1GB, United Kingdom: Elsevier Ltd.
66. Huang, J., et al., Robust stability conditions for remote SISO DMC controller in networked control systems. Journal of Process Control, 2009. 19(5): p. 743-750.
67. Kokate, R.D., L.M. Waghmare, and S.D. Deshmukh. Review of tuning methods of DMC and performance evaluation with PID algorithms on a FOPDT model. in 2nd International Conference on Advances in Recent Technologies in Communication and Computing, ARTCom 2010, October 15, 2010 - October 16, 2010. 2010. Kottayam, India: IEEE Computer Society.
68. Yan, H.-B., L.-E. Huang, and Z.-S. Liu. The application of improved DMC in remote networked measure-control system. in 3rd International Symposium on Information Science and Engineering, ISISE 2010, December 14, 2010 - December 26, 2010. 2011. Shanghai, China: IEEE Computer Society.
69. Mehra, R.K., et al. MODEL ALGORITHMIC CONTROL (MAC): REVIEW AND RECENT DEVELOPMENTS. in Chemical Process Control 2: Proceedings of the Engineering Foundation Conference. 1982. Sea Island, GA, USA: United Eng Trustees.
70. Guan, Y., et al. Research on MAC in zinc-air battery pole manufacturing line. in 2009 International Forum on Information Technology and Applications, IFITA 2009, May 15, 2009 - May 17, 2009. 2009. Chengdu, China: IEEE Computer Society.
71. Richalet, J., et al., MODEL PREDICTIVE HEURISTIC CONTROL: APPLICATIONS TO INDUSTRIAL PROCESSES. Automatica, 1978. 14(5): p. 413-428.

VITA

Yi Lu

EDUCATIONAL BACKGROUND

PhD. Candidate, Electrical Engineering, University of Kentucky, Lexington, KY

Dissertation: "Model Analysis and Predictive Control of Double Electrode Submerged Arc Welding Process for Fillet Joints with Root Opening"
Supervisor: Dr. YuMing Zhang

B.S., Electrical Engineering, University of Science & Technology Beijing, China

Thesis: "PID Control System Design and Simulation of Tobacco Drier"

PUBLICATIONS

- **Lu, Yi**, S.J. Chen, Y. Shi, X.R. Li, J.S. Chen, L. Kvidahl, and Y.M. Zhang, *Double-electrode arc welding process: Principle, variants, control and developments*, Journal of Manufacturing Processes, Sep. 2013.
- Li, X.R., **Y. Lu**, and Y.M. Zhang, *Accelerometer-based Position and Speed Sensing for Manual Pipe Welding Process.* The International Journal of Advanced Manufacturing Technology, p1-9, May 2013.
- Chen, J.S., **Y. Lu**, X.R. Li and Y.M. Zhang, *Gas Tungsten Arc Welding Using an Arcing Wire.* Welding Journal, Vol. 91 Issue 10, p261-s, Oct. 2012. (Citations: 3)
- **Lu, Yi**, Y.M. Zhang and Kvidahl, L., *Heat Input Reduction in Fillet Welding Using Bypass and Root Opening*, Welding Journal, 2013, Vol. 92, accepted for publication.
- **Lu, Yi**, J.S. Chen and Y.M. Zhang, *Dynamic Model of Consumable Double-Electrode Submerged Arc Welding Process*, Transactions of the ASME, accepted for publication.
- **Lu, Yi**, J.S. Chen, Y.M. Zhang and L. Kvidahl, *Predictive Control Based Double-Electrode Submerged Arc Welding for Fillet Joints*, in review for Control Engineering Practice.

CONFERENCE PROCEEDINGS

- **Lu, Yi** and Y.M. Zhang, *Modeling and Analysis of DE-SAW Process*, in *AWS Professional Program at FABTECH* 2012: Las Vegas, NV.
- Chen, J.S., **Y. Lu**, and Y.M. Zhang, *Improvement of GTAW Using Arcing-Wire* in *AWS Professional Program at FABTECH* 2012: Las Vegas, NV.

- Chen, J.S., **Y. Lu**, and Y.M. Zhang, *Double Electrode GMAW with One Welding Power Supply*, in *AWS Professional Program at FABTECH* 2011: Chicago, IL.

PATENTS PENDING

- Zhang, YuMing, J.S. Chen and **Y. Lu**, *Gas Tungsten Arc Welding Using Arcing-Wire*, Assignee: Adaptive Intelligent Systems LLC, US patent application #13/694,230, currently under review.
- Zhang, YuMing, **Y. Lu**, J.S. Chen and Z. Shao, *A Method to Make Fillet Welds*, Assignee: Adaptive Intelligent Systems LLC, US patent application #13/986,864, currently under review.

ACADEMIC HONORS AND AWARDS

University of Kentucky

- Graduate School Student Travel Funding – 2011 and 2012
- Kentucky Graduate Scholarship – 2008

University of Science and Technology Beijing

- People's Scholarship (Grade 3) – 2005 and 2006
- People's Scholarship (Grade 4) – 2004